

Developing Peptide Probes for Membrane Lipids via Phage Display

Michael A. Kelly

A dissertation

submitted to the Faculty

of the Department of Chemistry

in partial fulfillment

of the requirements for the degree of

Doctor of Philosophy

Boston College
Morrissey College of Arts and Sciences
Graduate School

May 2020

Developing Peptide Probes for Membrane Lipids via Phage Display

Michael A. Kelly

Advisor: Prof. Jianmin Gao, PhD

Lipid reporters are key signaling molecules in a number of biological processes ranging from apoptosis in mammalian cells to novel resistance mechanisms in pathogenic bacteria. Developing probes to target these lipids is a worthy endeavor, especially when better reporters could mean lives saved. This is particularly true considering new antibiotic resistant pathogens emerge every year with evolving lipid compositions. To combat these pathogens and prevent a potential global pandemic, it is imperative to continue the development of novel and innovative probes/drugs to meet this daunting challenge. To fulfill this demand, we must continue to establish new strategies, enhance current technologies and advance scientific understanding. Only by pushing the boundaries of what is currently possible will we remain one step ahead of these diseases. Diseases like *mcr-1* positive bacteria, first documented in 2016, remain largely uncontested.

Herein, we seek to expand the available probes specific to key lipid reporters for phosphatidylserine, lysyl-phosphatidylglycerol, and phosphoethanolamine lipid A. Cyclic phage libraries were first utilized to target phosphatidylserine, ultimately producing weak binders. Refining our phage display libraries to include reversible covalent warheads allowed for the identification of more potent lipid reporters. In doing so, we have created the tools necessary to interrogate the unique resistance mechanisms expressed by these drug-resistant pathogens. A strong correlation was observed between peptides binding *mcr-1*

positive strains, LPS modification on the surface of these bacteria, and level of colistin resistance. To our knowledge, these peptides are the only probes capable of demonstrating this correlation. We surmise that the methods discussed here will pave the way for better diagnostic tools for these resistant pathogens. A recurring method of resistance among gram-positive and gram-negative bacteria has been to decorate their surface with positive amines to repel cationic antimicrobial peptides. As such, our current APBA library and the libraries in development in the Gao lab would be ideally suited to target these and other undiscovered resistance mechanisms.

Table of Contents

List of Tables	v
List of Figures	vii
List of Abbreviations	x
Acknowledgments	xii
1.0 Chapter 1: Introduction to Phage Display	1
1.1 A Brief History of Phage Display	2
1.2 A Technical Introduction to M13 Phage Display	2
1.3 Disadvantages of Phage Display Technology	4
1.4 Chemical Modifications in Phage Display	6
1.5 Identifying and Evaluating Targets for Screening	8
1.6 Conclusions	10
1.7 References	11
2.0 Peptide Probes Identified for Phosphatidylserine Containing Membranes	14
2.1 Introduction	15
2.1.1 Phosphatidylserine and Its Importance in Lipid Signaling	15
2.1.2 PS Probes	16
2.1.3 Phage Display for Lipid Binding	18
2.2 Screening and Selections	19
2.2.1 Screening by Liposomes	19
2.2.2 Characterization of Phage Outputs from Liposome Screening	21
2.2.3 Selection of Physically Deposited PS Lipids	23
2.2.4 Characterization of Phage from Physical Deposition of Lipids	24
2.3 Peptide Characterization for PS Detection	25
2.3.1 Dansyl Emission Analysis of Peptides Against Liposomes	25
2.3.2 Testing MAK3 against Apoptotic Cells	29
2.4 Conclusions and Discussion	30
2.5 Experimental Protocols	33
2.5.1 Liposomes	33
2.5.2 Screening Against Lipids	34
2.5.3 ELISA of Selected Phage	35
2.5.4 Peptide Synthesis	36
2.5.5 Peptide Characterization by Dansyl Emission	36

2.5.6 Mammalian Cell Culture and Analysis by FACS and Microscopy	37
2.6 References	38
3.0 Targeting Lys-PG for Bacterial Recognition with an APBA-Modified Library	41
3.1 Introduction	42
3.1.1 Lysyl-Phosphatidylglycerol (Lys-PG) and Its Role in Bacteria	42
3.1.2 Phage Display Modification Strategies	43
3.1.3 Iminoboronate Chemistry	44
3.2 APBA Dimer Library Construction and Validation of Modifications	45
3.2.1 Library Modification	45
3.2.2 Confirmation of APBA Modification of Phage	46
3.3 Targeting Lys-PG	48
3.3.1 Screening Protocol Against Lys-PG	48
3.4 Peptide Characterization	51
3.4.1 Flow Cytometry Analysis	51
3.4.2 Microscopy Analysis	53
3.4.3 Selectivity Over Mammalian Cells	53
3.4.4 ELISA Characterization of Peptides	55
3.5 Inhibition by BSA and Second-Generation Peptide	57
3.5.1 BSA Inhibition Studies	57
3.5.2 Second Generation Peptides via Cell Screening with BSA Present	58
3.6 Conclusions and Discussion	59
3.7 Experimental Protocols	60
3.7.1 Materials and General Methods	60
3.7.2 Synthetic Scheme of 2-Acetylphenyl Boronic Acid Moiety: (2acetyl-5-(3-(2-iodoacetamido)propoxy)phenyl)boronic acid	61
3.7.3 Synthesis of <i>Tert</i> -butyl (3-bromopropyl)carbamate (2)	61
3.7.4 Synthesis of 2-Aetyl-5-(3-((<i>tert</i> -butoxycarbonyl)amino)propoxy) phenyl trifluoromethanesulfonate (3)	62
3.7.5 Synthesis of <i>tert</i> -butyl (3-(4-acetyl-3-(4,4,5,5-tetramethyl-1,3,2- dioxaborolan-2-yl)phenoxy)propyl)carbamate (4)	63
3.7.6 Synthesis of (2-acetyl-5-(3-(2-iodoacetamido)propoxy)phenyl) boronic acid (5)	64
3.7.7 Bacterial Cell Culture and Staining	66
3.7.8 Mammalian Cell Culture and Staining	67
3.7.9 Phage Display and Affinity Selection	67
3.7.10 Streptavidin Capture Assay	68
3.7.11 Solid Phase Peptide Synthesis	69

3.7.12 Microscopy and FACS Analysis	70
3.7.13 Fluorescent SDS-PAGE	71
3.7.14 ELISA Assay on Peptide Binding to Pure Lipids	71
3.8 References	72
4.0 Peptide Probes of Colistin Resistance Discovered via Chemically Enhanced Phage Display	76
4.1 Introduction	77
4.1.1 Colistin Resistance	77
4.2 Identification of Probes for <i>Mcr-1</i> Positive <i>E.coli</i>	80
4.2.1 Panning Against <i>Mcr-1</i> Positive <i>E.coli</i>	80
4.3 Characterization of the Peptide Hits for Detecting Colistin Resistance	84
4.3.1 Flow Cytometry Analysis of Peptide Hits	84
4.3.2 Scope of MAK30 for Detecting Colistin Resistant Pathogens	86
4.3.3 Lipopolysaccharide Analysis	92
4.4 Targeting Additional Colistin Resistant Strains	95
4.4.1 Identifying Probes Against Colistin Resistant <i>A. baumannii</i> and <i>K. pneumoniae</i>	95
4.4.2 Cross Examination of Peptide Probes Against Different Bacterial Species	100
4.5 Combination Therapies	103
4.5.1 Peptides in Combination with Antibiotics	103
4.6 Conclusions and Discussion	105
4.7 Experimental Protocols	107
4.7.1 Materials and Instrumentation	107
4.7.2 Peptide Synthesis	107
4.7.3 APBA-Dimer Library Panning Against Whole Cells	108
4.7.4 Fluorescence Microscopy	109
4.7.5 Flow Cytometry Analysis	109
4.7.6 Mass Spec Analysis of LPS	109
4.7.7 Cell Killing Assay	110
4.8 References	111
5.0 Conclusions: Unique Targets Require Innovative Screening Strategies	115
5.1 References	122
Additional Data	123

6.0 Targeting Proteins with APBA Libraries	124
6.1 Introduction	125
6.1.1 Expanding the Scope to Proteins	125
6.2 Targeting Proteins	127
6.2.1 Screening APBA Libraries Against Protein Targets	127
6.2.2 Creating Novel Mono APBA Cyclic Libraries	128
6.2.3 Human Lysozyme Screen and Peptide Characterization	131
6.2.4 Sortase A Screen and Peptide Characterization	135
6.3 Conclusions and Discussion	137
6.4 Experimental Protocols	139
6.4.1 General Methods and Procedures	139
6.4.2 Library Screening	139
6.4.3 Pulse Chase Assay	139
6.4.4 Protein Labeling with Biotin-NHS	140
6.4.5 ELISA Assay	141
6.5 References	142
7.0 Biocompatible Conjugation of Tris Base to 2-Acetyl and 2-Formyl Phenylboronic Acid	144
7.1 Introduction	145
7.1.1 Biocompatible Conjugation Chemistries with APBA	145
7.2 Discovery and Characterization of Tris APBA/FPBA Complex	147
7.2.1 LC-MS and X-ray Crystallography	147
7.2.2 Kinetic Studies	148
7.3 Conclusions and Discussion	150
7.4 Experimental Protocols	151
7.4.1 General Methods and Procedures	151
7.4.2 Crystallographic Information	151
7.4.3 Relaxation Kinetics	155
7.5 References	156

List of Tables

1.0 Introduction

2.0 Peptide probes identified for phosphatidylserine containing membranes

Table 2-1 Hits isolated from PS targeting phage display	26
--	----

3.0 Targeting Lys-PG for bacterial recognition with an APBA-modified library

Table 3-1 List of DNA and peptide sequences identified from Screen against Lys-PG	50
--	----

Table 3-2 Peptides hits made for further characterization	51
--	----

Table 3-3 Calculated and observed mass of the disulfide-cyclized peptides	69
--	----

Table 3-4 Calculated and observed mass of the 2-APBA labeled peptides	70
--	----

4.0 Peptide Probes of Colistin Resistance Discovered via Chemically Enhanced Phage Display

Table 4-1 List of bacterial strains used in this work	81
--	----

Table 4-2 Sequencing results for the output populations of <i>E. coli</i> (493 strain) screening	83
---	----

Table 4-3 Sequence and mass-spec data of peptide hits	84
--	----

Table 4-4 SEC18-20	96
---------------------------	----

Table 4-5 SEC5 & KAM20-21	98
----------------------------------	----

5.0 Conclusions: Unique targets require innovative screening strategies

Additional Data

6.0 Targeting Proteins with APBA Libraries

Table 6-1 Sequences identified for human lysozyme	131
--	-----

Table 6-2 Peptide sequences for human lysozyme made via SPPS	132
---	-----

Table 6-3 Sequences identified for SrtA	136
--	-----

Table 6-4 Peptide sequences for SrtA made via SPPS	136
---	-----

Table 6-5 Protein labeling with Biotin-NHS	141
---	-----

7.0 Biocompatible conjugation of Tris base to 2-acetyl and 2-formyl phenylboronic acid

Table 7-1 Masses of the same peptide labeled APBA head group in Tris vs PBS	147
Table 7-2 Crystallography data and structure refinement for APBA-Tris	152
Table 7-3 Atomic coordinates and equivalent isotropic displacement parameters for C ₁₂ H ₁₆ BNO ₄	153
Table 7-4 Crystallography data and structure refinement for FPBA-Tris	154
Table 7-5 Atomic coordinates and equivalent isotropic displacement parameters for C ₁₁ H ₁₄ BNO ₄ .	155

List of Figures

1.0 Introduction

Figure 1-1 The phage display panning process	3
Figure 1-2 Nonspecific chemical modification strategies on phage display scaffolds	7
Figure 1-3 Examples of site-specific phage modifications	8
Figure 1-4 Lipid targets of interest for developing peptide probes	9

2.0 Peptide probes identified for phosphatidylserine containing membranes

Figure 2-1 A healthy cell undergoing apoptosis	16
Figure 2-2 PS and previous peptide probes	18
Figure 2-3 Screening of phage display libraries against liposomes	21
Figure 2-4 Liposome ELISA	22
Figure 2-5 Screening of phage against directly deposited lipids	24
Figure 2-6 ELISA of physically deposited lipids and hydrophobicity scale	25
Figure 2-7 MAK1-4 dansyl emission assay against LUVs	27
Figure 2-8 MAK1-4 dansyl emission assay against SUVs	28
Figure 2-9 Testing MAK3 at physiologically relevant levels of PS	29
Figure 2-10 FACS analysis of MAK3	30
Figure 2-11 Lipid Packing	32

3.0 Targeting Lys-PG for bacterial recognition with an APBA-modified library

Figure 3-1 Illustration of PG (left) and Lys-PG (right)	43
Figure 3-2 Reversible covalent interaction of APBA and free amine to form a stable iminoboronate	45
Figure 3-3 C7C phage display library reduction and labeling with APBA functionality	46
Figure 3-4 Confirmation of phage labeling	48
Figure 3-5 Screening process for modified phage display libraries against Lys-PG	49
Figure 3-6 APBA modified peptides MAK5-8 FACS	52
Figure 3-7 <i>S. aureus</i> , <i>S. pyogenes</i> and <i>B. subtilis</i> , incubated with MAK7 peptide	53
Figure 3-8 Co-culture FACS with peptides	54

Figure 3-9 Confocal microscopic	55
Figure 3-10 Assessing lipid selectivity of the peptide hits by ELISA	57
Figure 3-11 MAK7 with and without 1mg/mL BSA	58
Figure 3-12 KAM5 ACVSPRSHECGGGDap with and without BSA present	59
Figure 3-13 Increased binding of KAM5 with increased concentration of BSA present	59
Figure 3-14 Synthetic scheme of APBA	61

4.0 Peptide Probes of Colistin Resistance Discovered via Chemically Enhanced Phage Display

Figure 4-1 Illustration of surface modifications of colistin resistant bacteria	80
Figure 4-2 Schematic illustration of phage panning against live bacterial cells	82
Figure 4-3 Flow cytometry analysis of <i>mcr-1 E. coli</i> peptides	85
Figure 4-4 MAK30 and fluorescein alone tested against 493 and 348	86
Figure 4-5 Microscopy and flow cytometry analyses showing MAK30	87
Figure 4-6 MAK30 is a pan- <i>mcr-1</i> (+) strain selective probe for <i>E. coli</i>	88
Figure 4-7 Flow cytometry analysis of MAK30 against a variety of <i>E. coli</i>	89
Figure 4-8 Microscopy analysis of KAM5	90
Figure 4-9 Microscopy images of linear MAK30 precursor	91
Figure 4-10 Lipopolysaccharide (LPS) with and without the addition of PE	92
Figure 4-11 Mass-spec analysis of bacterial lipids showing <i>mcr-1</i> induced PE modification of LPS	93
Figure 4-12 Bar graph showing the apparent percentages of lipid A modification with PE	94
Figure 4-13 <i>K. pneumoniae</i> binding curves of SEC18-SEC20	96
Figure 4-14 Mass spec LPS analysis of <i>K. pneumoniae</i>	97
Figure 4-15 Flow cytometry analysis of <i>A. baumannii</i> staining by SEC5, KAM20, and KAM21	99
Figure 4-16 LPS modification in colistin resistant <i>A. baumannii</i>	100
Figure 4-17 Cross examination of SEC5 and SEC18 against various bacterial species	102
Figure 4-18 Cell killing curves were generated for rifampicin and clarithromycin in combination with colistin	104

5.0 Conclusions: Unique targets require innovative screening strategies

Additional Data

6.0 Targeting Proteins with APBA Libraries

Figure 6-1 3D structure of human lysozyme	126
Figure 6-2 3D structure of Sortase A	127
Figure 6-3 Summary of screens performed and the manner of immobilization of each protein target	128
Figure 6-4 Confirmation of Mono APBA library	130
Figure 6-5 ELISA human lysozyme peptides	133
Figure 6-6 Images of MAK21 incubated with streptavidin beads and human lysozyme	134
Figure 6-7 Fluorescent microscopy imaging of positive control WW6 and MAK35-37	137

7.0 Biocompatible conjugation of Tris base to 2-acetyl and 2-formyl phenylboronic acid

Figure 7-1 Biocompatible conjugation chemistries of 2-FPBA/APBA	146
Figure 7-2 Characterization of the FPBA/APBA	148
Figure 7-3 Kinetics analysis of Tris conjugation with 2-FPBA/APBA	149

Abbreviations

DNA	Deoxyribonucleic Acid
NGS	Next Generation Sequencing
cPTM	Chemical Post-Translational Modifications
TFP	Tetrafluorophenyl
NHS	N-Hydroxysuccinimide
PS	Phosphatidylserine
Lys-PG	Lysyl-Phosphatidylglycerol
PE	Phosphoethanolamine
kDa	Kilodalton
APBA	Acetylphenylboronic Acid
cLac-2	Cyclic Lactadherin Peptide
PC	Phosphatidylcholine
LUV	Large Unilamellar Vesicles
(Biotin-PE)	Biotinylated Phosphatidylethanolamine
HRP	Horseradish Peroxidase
ELISA	Enzyme Linked Immunosorbent Assay
pfu	Plaque Forming Units
PBS	Phosphate Buffered Saline
SPPS	Solid Phase Peptide Synthesis
Dap	Diaminopropionic Acid
RP-HPLC	Reverse Phase High-Performance Liquid Chromatography
LC-MS	Liquid Chromatography Mass Spectrometry
DMF	Dimethylformamide
SUV	Small Unilamellar Vesicles
CPT	Camptothecin
FAM	5-Carboxyfluorescein
FACS	Fluorescence Activated Cell Sorting
FITC	Fluorescein Isothiocyanate
DCM	Dichloromethane
TMB	Tetramethylbenzidine
Fmoc	Fluorenylmethyloxycarbonyl
HBTU	Hexafluorophosphate Benzotriazole Tetramethyl Uronium
HCl	Hydrochloric Acid
Alloc	Allyloxycarbonyl
NMM	<i>N</i> -Methylmorpholine
TFA	Trifluoroacetic Acid

uv-vis	Ultraviolet Visible
FBS	Fetal Bovine Serum
PG	Phosphatidylglycerol
FPBA	Formyl Phenylboronic Acid
APBA-IA	Acetyl Phenylboronic Acid Iodoacetamide
iTCEP	Immobilized Tris(2-carboxyethyl) phosphine
Biotin-IA	Biotin Iodoacetamide
SCZ	Semicarbazide
SDS-PAGE	Sodium Dodecyl Sulfate Polyacrylamide Gel Electrophoresis
CHL	Cholesterol
BSA	Bovine Serum Albumin
PEG	Polyethylene glycol
ESKAPE	<i>Enterococcus faecium, Staphylococcus aureus, Klebsiella pneumoniae, Acinetobacter baumannii, Pseudomonas aeruginosa</i> and <i>Enterobacter</i> species
LPS	Lipopolysaccharides
LOS	Lipooligosaccharide
CDC	Centers for Disease Control and Prevention
NAG	N-Acetylglucosamine
NAM	N-Acetylmuramic Acid
SrtA	SortaseA
APBA-DCA	APBA Dichloroacetamide
TzB	Thiazolidinoboronate
IzB	Imidazolidoboronate
OzB	Oxazolidinoboronate

Acknowledgments

I would like to sincerely thank my advisor Professor Jianmin Gao who's mentorship and guidance has helped me to grow and learn as a scientist. Without his help I would not have accomplished all that I have today. His dedication and drive for science has been an inspiration to me, and I will take the tools and knowledge I have gained here with me into my future endeavors.

I would like to thank my committee members Professor Ahbishek Chatterjee, and Professor Eranthie Weerapana for taking the time to read my dissertation. Your help and advice throughout these years has been invaluable to me.

I would like to thank the office staff for all the work you do behind the scenes in Merkert to keep this place running.

I would like to thank all my coworkers who have shown me techniques, taught me how to use the instrumentation, and helped me with various projects throughout the years. It really is a collaborative effort working in Merkert and you all have been a pleasure to work with. Kaicheng you have been an amazing desk buddy in my time here and I couldn't have asked for a better lab mate to work with. The entirety of the Gao lab has been wonderful to work with and I thank you all. Thank you especially to Katie and Breanna for helping to edit my thesis.

I'd like to thank all the friends I've made at BC for the fun times both in and outside of Merkert. You've made Boston feel like home.

I'd like to thank my family, especially my parents who have been patient with me throughout this whole process. I could not have done this without your support. I'd like to thank my sister for letting me know that even though I'm getting my PhD, I still don't know anything. I would like to acknowledge all my family and friends who saw me begin this journey but passed before I could finish it. I love you all and you will always be in my heart.

Above all, I would like to thank my amazing wife, Rachel. I can't thank you enough for all your love and support throughout this time. You make me smile every day and lift me up when I need encouragement. You have been at my side every step of the way, helping me to achieve my goals. You truly are an incredible person and I can't wait to see what our future holds.

Chapter 1

Introduction to Phage Display

1.1 A Brief History of Phage Display

In 2018, the Nobel Prize in Chemistry was jointly awarded to Frances H. Arnold, George P. Smith, and Sir Gregory P. Winter for their work in phage display and directed evolution of enzymes.¹ Phage display, as a platform, was created in 1985 when G. Smith first expressed polypeptides on the surface of lysogenic filamentous bacteriophage.² Not long after that first report, the phage display platform was used for screening and panning affinity selections.³ Since the early days of discovery, the technology for phage display has rapidly evolved. From simple peptides to whole antibody selection, phage display has developed into an extremely powerful tool.⁴ This year, phage display celebrates its 35th anniversary and continues to have a major impact on drug discovery and the life sciences field.

1.2 A Technical Introduction to M13 Phage Display

The screening platform of phage display leverages the innate characteristics and life cycle of filamentous bacteriophage. One key aspect that phage display relies on is the natural connection between genotype and phenotype of these filamentous viruses.¹⁻³ This relationship allows for easy identification of peptides and antibodies expressed on the surface of phage by sequencing their DNA. Large, chemically diverse polypeptide libraries can be created through designing and cloning synthetic oligonucleotide inserts, which once incorporated into the phage vector, will express their corresponding peptide on the surface of the phage.

Another important aspect of phage display is its replication in bacteria. In M13 phage display, the phage attaches to the F pilus, an extracellular appendage expressed in

specific *E. coli* strains.⁵ Once attached, the appendage retracts, and the phage DNA is then passed into the bacterial cell. From there, the cell replicates the phage DNA, expresses the various viral proteins, packages new filamentous phage, and exports the phage to repeat the process.^{6,7}

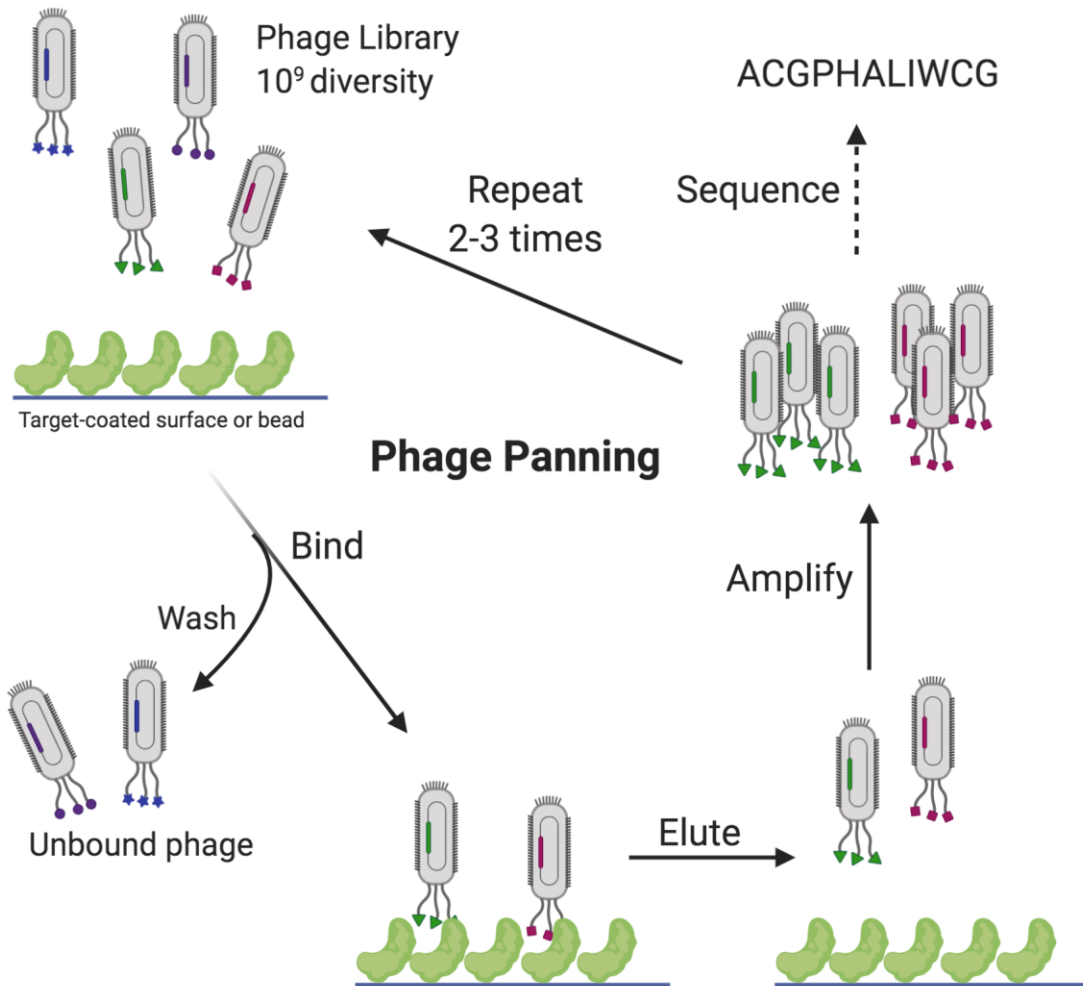


Figure 1-1 The phage display panning process. Phage are incubated with a target of interest. Non-binders are washed away. Phage bound to the target are eluted and then amplified in *E. coli*. The process repeats and phage plaques are sequenced after rounds two and three.

By combining the diversity of peptides expressed with the short, easily-managed replication process, screening processes have become straightforward: one simply needs to apply the phage libraries to a target of interest and allow the affinity selection process to generate ligands for the target. The selection process follows five key steps, with some variation depending on setup: identify and immobilize a target, incubate phage libraries with the target of interest, wash away non-binding phage, elute bound phage from the target, amplify isolated phage, and repeat the process.^{8,9} The full process (**Figure 1-1**) can be repeated multiple times to enrich for higher affinity binders, and phage isolated after each round can be sequenced to identify potential hits for further analysis.

1.3 Disadvantages of Phage Display Technology

The straightforward panning process and the commercial availability of phage libraries has allowed phage display to become one of the most widely used high-throughput screening processes.¹¹ Phage display libraries are capable of exploring a diverse sequence space with library diversities of 10^9 and greater, giving the phage display platform a major advantage over other screening methodologies.¹² However, there are a number of drawbacks to using phage display technology; one such drawback is the necessity of a large phage scaffold. A large, filamentous phage structure can participate in nonspecific interactions with targets of interest or possibly non-target related material, leading to false positives in the screening process.¹³ Furthermore, it is critical that the entirety of the phage virus remains intact. Phage can be killed through disruption of its overall structure, which limits the conditions in which screening can be conducted.¹⁴

For screening purposes, the phage library is often expressed at the N-terminal of the PIII protein, though there are other potential locations for library expression.¹⁵ The PIII protein attaches to the F pilus appendage and initiates the injection of DNA into the bacterial cell.⁵ Any library, or specific library member, expressed at this site that interrupts any aspect of the phage life cycle in *E. coli* effectively renders the phage inert. When this occurs, biases or censorships can occur in phage libraries.¹⁶ Censorship of charged sequences through the general secretory pathway in *E. coli* is well-documented and can lead to significantly reduced peptide diversity when compared to theoretical diversity.¹² One key mitigation method for this drawback is the use of next generation sequencing (NGS).¹² This deep sequencing allows for identification of initial library biases and censorships, helping to more accurately assess screening outputs. Improved analysis of output populations ultimately helps identify false positives and increases the likeliness of screens producing high affinity binders for targets.

The last major drawback of phage display as a platform for screening is the phage's reliance on biological machinery. Phage production in *E. coli* is straightforward and reliable, however, it limits the expressed library to natural amino acids. This drawback has been overcome by the development of unnatural amino acid expression systems, allowing for the incorporation of unique residues.^{17,18} Nonetheless, unnatural amino acid incorporation in phage display has yet to see broad implementation. Alternatively, introduction of chemical post-translational modifications (cPTM) into phage can dramatically expand the diversity of libraries without the need for heavily engineered *E. coli* expression systems.¹²

1.4 Chemical Modifications in Phage Display

CPTM can access diverse functionalities and gain added benefits like constrained topology, proteolytic stability, and glycosylation among others.¹² Early cPTM aimed at modifying the free amines of lysine residues, carboxylic acid residues like glutamate and aspartate, and tyrosine.¹⁹ These modifications had diverse applications, including drug delivery, imaging, photosensitivity, and biosensing.¹⁹ However, modifications were not limited to the PIII-expressed library, and labeled the entirety of the phage scaffold. This was by design, and these methods utilized the entirety of the phage for specific applications, but entire phage modifications are less than ideal for ligand discovery purposes. Despite their shortcomings, these modifications opened the door to new possibilities for phage platforms.

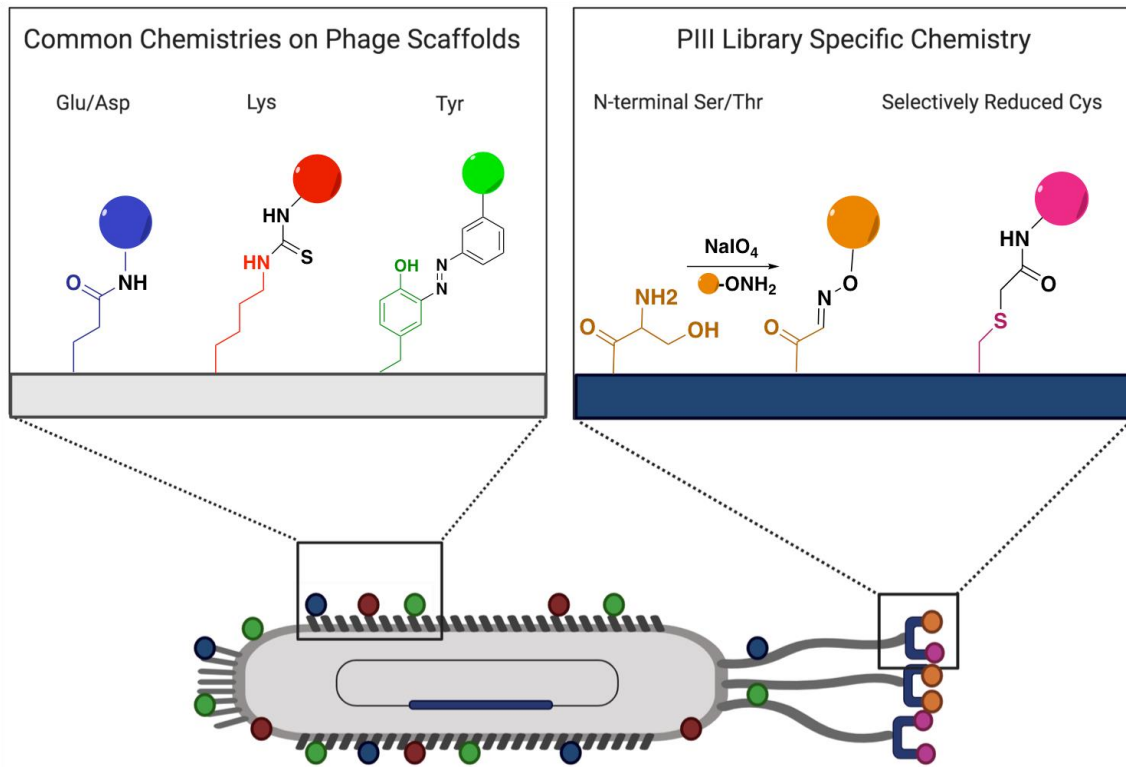


Figure 1-2 Nonspecific chemical modification strategies on phage display scaffolds (left) and PIII library specific chemistries (right).

Building on the success of previous modifications, recent designer functionalities were introduced in a site-specific manner through two main methods. The first method works via selective modification of a strategically placed N-terminal serine or threonine.²⁰ The second method uses selective alkylation of N-terminal cysteines.²¹ This method of cysteine modification is easily accessible, due to the commercial availability of a C7C library, a library consisting of seven randomized amino-acids flanked by two cysteines. Modifications like the introduction of biotin and carbohydrate handles or staples to create rigid bicyclic peptides have been reported as successful methods for screening to identify high affinity ligands for their targets of interest.²²

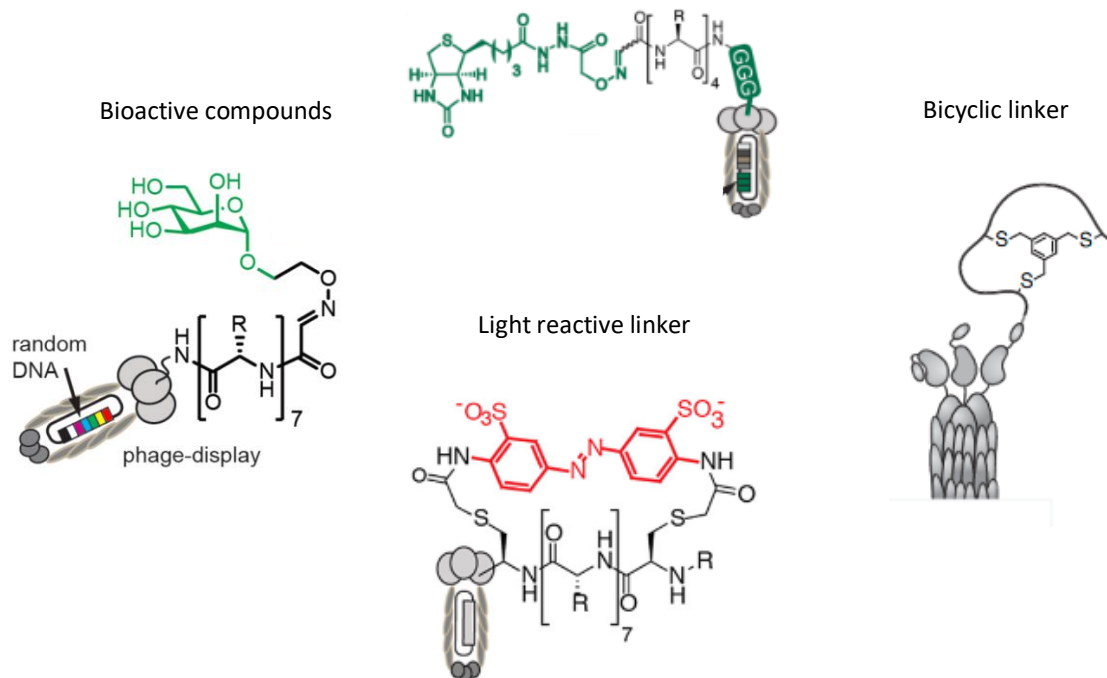


Figure 1-3 Examples of site-specific phage modifications for screening purposes. Modifications utilize N-terminal serine/threonine²⁰ or selectively reduced cysteines^{21,22} in peptide libraries.

1.5 Identifying and Evaluating Targets for Screening

Screening and the development of probes for targets of interest can consume a significant amount of time, energy, and resources. This is especially true when trying to develop drugs for clinical trials, where it can take 10 to 15 years to successfully complete all phases and reach the market.²³ As the process of drug discovery and implementation can be extensive and arduous, it is important to fully analyze potential targets before the commencement of screening. It is crucial that the current landscape of a particular target is fully understood to streamline efforts for the greatest yield in screening.

A considerable focus of the Gao lab research has been to identify probes for lipid recognition. Lipid composition and distribution in cell membranes can play an important

role in many physiological aspects of the cell. For example, phosphatidylserine (PS) is an indicator of apoptosis in mammalian cells.²⁴ In gram-positive bacteria high percentages of lysyl-phosphatidylglycerol (lys-PG) act as a resistance mechanism for cationic antimicrobials.²⁵ The same can be said for phosphoethanolamine (PE) modifications to lipid A in gram-negative bacteria.²⁶ However, these lipids present a difficult target for probe development due to their small size. Despite this challenge, we have decided to pursue these lipids as targets with unique peptide-based strategies to expand on the limited number of probes currently available.

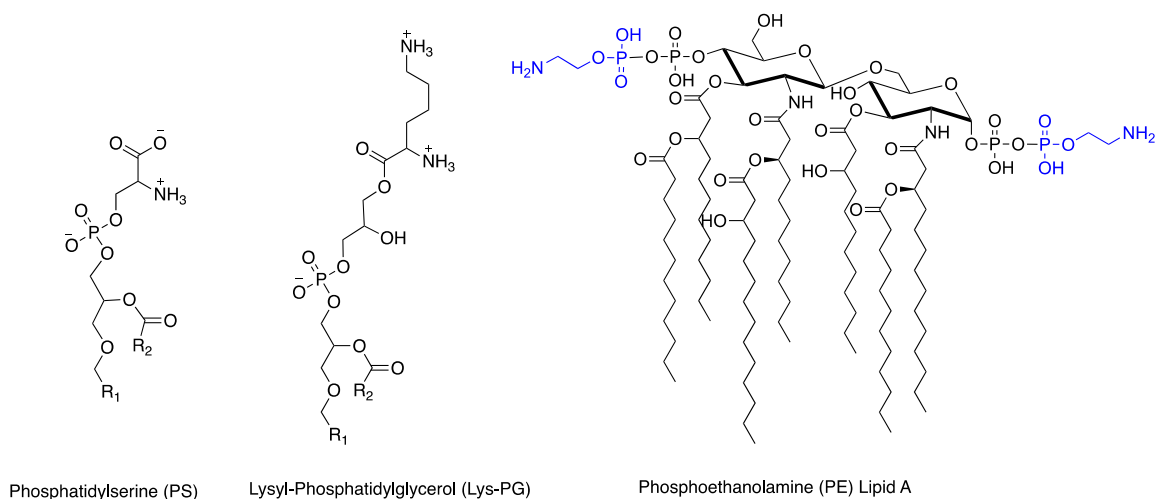


Figure 1-4 Lipid targets of interest for developing peptide probes.

An aspect of examination for these lipid targets is their currently available probes and identification of opportunities for improvement. For example, the current gold standard for detecting PS is annexin V, a 36.8 kDa protein that relies on calcium to bind.²⁷ A small peptide probe that does not rely on calcium for binding could be a significant improvement. Similarly, PE modifications in gram-negative bacterial cells have recently become a topic of concern and potential global threat to public health.²⁸ Despite the

seriousness of this threat, there are currently no known probes that can identify these PE modifications, leaving opportunity for exploration. Identification of high affinity ligands for these targets could be beneficial in facilitating accurate clinical diagnoses. That said, these small molecule targets present unique challenges for screening, so careful forethought must be given for choosing an appropriate phage display library. To this end, we have developed novel, reversible covalent phage display libraries to identify potent peptide probes. Specifically, we attached acetylphenylboronic acid (APBA) moieties for targeting amine-presenting lipids.²⁹ The unique libraries described in this work expand on the modification strategies employed by phage display technology and ultimately provide a powerful tool for targeting free amines on a variety of targets.

1.6 Conclusions

The concept of phage display as a screening platform has significantly improved since its original report in 1985. The simple polypeptide library reported by George P. Smith has been refined and reinvented for a wide array of applications. Gregory P. Winter augmented phage display to include humanized antibody libraries, which greatly expanded the applications of this technology for medical purposes. Today, this platform continues to advance with unique libraries, creative screening methods, and mitigation of its drawbacks. Phage display has had a major impact in the field of life science, and the contributions in this work aim to further expand the applications of phage technology.

1.7 References

1. Barderas, R., & Benito-Peña, E. (2019). The 2018 Nobel Prize in Chemistry: phage display of peptides and antibodies. *Analytical and bioanalytical chemistry*, 411(12), 2475-2479.
2. Smith, G. P. (1985). Filamentous fusion phage: novel expression vectors that display cloned antigens on the virion surface. *Science*, 228(4705), 1315-1317.
3. Parmley, S. F., & Smith, G. P. (1988). Antibody-selectable filamentous fd phage vectors: affinity purification of target genes. *Gene*, 73(2), 305-318.
4. McCafferty, J., Griffiths, A. D., Winter, G., & Chiswell, D. J. (1990). Phage antibodies: filamentous phage displaying antibody variable domains. *nature*, 348(6301), 552-554.
5. Sidhu, S. S. (2001). Engineering M13 for phage display. *Biomolecular engineering*, 18(2), 57-63.
6. Wickner, William, and Teresa Killick. "Membrane-associated assembly of M13 phage in extracts of virus-infected Escherichia coli." *Proceedings of the National Academy of Sciences* 74.2 (1977): 505-509.
7. Kuhn, A., & Wickner, W. (1985). Isolation of mutants in M13 coat protein that affect its synthesis, processing, and assembly into phage. *Journal of Biological Chemistry*, 260(29), 15907-15913.
8. Watters, J. M., Telleman, P., & Junghans, R. P. (1997). An optimized method for cell-based phage display panning. *Immunotechnology*, 3(1), 21-29.
9. Clackson, T., & Lowman, H. B. (Eds.). (2004). *Phage display: a practical approach* (No. 266). Oxford University Press.
10. Ph.d.[™]-7 Phage Display Peptide Library New Biolabs - <https://www.nebiolabs.com.au/products/e8102-phd-7-phage-display-peptide-library#Product%20Information>
11. Peltomaa, R., Benito-Peña, E., Barderas, R., & Moreno-Bondi, M. C. (2019). Phage Display in the Quest for New Selective Recognition Elements for Biosensors. *ACS omega*, 4(7), 11569-11580.

12. He, B., Tjhung, K. F., Bennett, N. J., Chou, Y., Rau, A., Huang, J., & Derda, R. (2018). Compositional bias in naïve and chemically-modified phage-displayed libraries uncovered by paired-end deep sequencing. *Scientific reports*, 8(1), 1-14.
13. AC't Hoen, P., Jirka, S. M., Bradley, R., Schultes, E. A., Aguilera, B., Pang, K. H., ... & den Dunnen, J. T. (2012). Phage display screening without repetitious selection rounds. *Analytical biochemistry*, 421(2), 622-631.
14. Olofsson, L., Ankarloo, J., & Nicholls, I. A. (1998). Phage viability in organic media: insights into phage stability. *Journal of Molecular Recognition: An Interdisciplinary Journal*, 11(1-6), 91-93.
15. Fagerlund, A., Myrset, A. H., & Kulseth, M. A. (2008). Construction and characterization of a 9-mer phage display pVIII-library with regulated peptide density. *Applied microbiology and biotechnology*, 80(5), 925-936.
16. Zade, H. M., Keshavarz, R., Shekarabi, H. S. Z., & Bakhshinejad, B. (2017). Biased selection of propagation-related TUPs from phage display peptide libraries. *Amino acids*, 49(8), 1293-1308.
17. Tian, F., Tsao, M. L., & Schultz, P. G. (2004). A phage display system with unnatural amino acids. *Journal of the American Chemical Society*, 126(49), 15962-15963.
18. Day, J. W., Kim, C. H., Smider, V. V., & Schultz, P. G. (2013). Identification of metal ion binding peptides containing unnatural amino acids by phage display. *Bioorganic & medicinal chemistry letters*, 23(9), 2598-2600.
19. Mohan, K., & Weiss, G. A. (2016). Chemically modifying viruses for diverse applications. *ACS chemical biology*, 11(5), 1167-1179.
20. Ng, S., Jafari, M. R., Matochko, W. L., & Derda, R. (2012). Quantitative synthesis of genetically encoded glycopeptide libraries displayed on M13 phage. *ACS chemical biology*, 7(9), 1482-1487.
21. Jafari, M. R., Deng, L., Kitov, P. I., Ng, S., Matochko, W. L., Tjhung, K. F., ... & Derda, R. (2014). Discovery of light-responsive ligands through screening of a light-responsive genetically encoded library. *ACS chemical biology*, 9(2), 443-450.

22. Heinis, C., Rutherford, T., Freund, S., & Winter, G. (2009). Phage-encoded combinatorial chemical libraries based on bicyclic peptides. *Nature chemical biology*, 5(7), 502.
23. Step 3: Clinical Research -Office Commissioner -
<https://www.fda.gov/patients/drug-development-process/step-3-clinical-research>
24. Mariño, G., & Kroemer, G. (2013). Mechanisms of apoptotic phosphatidylserine exposure. *Cell research*, 23(11), 1247-1248.
25. Killee, E., Pokorny, A., Yeaman, M. R., & Bayer, A. S. (2010). Lysyl-phosphatidylglycerol attenuates membrane perturbation rather than surface association of the cationic antimicrobial peptide 6W-RP-1 in a model membrane system: implications for daptomycin resistance. *Antimicrobial agents and chemotherapy*, 54(10), 4476-4479.
26. Gao, R., Hu, Y., Li, Z., Sun, J., Wang, Q., Lin, J., ... & Zhu, B. (2016). Dissemination and mechanism for the MCR-1 colistin resistance. *PLoS pathogens*, 12(11).
27. Zhang, G., Gurtu, V., Kain, S. R., & Yan, G. (1997). Early detection of apoptosis using a fluorescent conjugate of annexin V. *Biotechniques*, 23(3), 525-531.
28. Wang, R., van Dorp, L., Shaw, L. P., Bradley, P., Wang, Q., Wang, X., ... & Dorai-Schneiders, T. (2018). The global distribution and spread of the mobilized colistin resistance gene mcr-1. *Nature communications*, 9(1), 1-9.
29. McCarthy, K. A., Kelly, M. A., Li, K., Cambray, S., Hosseini, A. S., van Opijnen, T., & Gao, J. (2018). Phage display of dynamic covalent binding motifs enables facile development of targeted antibiotics. *Journal of the American Chemical Society*, 140(19), 6137-6145.

Chapter 2

Peptide Probes Identified for Phosphatidylserine Containing Membranes

2.1 Introduction

2.1.1 Phosphatidylserine and its Importance in Lipid Signaling

The cell membrane is a double layer of lipids and proteins that plays a key role in everyday cellular life. One obvious role is its ability to separate the cell from the external environment while also being selectively permeable, only allowing certain molecules and nutrients to enter.¹ However, there is an additional, quite important role the membrane plays, and that is in cell signaling. Cell signaling can happen through a variety of methods and mechanisms but they all generally follow the same specific steps: (1) synthesis and release of the signaling molecules, (2) transport of the signal to the target cell, (3) binding of the signal to the target cell and activation, and (4) initiation of signal transduction pathways.² One pathway in particular that we in the Gao lab are interested in exploring is the apoptotic pathway.

Apoptosis is one mechanism for programmed cell death, with a number of characteristic features that occur, namely blebbing, cell shrinkage, and PS externalization, among other changes that occur internal to the cell.³ PS is an abundant anionic lipid that is a key signaling molecule in apoptosis.⁴ Live mammalian cells actively maintain an asymmetric distribution of PS, restricting it to the cytosolic leaflet of the plasma membrane; however, upon apoptosis, PS is flipped to the outer leaflet where it then composes between 10%-15% of phospholipids present on the cell surface (**Figure 2-1**).⁵ Many cancer treatments work by initiating apoptosis in tumor cells and thus the exposure and detection of PS could be a useful tool in assessment of treatment efficacy.

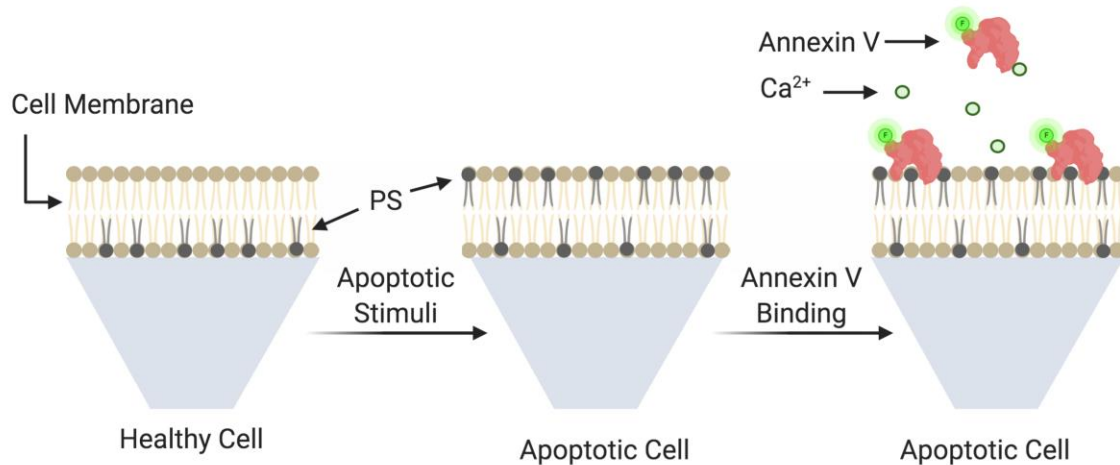


Figure 2-1 A healthy cell undergoing apoptosis, demonstrating the transition of PS from the inner membrane to the outer membrane.

2.1.2 PS Probes

Currently the most widely used assessment of cancer treatment efficacy is to take before and after images of a tumor and monitor any shrinking that may occur.⁷ This process could take weeks before any difference in size is substantial enough to be imaged and by that point, valuable time has been lost. A more direct indication of efficacy of anticancer drugs would be the direct detection of exposed PS at the site of a tumor. There is a limited number of PS binding ligands but perhaps the gold standard in the field is the use of annexin V.⁸ This 36 kDa protein has been used both *in vitro* and in living organisms by attaching fluorophores or radioactive nuclides for imaging cell death in animals and humans.⁹ However, there are serious drawbacks to the use of annexin V, namely its high molecular weight and reliance on calcium to bind.¹⁰ High costs of production and the potential for protein degradation have lead us and others to look for suitable alternatives to annexin V as an indicator of apoptosis.

Previously, our lab had used a rational design approach of modeling short cyclic peptides after lactadherin. Lactadherin is 47 kDa protein whose key function is to mediate phagocytosis of apoptotic cells by recognition of surface exposed PS.¹¹ The docking pocket of the protein was assessed for key residues that interact with PS and a short cyclic peptide (cLac-2) was modeled based on that pocket. cLac-2 was shown to be an effective at binding to surface exposed PS with an apparent dissociation constant of $\sim 8\mu\text{M}$ and confirmed to target only apoptotic cells in a similar manner to annexin V, but without the need for calcium ligands.^{12,13} With the success of this rationally designed approach, we then sought to discover new peptides that could bind to PS as an apoptotic reporter with greater affinities. We decided to do screening of large peptide libraries in order to further expand the arsenal of PS detecting tools.

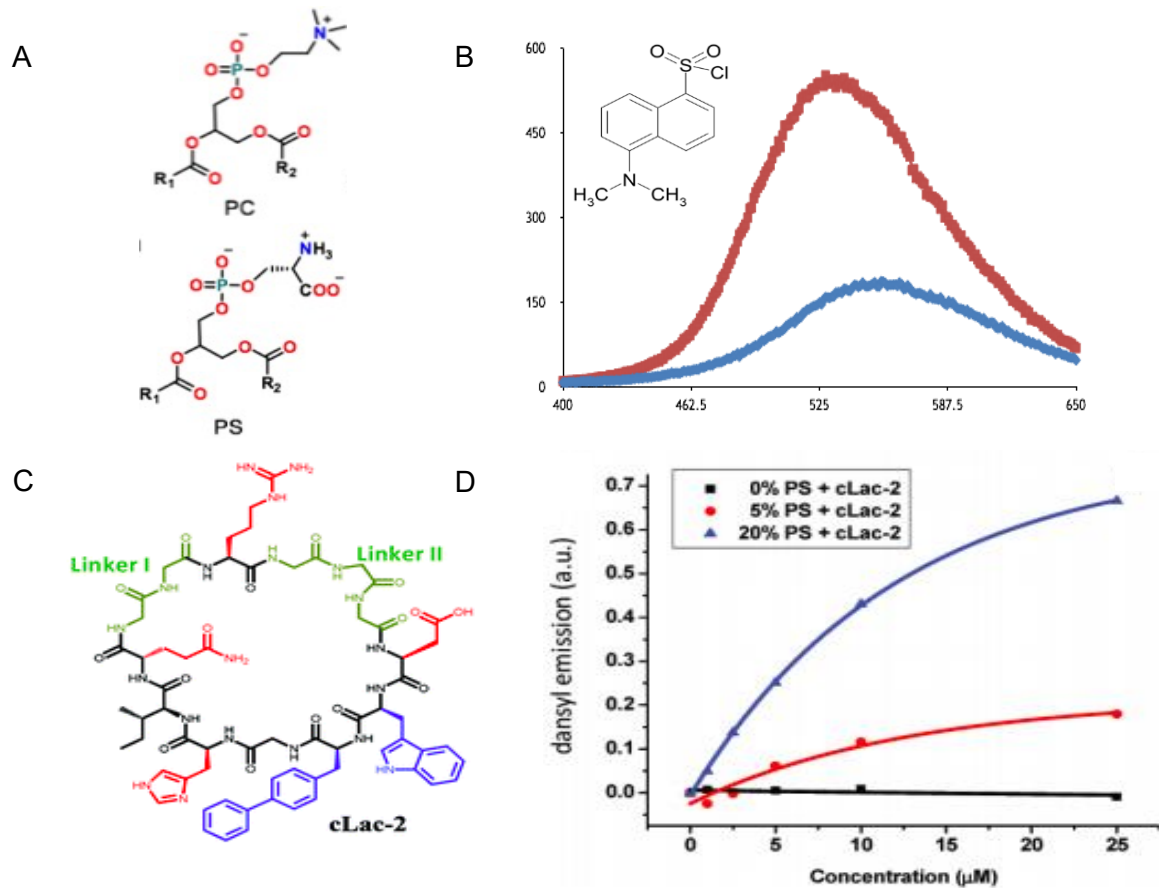


Figure 2-2 PS and previous peptide probes. A) Head groups of phosphatidylcholine (PC) (top) and PS (bottom). B) Demonstration of the increase in fluorescent intensity of dansyl chloride when it interacts with a membrane. C) cLac-2 a cyclic peptide designed to bind to PS containing membranes. D) cLac-2 binding to liposomes with and without PS.

2.1.3 Phage Display for Lipid Binding

Phage display has long been used as a platform for identification of peptides, proteins, and antibodies as ligands to a variety of targets including membranes.¹⁴ Membrane targeting can be a unique challenge due to the fluidity and ever-changing structure to the surface of the cell. With this in mind, it is appropriate to consider your target and choose an appropriate phage library for the selection process. Seeing as how we wanted to identify short stable peptides as ligands to PS, that eliminated large protein

and antibody libraries, which have also been fully characterized and previously screened against PS.^{15,16} However, due to the small nature of a PS lipid molecule in a dynamic shifting environment, we wanted a structurally rigid peptide that would have a reduced entropic cost when binding to a PS containing membrane. For these reasons, we chose the commercially available C7C library, which consists of two cysteine residues flanking 7 randomized amino acids. The cysteines form a disulfide bond creating a cyclic library. This library is expressed at the N-terminal of the PIII protein on M13 phage with five copies of the peptide per phage scaffold. The structural rigidity of this cyclic peptide library was thought to have an advantage over a linear library as it would be already pre- “folded,” whereas the flexible linear peptides would be less likely to bind due to their fluid structure and multiple conformations resulting in a higher entropic cost to binding.

2.2 Screening and Selections

2.2.1 Screening by Liposomes

Screening against lipids was first carried out by whole liposome capture of large unilamellar vesicles (LUVs) in wells. LUV's were deemed to be an ideal mimic to the natural cell surface with minimally exposed lipid tails and with tight packing of lipid head groups. By controlling the amount of phosphatidylcholine (PC) and PS lipids present we could generate a composition similar to the expression of PS in apoptotic cells. Incorporation of 1% biotinylated phosphatidylethanolamine (Biotin-PE) lipids allowed for these liposomes to be captured by streptavidin protein, which had been deposited onto 96 well high binding plates. As a negative selection, LUV's containing 100% PC were used to select against any peptides that might bind to lipid membranes in general and not

specifically to the anionic PS-containing membranes. 60:40 PC:PS LUV's were made for positive selection with decreasing amounts (70:30 PC:PS followed by 80:20 PC:PS) in further selection rounds, in order to increase stringency and hopefully identify peptides with increased potency. In wells 1 μg of streptavidin was deposited to capture biotinylated liposomes and as a positive control, to ensure the liposomes were present and successfully deposited on the surface of these wells, annexin V conjugated to horseradish peroxidase (HRP) was used in an enzyme linked immunosorbent assay (ELISA).

As mentioned previously, the library chosen for screening was the commercially available C7C phage display library. The theoretical diversity of the library is 10^9 different cyclic peptide sequences, and used in these experiments was a total phage count of 10^{11} plaque forming units (pfu). At these numbers, our library should be fully covered with every sequence present 100 times, assuming minimal sequence bias. The cyclic library was diluted in PBS pH 7.4 buffer and incubated first with the PC liposomes captured in wells, followed by positive selection of phage by incubation with PS liposomes. Three rounds of affinity selection were carried out with an input population of $\sim 10^{11}$ (pfu) with extensive washing to eliminate non-binders (**Figure 2-3**). Sequences were isolated after each round for characterization.

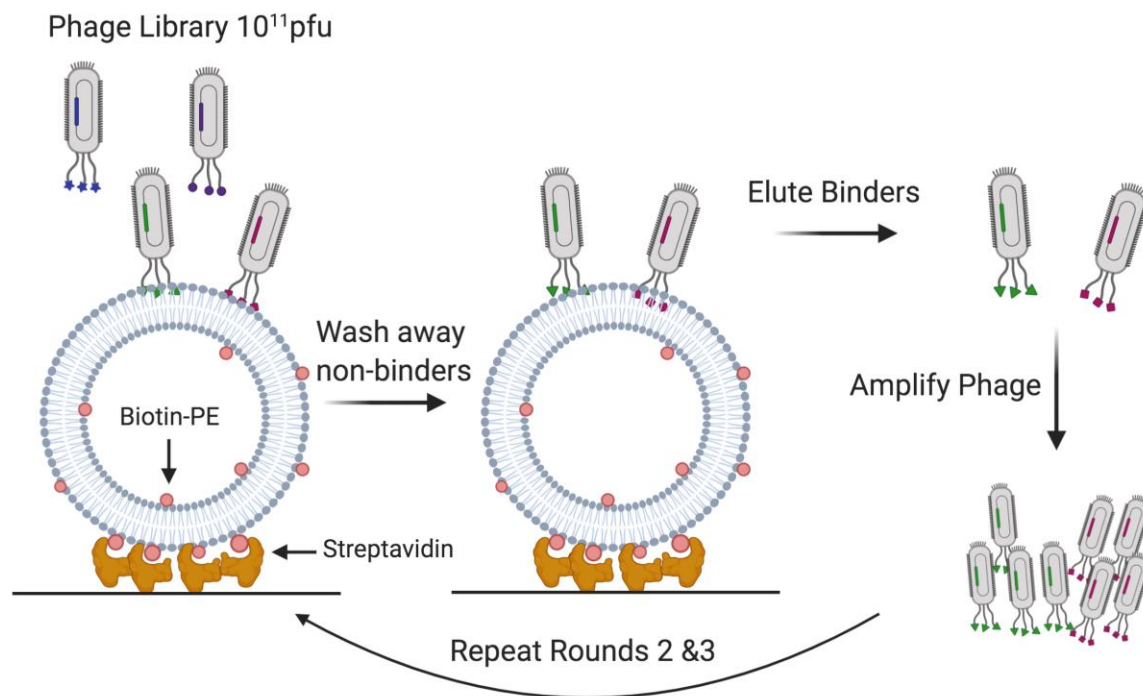


Figure 2-3 Screening of phage display libraries against liposomes captured by physically deposited streptavidin.

2.2.2 Characterization of Phage Outputs from Liposome Screening

Due to the large number of phage hits identified from the screening process, it is ideal to attempt to eliminate false positives by further characterizing phage hits before making peptide sequences. To this end, we sought to do ELISA assays with isolated phage sequences in an attempt to further identify peptide binders. Again, liposomes were deposited into wells and phage were incubated with the target liposomes. Washing away any non-binders followed by incubation with anti-M13 antibody conjugated to HRP, we could see that phage sequences appear to have similar binding to both PC and PS containing liposomes. With no hits showing any real preference for PS containing liposomes (**Figure 2-4B**), an additional experiment was conducted to probe the overall

efficiency of the screening process by looking at the whole phage output population against streptavidin alone, PC liposomes and PS liposomes (**Figure 2-4C**).

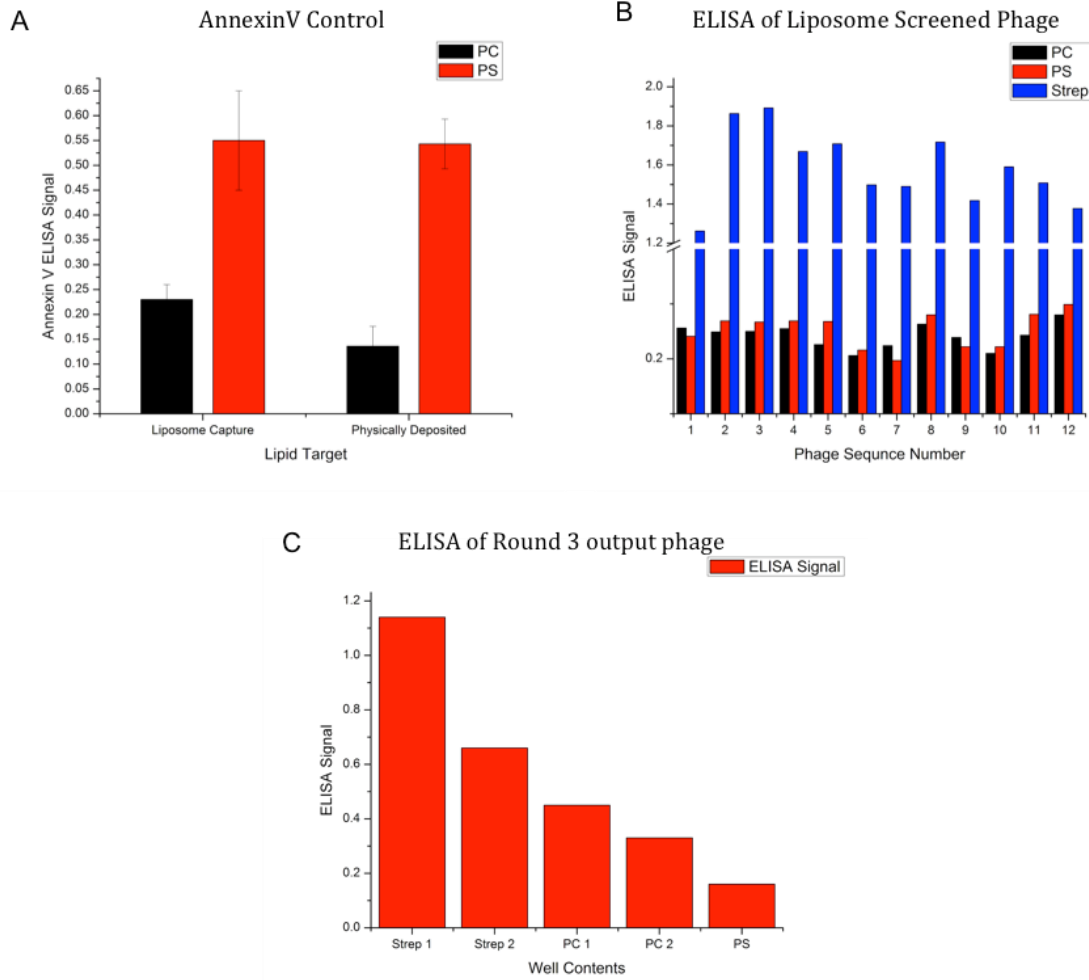


Figure 2-4 Liposome ELISA A) Annexin V positive control to demonstrate deposition of lipids in wells. B) ELISA of selected phage against liposomes. ELISA results indicate phage bind preferentially to streptavidin C) The whole output of round 3 phage was serially incubated with streptavidin, PC, and PS. The ELISA results would indicate isolated phage preferentially bind to streptavidin.

In this assay, we clearly observe a marked binding of phage to streptavidin containing wells with a noticeable drop in binding to wells with PC and PS containing liposomes. This would indicate that the phage identified in this pull down may have been

unknowingly selected for streptavidin and not the PS containing liposomes, despite our best efforts to eliminate this with a negative selection process. With this in mind, we decided to remove streptavidin from the process and only incorporate the lipids of interest into each well. This method has its drawbacks in that lipids may not be perfectly “membrane like” as they would appear on the surface of the cell, however we do not run the risk of selecting for streptavidin as was just seen in the LUV screening process.

2.2.3 Selection of Physically Deposited PS Lipids

Physically deposited lipids do not require the use of streptavidin for binding. However, this technique has drawbacks in that the shape of the lipids deposited cannot be fully characterized as they could be tightly packed, similar to a cell membrane, or less densely packed about the surface of the well in an unorganized manner. The presence of PS can still be characterized by the use of annexin V ELISA assay as done previously, and so screening can be carried out still with a high degree of confidence. Screening was carried out as outlined previously with a negative selection against PC lipids in wells followed by positive selection of PC:PS wells with decreasing concentrations of PS in order to gain more potent binders. Input and output populations were measured before and after each round followed by sequencing of plaques for analysis after all three rounds. A summary of repeating sequences obtained are outlined in **Table 2-1**.

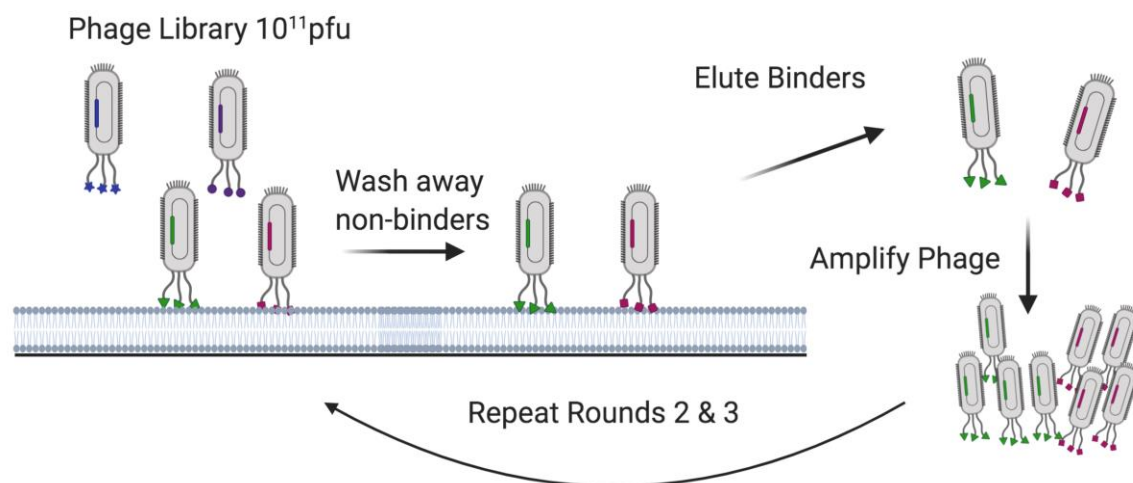


Figure 2-5 Screening of phage against directly deposited lipids.

2.2.4 Characterization of Phage from Physical Deposition of Lipids

With so many sequences identified from several rounds, one method for deciding which peptides to pursue is simply looking at sequences with the highest number of repeats. However, as mentioned previously the process of making peptides is both time and resource consuming, so elimination of false positives as soon as possible is a worthy endeavor. Before making sequences as peptides to test *in vitro*, an analysis of phage was done in order to best decide which peptides to move forward with for testing. In a similar manner phage hits were isolated and assessed for their ability to bind to wells containing PS lipids over those containing PC lipids. Four peptide sequences showed promise with higher ELISA signal for PS over PC wells. In addition to this, peptide sequences were assessed based on their whole residue hydrophobicity scale, estimating each sequence's potential to fold into membranes.¹⁷ A variety of peptides, both hydrophobic and hydrophilic, were chosen as potential hits for further analysis. At the time, it was hypothesized that choosing a wide variety of peptides that might interact at the surface

or also delve into the hydrophobic portion of the membrane might be ideal and increase chances of finding a PS membrane binder.

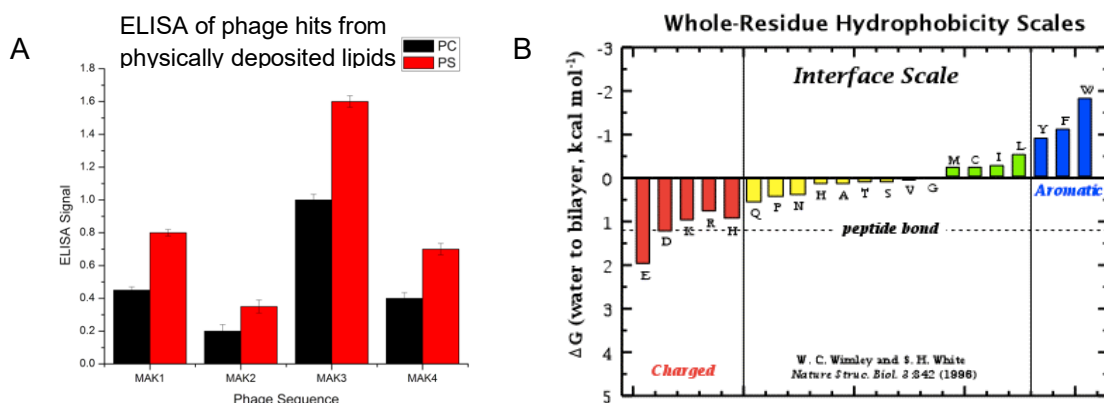


Figure 2-6 ELISA of physically deposited lipids and hydrophobicity scale A) ELISA assay of selected phage sequences from physically deposited lipid screening. B) Whole residue hydrophobicity scale for determination of peptides ability to fold into membranes.¹⁷ The more negative their value, the more likely they are to fold into membranes.

2.3 Peptide Characterization for PS Detection

2.3.1 Dansyl Emission Analysis of Peptides Against Liposomes

Four particular sequences MAK1-MAK4 (**Table 2-1**) all displayed significant binding to PS over PC and produced mixed overall hydrophobicities. With this in mind, we made each peptide by solid phase peptide synthesis (SPPS) on Rink amide resin with an orthogonally protected diaminopropionic acid (Dap) residue on the C-terminus, which allowed for on-resin coupling of dansyl chloride. A single glycine residue was installed between the Dap residue and the rest of the peptide to minimize interference of the dansyl group but such that it was not too far to still be useful for membrane interaction studies. Peptides were purified by reverse phase high-performance liquid chromatography (RP-HPLC) and their identity and purity confirmed by Liquid

chromatography- mass spectrometry (LC-MS) before being lyophilized and prepared as 1mM stocks made in dimethylformamide (DMF).

Table 2-1 Hits isolated from PS targeting phage display; the number of times they appeared after selection and their overall hydrophobicity as calculated from (**Figure 2-6B**) is provided.

Peptide Name	Sequence	Occurrences	Hydrophobicity
MAK1	CSWQIGGNCGDap	3	-1.49
MAK2	CTVRTSADCGDap	2	2.21
MAK3	CTLLPHSCGDap	2	-0.54
MAK4	CLKLGEKWCGDap	3	0.56

These peptides were first assessed for their ability to bind to PS-containing LUV's by a dansyl emission assay, where by a constant concentration of dansyl-labeled peptide in PBS would be measured initially and then increasing concentrations of liposomes would be titrated into the sample. Increases in dansyl emission as seen in **Figure 2-2B**, would be recorded if the peptide is interacting with the membrane in any way. LUVs were titrated with measurements taken at 0 μ M, 5 μ M, 10 μ M, 50 μ M, 100 μ M, 250 μ M, 500 μ M, and 1000 μ M. Minimal to no increase in fluorescence was observed against LUVs and, in fact, a slight decrease was seen at higher concentrations of LUVs that likely occurred due to slight changes in concentration of the peptide caused by dilution with liposomes as well as scattering of the signal from the liposomes.

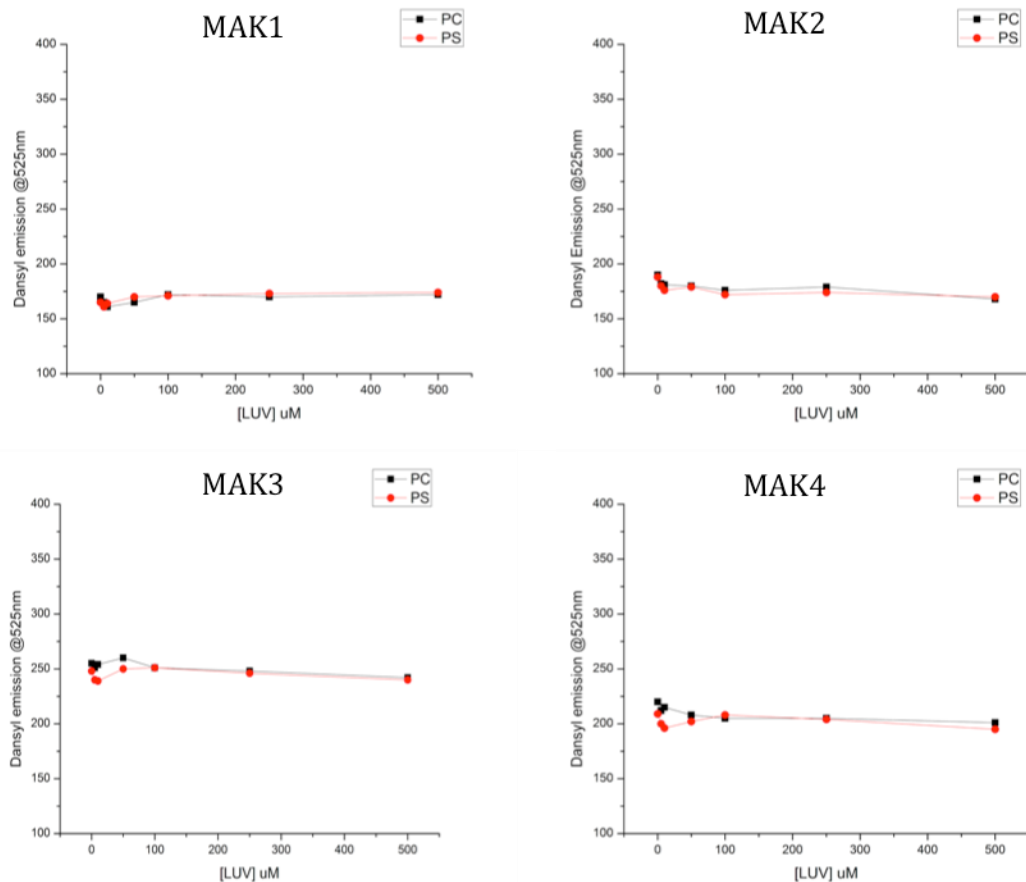


Figure 2-7 MAK1-4 dansyl emission assay against LUVs.

With this in mind, we decided to test these peptides against small unilamellar vesicles (SUVs), as they are not packed as tightly as LUVs. The less densely packed lipids of SUVs leads to slight exposure of the hydrophobic interior of the membranes.¹⁸ Our theory was that the screening process was likely more akin to these SUVs and thus peptides would be more likely to bind. Composition of SUV's were made in 1:1 PC:PS with 100% PC liposomes as a negative control to ensure binding was not to membranes in general. SUVs were titrated in the same concentrations as previously used with 10 μ M of peptides remaining constant. As **Figure 2-8A** indicated, 1 of the 4 peptides (MAK1) showed some partitioning into membranes in general (PC:PS and just PC) while two of the

peptides (MAK3 and MAK4) appeared to be specific for PS containing membranes. MAK3 and MAK4 each demonstrated a significant increase in dansyl emission at concentrations of liposomes as low as 50 μ M. These initial experiments were conducted at 50% PS, which is much higher than concentrations that would be found in cellular membranes (10-15%).

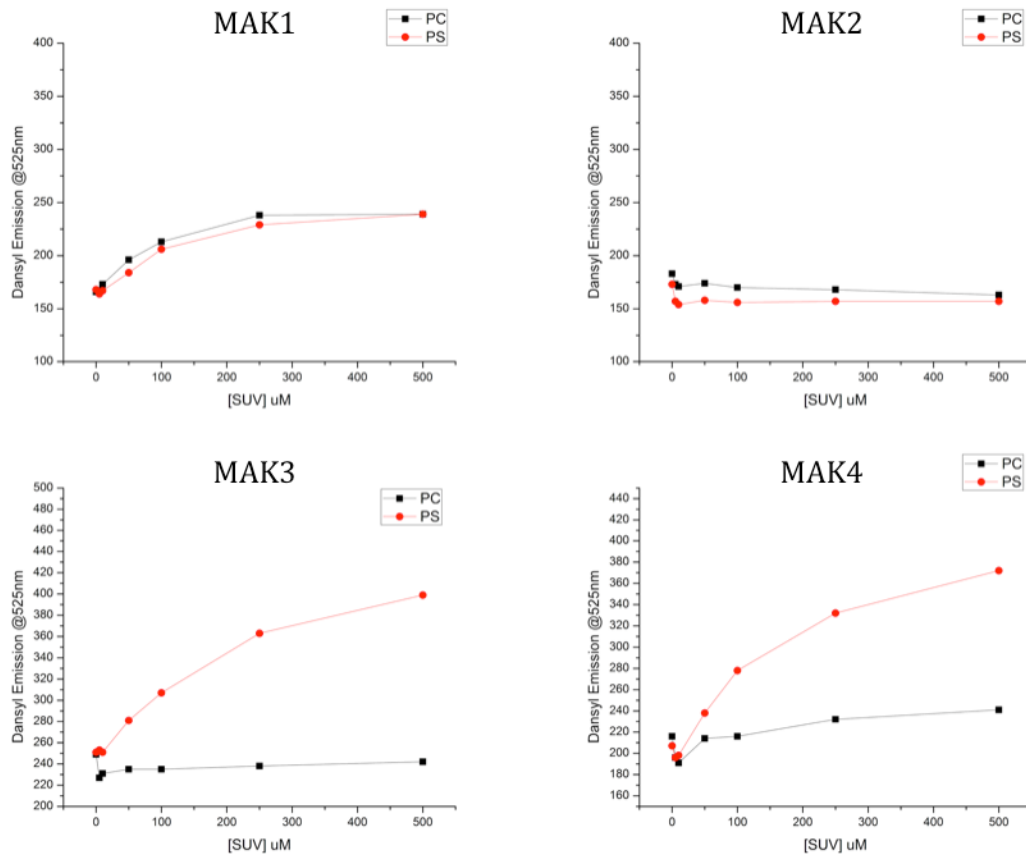


Figure 2-8 MAK1-4 dansyl emission assay against SUVs.

To test whether or not these peptides could bind under conditions more likely to be encountered in membranes, we tested concentrations of PS at 10% composition. It was also hypothesized that for MAK3, the positively charged histidine residues played a role in binding to the anionic lipid head groups of PS. To test this theory, we conducted similar experiments at pH 5 (below the pK_a of histidine) and essentially increased the

positive charges at these residues. As can be seen when dropping the concentration of PS in membranes to physiologically relevant levels, binding of MAK3 is essentially lost; however, the activity is rescued by lowering the pH to 5.

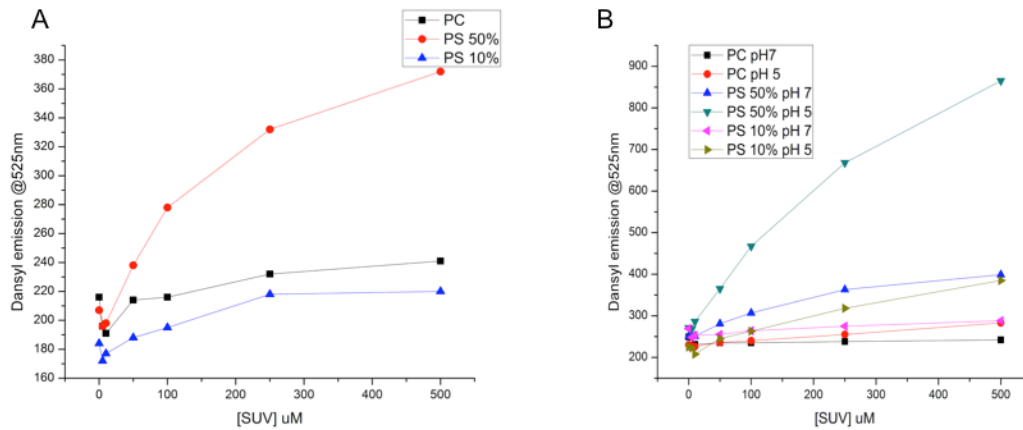


Figure 2-9 Testing MAK3 at physiologically relevant levels of PS (A) and at varying pH (B).

2.3.2 Testing MAK3 Against Apoptotic Cells

Taking MAK3 further, we wanted to see if this peptide could bind to cells undergoing apoptosis. To this end, Jurkat cells were used and incubated with camptothecin (CPT) to induce apoptosis. CPT induces apoptosis through the selective inhibition of the nuclear enzyme DNA topoisomerase, type 1.¹⁹ Peptides were incubated with apoptotic cells for flow cytometry analysis. Fluorescein labeled annexin V was used as a positive control to ensure these cells were indeed undergoing apoptosis. Samples were submitted for flow cytometry analysis with 5-carboxyfluorescein (FAM) as a negative control and annexin V labeled with fluorescein as a positive control. Triggering apoptosis with CPT does not cause an even distribution of apoptotic cells. Indeed, samples treated with CPT will have cells at a variety of stages of apoptosis, depending on

treatment length and concentration of CPT. Therefore, some cells will be in the early or late stages of apoptosis, while other cells will not have started the apoptosis process yet. Due to this wide range in apoptotic states, two populations of cells are typically visible: those undergoing apoptosis and those that have not yet started apoptosis. These two distinct populations are clearly visible by flow cytometry analysis in annexin V treated samples. Apoptotic cells are shifted to the right on the fluorescein isothiocyanate (FITC) channel. However, upon treatment with FAM and MAK3 you can see there is no distinction between these two populations. In fact, both the negative control and MAK3 appear to be shifting to the right, indicating that the peptide perhaps labels the cells regardless of their apoptotic state.

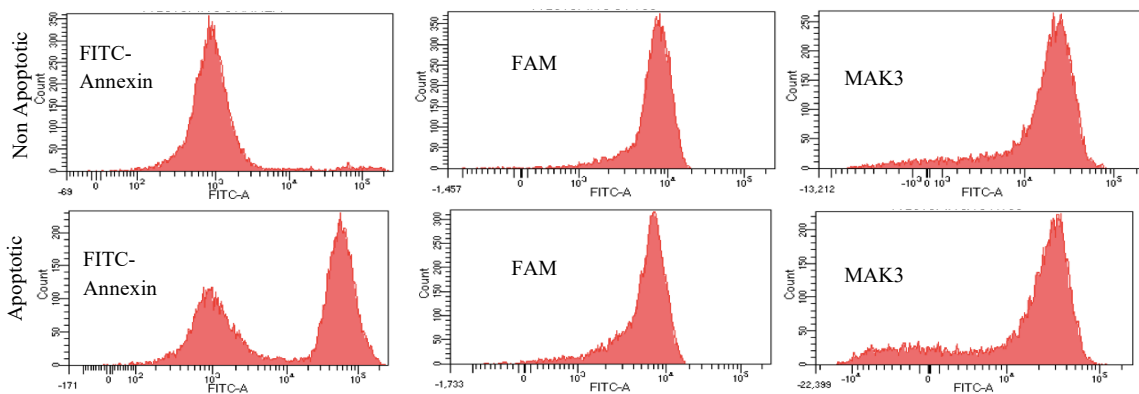


Figure 2-10 FACS analysis of MAK3 with annexin V as a positive control and FAM as a negative control.

2.4 Conclusions and Discussion

The binding of these peptides to SUVs but not LUVs or mammalian cells is perhaps not surprising. The screening conditions under which these peptides were isolated would potentially make the hydrophobic portions of the lipid molecules more accessible. While care was taken to ensure that PS was indeed present in the wells using an annexin V ELISA

assay, it is not clear how structured the physically deposited lipids actually are. This is the draw to screening against liposomes captured by streptavidin, as there is more certainty in the membrane-like properties of the lipid target. However, as was observed under these circumstances, the possibility arises of selecting for phage that bind to streptavidin. In theory, streptavidin binders would have been removed during the negative subtraction with PC liposomes, as streptavidin was present in PC wells as well, but the ELISA results in **Figure 2-4** indicate that is not the case. Lipids physically deposited into wells may not form a uniform membrane like structure as indicated in **Figure 2-11**. In actuality, it could be disordered. So peptides screened under these conditions would have had access to the lipid interiors of the membrane and this could be why the peptides bound to SUVs, where the hydrophobic regions would be more exposed. Whereas in the LUVs and in mammalian cells the lipids are more tightly packed and only the head groups are exposed, thus preventing peptides from binding.

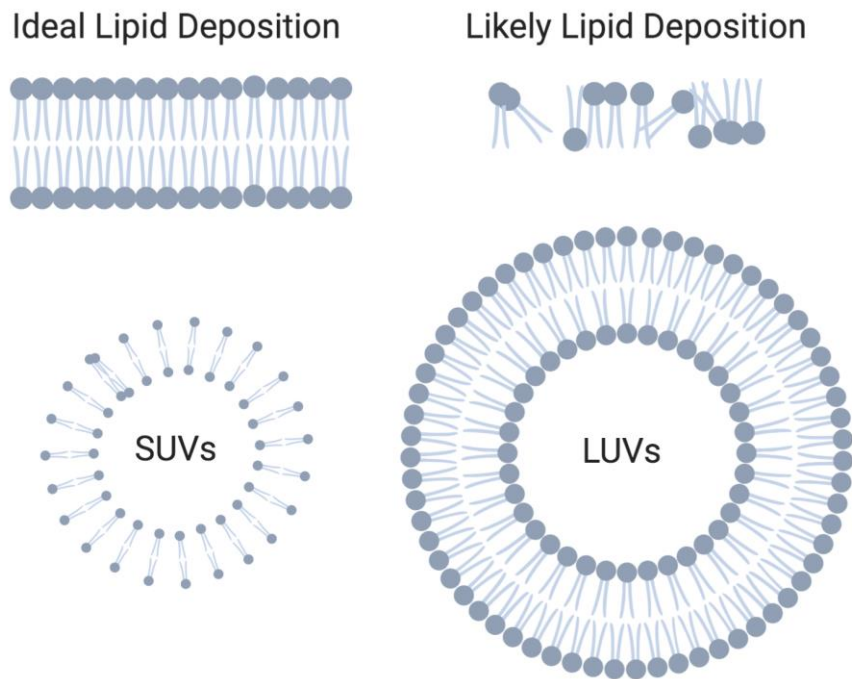


Figure 2-11 Lipid Packing. Ideal lipid deposition would not have any hydrophobic areas exposed. Likely the lipids were not packed tightly during the screening process, exposing the hydrophobic tails. This could be one explanation as to why peptides bound SUVs over LUVs and Jurkat cells which likely contain better lipid packing.

The dansyl assay shows that the anionic nature of the PS head group plays a role and does not solely require the exposed hydrophobic regions of the lipid. Two out of the 4 peptides (MAK3 and MAK4) showed preferential binding to PS containing membranes over membranes containing only PC and MAK3 even showed a meaningful relationship with pH. As pH was lowered to 5, below the pKa of histidine, binding drastically increased. While at first this may seem not relevant due to the body's natural pH laying in a tight range between 7.35-7.45, tumor microenvironments are considerably more acidic between 6.5- 6.9.²⁰ Though this range is still too basic for MAK3 to really be effective in binding to 10% PS lipid compositions, perhaps with some fine-tuning this peptide could

work well in a more neutral range. Structure activity relationships could be beneficial to this peptide. Starting with a simple alanine scan to probe the nature in which MAK3 binds could lead to optimization of hydrophobic and charged residues to yield a potent and specific peptide for PS membranes that are capable of binding to LUVs and mammalian cells. Taking this one step further, it would be interesting to test whether changing the positively charged histidines to lysines or arginines would increase binding at neutral pH. Moreover, switching to glutamate and aspartate perhaps could be used to target cationic lipids.

The peptides overall are quite interesting and could be pursued as general membrane binders. For example, a short 9 amino acid sequence expressed at the end of a protein sequence could be an effective tool for general membrane docking. MAK1 showed binding to membranes regardless of composition. This peptide too could be optimized for the purposes of general membrane targeting, with a cargo of interest.

2.5 Experimental Protocols

2.5.1 Liposomes

Phosphatidylcholine, phosphatidylserine, and biotinylated phosphatidylethanolamine lipids were obtained from Avanti Polar Lipids. Lipids were weighed out in appropriate ratios in a total of 10mg solution and mixed thoroughly in DCM. In samples for liposome capture by streptavidin biotinylated PE was present at 1% by mass of total lipid. DCM was then completely removed under vacuum overnight and lipid samples resuspended in 1mL of PBS buffer pH 7.4. LUVs samples were freeze-thawed five times and then extruded using an Avanti Polar Lipids extruder which allows for the

preparation of large unilamellar vesicles in an efficient manner with 0.1 μm membranes used. A small amount was then used in the Stewart assay to get an accurate measure of lipid concentration. SUVs were prepared in a similar manner except instead of extrusion samples were sonicated 5 seconds on 5 seconds off at 40% amplification until cloudy lipid solutions began to be clear (roughly 5-7 cycles). Samples were again measured for lipid concentration by Stewart assay.

2.5.2 Screening Against Lipids

1 μg of streptavidin in PBS buffer were incubated in high binding wells in a 96 well plate overnight with gentle shaking at 4°C. The next day excess sample was removed and washed once with PBS 0.1% tween (PBST). Following this, liposomes containing 1% biotinylated PE were incubated with wells for 1 hour to allow capture of liposomes to deposited streptavidin. Wells were washed 2 times with PBST to remove excess LUVs and the phage were added to wells at 10^{10} pfu/mL and allowed to incubate with targets for 1 hour. Liposomes containing only PC were used as a negative control to remove any binders that might be nonspecific for membranes in general followed by an incubation in wells with 1:1 PC:PS for positive selection. The phage library was incubated with lipids for 1 hour with gentle shaking at room temperature. Wells were then washed 8 times with PBST to remove any non-binders followed by elution of binders with 100 μL of 0.2 M glycine HCl pH 2.2 for 15 min. Eluted binders were transferred to an Eppendorf tube and neutralized with 25 μL of Tris pH 9.1. Samples were tittered to measure output populations and then amplified in 20mL of ER2738 *E. coli* culture for 4.5 hours. Cells were spun down to separate phage in the supernatant. And then PEG/NaCl was added to

precipitate phage. Phage were spun down at 7000xg for 10 min and then resuspended in 1mL of PBS buffered and then tittered to find out concentration of amplified phage. Amplified phage were then subjected to rounds two and three of panning following the same protocol. At the end of each round plaques were chosen and grown up individually for sequencing to identify the peptide sequence of selected phage. Phage from the sequencing process was set aside and concentrated by PEG precipitation in order to conduct ELISA for further analysis on phage.

Screening against physically deposited lipids was done in a similar manner depositing 1µg of lipid per well incubating overnight with gentle shaking at 4°C. Excess lipid was removed the following day and washed with PBST. As was done for streptavidin captured lipids, a negative selection of PC occurred followed by a positive selection against PC:PS containing wells.

2.5.3 ELISA of Selected Phage

Phage samples from the end of each round of screening were precipitated and resuspended to assess on phage binding. Phage were incubated with PC and PC:PS wells with lipids in the same manner that they were screened for. Phage samples were incubated in 96 well plates for 1 hour with gentle rocking at room temperature. Following this, wells were washed with PBST 8 times followed by incubation of Anti M13 antibody conjugated to HRP for 30 min. After antibody incubation, wells were washed an additional three times to remove excess antibody. 100µL of ELISA-TMB were added to each well using a multichannel to ensure TMB was added at the same time for PC and PS wells. Color was allowed to develop for 20-45 min before absorbance measurements on a plate

reader at 600nm. Controls of annexin V conjugated to HRP were used throughout the process to confirm the presence of PS containing wells and to show what a positive signal might look like.

2.5.4 Peptide Synthesis

SPPS was carried out on Rink Amide MBHA resin with Fmoc/Tbu chemistry on a 0.05 mmol scale. Five equivalents of commercially available amino acids and 4.9 equivalents of HBTU were used for each coupling reaction. An Alloc-protected Dap residue was installed at the C-terminus for on-resin coupling of the 5(6)-FAM/Dansyl Chloride fluorophores, followed by a single glycine linker and the peptide hit sequence at the N-terminus. 5(6)-FAM or Dansyl group were conjugated to the peptide on resin after removal of the Alloc protecting group with palladium tetrakis and phenylsilane in DCM, followed by HBTU- mediated amide bond coupling of the fluorophore in 0.4M NMM in DMF. The peptides were cleaved off resin and globally deprotected with 95% TFA, 2.5% water and 2.5% TIS. Crude peptides were obtained by ether precipitation and purified by RP-HPLC. All peptides were confirmed by LC-MS analysis.

2.5.5 Peptide Characterization by Dansyl Emission

Stock concentrations of Dansyl-labeled peptides were measured by recording the UV-Vis absorbance at 312 nm ($\epsilon = 3900 \text{ M}^{-1} \text{ cm}^{-1}$). Fluorescence monitoring experiments were carried out on a Cary Eclipse Spectrophotometer (Agilent Technologies) with a 10 mm path length quartz cuvette. The dansyl-labeled cyclic peptides were dissolved in DMF to give a 1 mM stock, which was diluted (with 50 mM Tris buffer, pH 7.4) to a 10 μM peptide concentration for the vesicle binding measurements. The samples were excited

at 312 nm and their emissions were monitored over a range from 400nm to 600nm. Membrane binding was assessed by adding increasing amounts of concentrated vesicles into a fixed peptide sample so as not to dilute the sample by too much in regards to peptide concentration. Max emission values at 525nm were plotted against liposome concentrations to generate the binding curves.

2.5.6 Mammalian Cell Culture and Analysis by FACS and Microscopy

Jurkat cells were grown and maintained in RPMI 1640 media with 10% FBS and 1% penicillin/streptomycin at 37 °C, 5% CO₂ and passed for less than 50 generations. The cell viability and density was checked and counted daily by using 0.2 μM trypan blue as a viability testing dye on a haemocytometer. Before staining with peptides or annexin V, the cells were cultured to a density of 1.5–2.0 × 10⁶ cells per ml in a Corning cell culture flask (with vent cap). Apoptosis induction was achieved by adding Camptothecin to a final concentration of 100μM in the media and the cells were left in the incubator for 6 hours. Cells were spun down at 200 x g and then washed once with PBS buffer. 1μM of MAK3 or FAM was added to apoptotic cells and allowed to incubate for 30 min before submission for FACS analysis. The samples were analyzed on a BD FACSAria cell sorter (BD Biosciences). Data analysis was performed with FlowJo (Tree Star, Inc.).

For confocal analysis, 5 μl of cells were placed on a glass slide and a 22 × 22 × 1.5 Fisherbrand microscope cover glass was placed on top. Images were taken on a Leica SP5 confocal fluorescence microscope with filters that allowed detection of AF488 (488 nm excitation, 496–564 nm emission). A × 63 oil objective was used with an Argon laser at 10% laser power. Gain was adjusted to between 900 HV and 1,100 HV with an offset of

-0.5%. The images were captured with the software LAS 2.6 and then processed with Fiji ImageJ.

2.6 References

1. Siontorou, C. G., Nikoleli, G. P., Nikolelis, D. P., & Karapetis, S. K. (2017). Artificial lipid membranes: past, present, and future. *Membranes*, 7(3), 38.
2. Lodish, H., Berk, A., Zipursky, S. L., Matsudaira, P., Baltimore, D., & Darnell, J. (2000). *Molecular cell biology* 4th edition. *National Center for Biotechnology Information, Bookshelf*.
3. Henry, C. M., Hollville, E., & Martin, S. J. (2013). Measuring apoptosis by microscopy and flow cytometry. *Methods*, 61(2), 90-97.
4. Balasubramanian, K., Mirnikjoo, B., & Schroit, A. J. (2007). Regulated externalization of phosphatidylserine at the cell surface implications for apoptosis. *Journal of Biological Chemistry*, 282(25), 18357-18364.
5. Kay, Jason G., and Gregory D. Fairn. "Distribution, dynamics and functional roles of phosphatidylserine within the cell." *Cell Communication and Signaling* 17.1 (2019): 1-8.
6. Phosphatidylserine Externalization in Apoptosis <https://www.novusbio.com/research-topics/apoptosis/phosphatidylserine-externalization>
7. Erridge, S. C., Seppenwoolde, Y., Muller, S. H., van Herk, M., De Jaeger, K., Belderbos, J. S., ... & Lebesque, J. V. (2003). Portal imaging to assess set-up errors, tumor motion and tumor shrinkage during conformal radiotherapy of non-small cell lung cancer. *Radiotherapy and Oncology*, 66(1), 75-85.
8. VaVermes, I., Haanen, C., Steffens-Nakken, H., & Reutellingsperger, C. (1995). A novel assay for apoptosis flow cytometric detection of phosphatidylserine expression on early apoptotic cells using fluorescein labelled annexin V. *Journal of immunological methods*, 184(1), 39-51.

9. de Wiele, C., Vanderheyden, J. L., Cuvelier, C. A., Slegers, G., & Dierck, R. A. (2003). Quantitative Tumor Apoptosis Imaging Using Technetium-99m-HYNIC Annexin V Single Photon Emission. *Journal of clinical oncology*, *21*(18), 3483-3487.
10. Lu, Y., Bazzi, M. D., & Nelsestuen, G. L. (1995). Kinetics of annexin VI, calcium, and phospholipid association and dissociation. *Biochemistry*, *34*(34), 10777-10785.
11. Shi, J., Heegaard, C. W., Rasmussen, J. T., & Gilbert, G. E. (2004). Lactadherin binds selectively to membranes containing phosphatidyl-L-serine and increased curvature. *Biochimica et Biophysica Acta (BBA)-Biomembranes*, *1667*(1), 82-90.
12. Hosseini, A. S., Zheng, H., & Gao, J. (2014). Understanding lipid recognition by protein-mimicking cyclic peptides. *Tetrahedron*, *70*(42), 7632-7638.
13. Zheng, H., Wang, F., Wang, Q., & Gao, J. (2011). Cofactor-free detection of phosphatidylserine with cyclic peptides mimicking lactadherin. *Journal of the American Chemical Society*, *133*(39), 15280-15283.
14. Willats, W. G. (2002). Phage display: practicalities and prospects. *Plant molecular biology*, *50*(6), 837-854.
15. Pregolato, F., Chighizola, C. B., Encabo, S., Shums, Z., Norman, G. L., Tripodi, A., ... & Meroni, P. L. (2013). Anti-phosphatidylserine/prothrombin antibodies: an additional diagnostic marker for APS?. *Immunologic research*, *56*(2-3), 432-438.
16. Caberoy, N. B., Zhou, Y., Alvarado, G., Fan, X., & Li, W. (2009). Efficient identification of phosphatidylserine-binding proteins by ORF phage display. *Biochemical and biophysical research communications*, *386*(1), 197-201.
17. Wimley, W. C., & White, S. H. (1996). Experimentally determined hydrophobicity scale for proteins at membrane interfaces. *Nature structural biology*, *3*(10), 842-848.
18. Nordlund, J. R., Schmidt, C. F., Dicken, S. N., & Thompson, T. E. (1981). Transbilayer distribution of phosphatidylethanolamine in large and small unilamellar vesicles. *Biochemistry*, *20*(11), 3237-3241.

19. Liu, L. F., Desai, S. D., LI, T. K., Mao, Y., Sun, M. E. I., & SIM, S. P. (2000). Mechanism of action of camptothecin. *Annals of the New York Academy of Sciences*, 922(1), 1-10.
20. Estrella, V., Chen, T., Lloyd, M., Wojtkowiak, J., Cornell, H. H., Ibrahim-Hashim, A., ... & Johnson, J. (2013). Acidity generated by the tumor microenvironment drives local invasion. *Cancer research*, 73(5), 1524-1535.

Chapter 3

Targeting Lys-PG for Bacterial Recognition with an APBA-Modified Library

3.1 Introduction

3.1.1 Lysyl Phosphatidylglycerol (Lys-PG) and its Role in Bacteria

Bacterial resistance to current antibiotics poses a serious threat to our society, calling for facile diagnosis of infection as well as prudent use of antibiotics. Membrane lipids that are unique to pathogenic bacteria may serve as reliable targets toward diagnosis of infection.¹⁸

One signature lipid in particular, is Lys-PG (**Figure 3-1**) a lysine modified phosphatidylglycerol overexpressed by the prevalent human pathogen *Staphylococcus aureus*.¹⁹ This cationic lipid greatly reduces the electronegative potential of the cell membrane, which enables the bacteria to evade cationic host defense peptides and neutrophils.²⁰ Being able to target and identify bacterial species containing Lys-PG could have great potential in diagnostic tools as well as treatment of bacterial infections. However, due to the lipids relatively small size and its head group being similar to a wide range of amines present in biological milieu, developing probes specific to this lipid poses a unique challenge. For a target as unique as Lys-PG lipids, unique and unconventional targeting strategies are required.

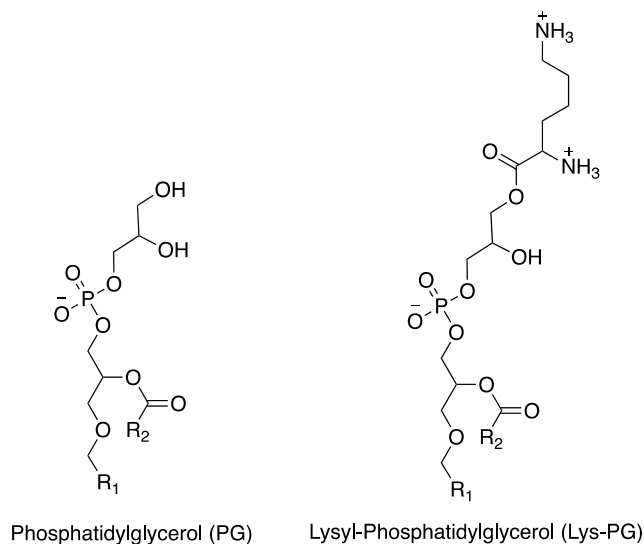


Figure 3-1 Illustration of PG (left) and Lys-PG (right).

3.1.2 Phage Display Modification Strategies

Phage display has proven to be a powerful high-throughput screening system which has been utilized in numerous applications.¹⁻³ A major drawback of phage display is the reliance on the canonical set of 20 proteinogenic amino acids, which often fail to yield peptide hits with desirable potency and selectivity for challenging targets such as membrane lipids and carbohydrates. Recently, several strategies have been attempted to allow for the incorporation of unnatural moieties into phage libraries. For example, the pioneering work by Schultz and coworkers has shown the feasibility of incorporating unnatural amino acids into phage libraries using the amber codon suppression technology.^{4,5} However, this strategy has not yet seen wide applications due to the less optimal efficiency of unnatural amino acid incorporation. To circumvent phage displays limitations, designer functionalities can be introduced via chemo selective modification of the phage-displayed peptide.^{6,7} For instance, chemo selective oxidation of an N-terminal serine yields an aldehyde, which can then serve as a handle to allow the

incorporation of various designer functionalities via oxime formation.^{8,9} Additionally, by taking advantage of the unique reactivity of cysteine, chemical functionalities can be introduced to induce cyclic and bicyclic peptide formation on phage (**Figure 1-3**).^{10,11} These modification strategies have proven to be effective for a wide range of targets, and with the right functionality could be a powerful tool for targeting Lys-PG and ultimately various bacterial species.

3.1.3 Iminoboronate Chemistry

Rarely seen in the interactions of endogenous biomolecules, reversible covalent bond formation is emerging as a powerful strategy in the development of molecular probes or inhibitors for biomolecules of interest.^{12, 13} While reversible covalent warheads have been documented for alcohols and thiols, we and others have recently introduced the iminoboronate chemistry as a way to target molecules with primary amines.^{14, 15} Specifically, 2-formyl and 2-acetyl phenylboronic acids (FPBA and APBA) were found to readily conjugate with primary amines under physiological conditions. In comparison to simple imines, an iminoboronate enjoys much greater thermodynamic stability, the formation of which displays accelerated kinetics as well achieving a K_d of 1-10mM. Strategic utilization of the iminoboronate warheads (e.g., APBA) has given rise to potent molecular probes of bacterial lipids¹⁵ as well as inhibitors of therapeutically relevant proteins.¹⁶ We envision that incorporating reversible covalent warheads into phage libraries may allow facile identification of reversible covalent probes or inhibitors for any target of interest. To test the hypothesis, we have chemically modified a phage library to display a pair of APBA moieties.

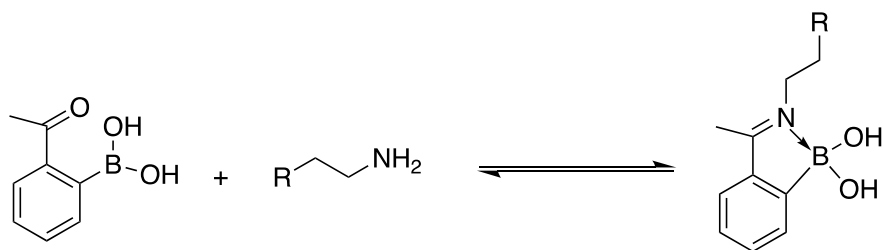


Figure 3-2 Reversible covalent interaction of APBA and free amine to form a stable iminoboronate. $K_d \sim 10\text{mM}$ at pH 7.4

3.2 APBA Dimer Library Construction and Validation of Modifications

A collaboration with Dr. Li was established for synthesis of APBA-IA.

3.2.1 Library Modification

The commercially available C7C library that was used previously for the screening against PS was used for modification. To expand the scope of phage display, several groups¹⁹⁻²¹ including our own²⁴ have been developing *chemically enhanced* phage libraries, which incorporate non-natural functional groups. For the purposes of this study the library was modified with APBA warheads by disulfide reduction and then selective alkylation of cysteines as previously described by Derda and co-workers. In order to selectively reduce cysteines expressed at the N-terminal end of the PIII protein immobilized TCEP (iTCEP) was incubated with the phage for 48 hr at 4°C. Reduced cysteines were then alkylated with an APBA derivative, APBA-IA for 2 hr to yield the APBA dimer library.

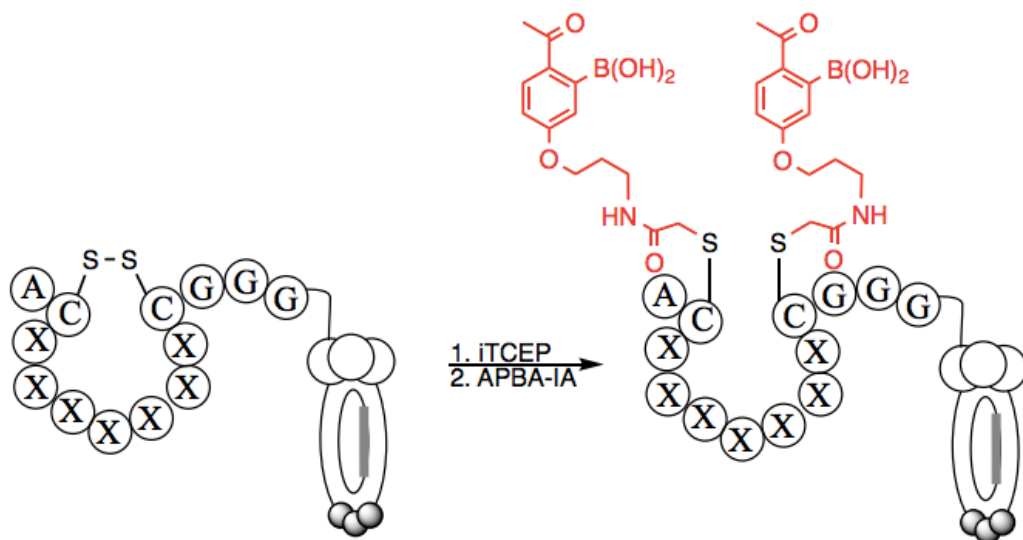


Figure 3-3 C7C phage display library reduction and labeling with APBA functionality.

3.2.2 Confirmation of APBA Modification of Phage

Labeling conditions had been previously worked out by Derda and co-workers, and confirmed in these experiments in a similar manner.⁹⁻¹¹ However, the extent of APBA-IA labeling needed additional step of a pulse-chase in which biotin-iodoacetamide (Biotin-IA) treatment and streptavidin capture after APBA-IA labeling allowed the quantification of phage that was not labeled with APBA-IA. Two separate phage populations were used for labeling studies, the first being C7C phage for labeling and screening, the second was a control phage “blank phage” with no peptide insert. Both phage populations were reduced and labeled under the same conditions however only C7C containing phage showed any labeling in the streptavidin capture assay indicating labeling was specific to N-terminal of the PIII protein. For the pulse chase neither population was labeled with biotin extensively indicating high APBA labeling. More direct evidence of APBA conjugation to phage was established by treating modified phage with a fluorophore

labeled semicarbazide (Scz-FITC), provided by Dr. Anupam Bandyopadhyay and Dr. Samantha Cambray, which is shown to form a stable diazaborine. This chemoselective conjugation allowed for the APBA labeled PIII protein to be fluorescently tagged, heat denatured, and the proteins subjected to fluorescence gel electrophoresis analysis. Reduced phage and biotin labeled phage were included as negative controls to demonstrate that Scz-FITC was specific to APBA labeled phage. For APBA labeled phage, a single distinct band was observed that corresponds to the PIII protein, which is known to run on sodium dodecyl sulfate polyacrylamide gel electrophoresis (SDS-PAGE) with an apparent molecular weight of 60-65 kDa, larger than its actual molecular weight of 43 kDa.

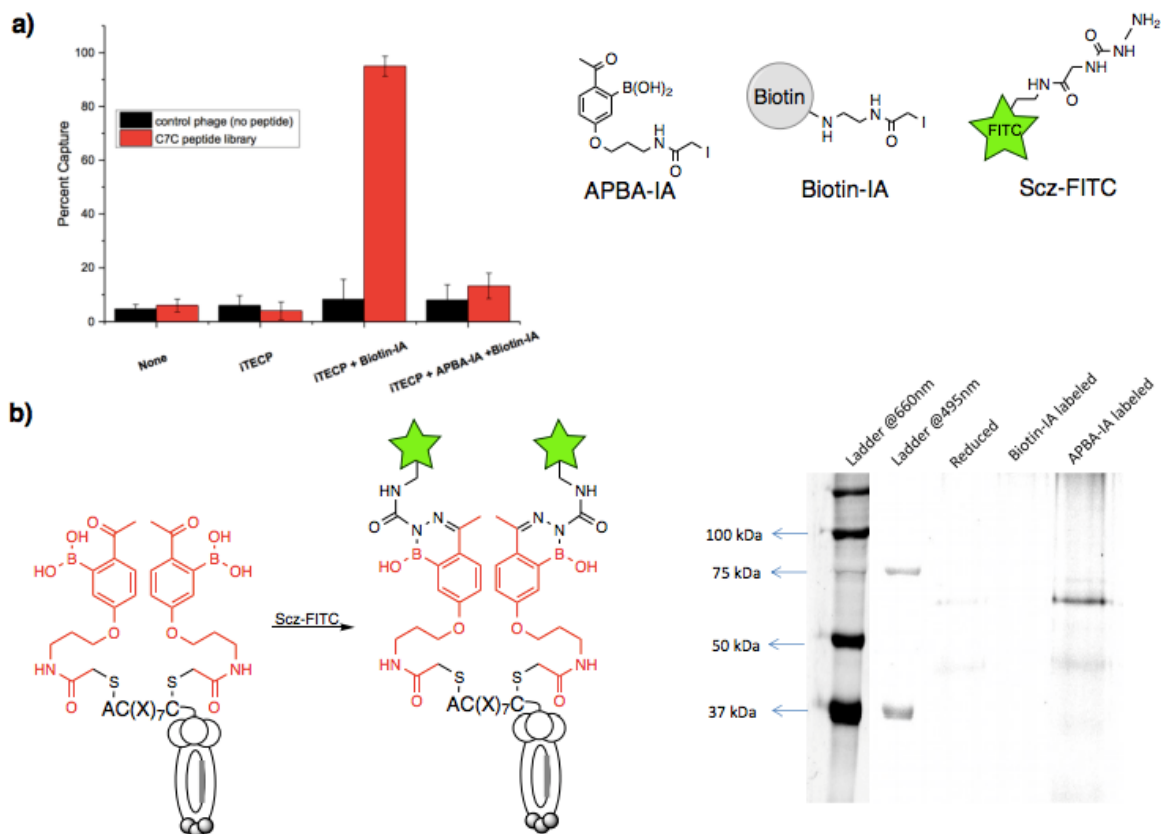


Figure 3-4 Confirmation of phage labeling A) Confirmation of conditions for phage labeling with Biotin. Only capture was seen for C7C containing phage treated with iTECP and Biotin-IA. B) Additional confirmation of APBA labeling with direct labeling of APBA with Scz-FITC and confirmation by fluorescent SDS page gel.

3.3 Targeting Lys-PG

3.3.1 Screening Protocol Against Lys-PG

Due to the limited success of screening against physically deposited lipids in the phosphatidylserine screen, a similar approach was used for targeting Lys-PG. Lipids were deposited into wells and three rounds of affinity selection were initiated with an input population of $\sim 10^{10}$ pfu in each round along with extensive washing steps to eliminate non-binders. After washing the phage were eluted off the target with output populations ranging from 10^4 to 10^6 pfu. Recovered phage were amplified, labeled and subjected to

the next round of panning. A negative selection against wells containing PC:PG lipids was done at the start of the second round to eliminate any nonspecific lipid binders.

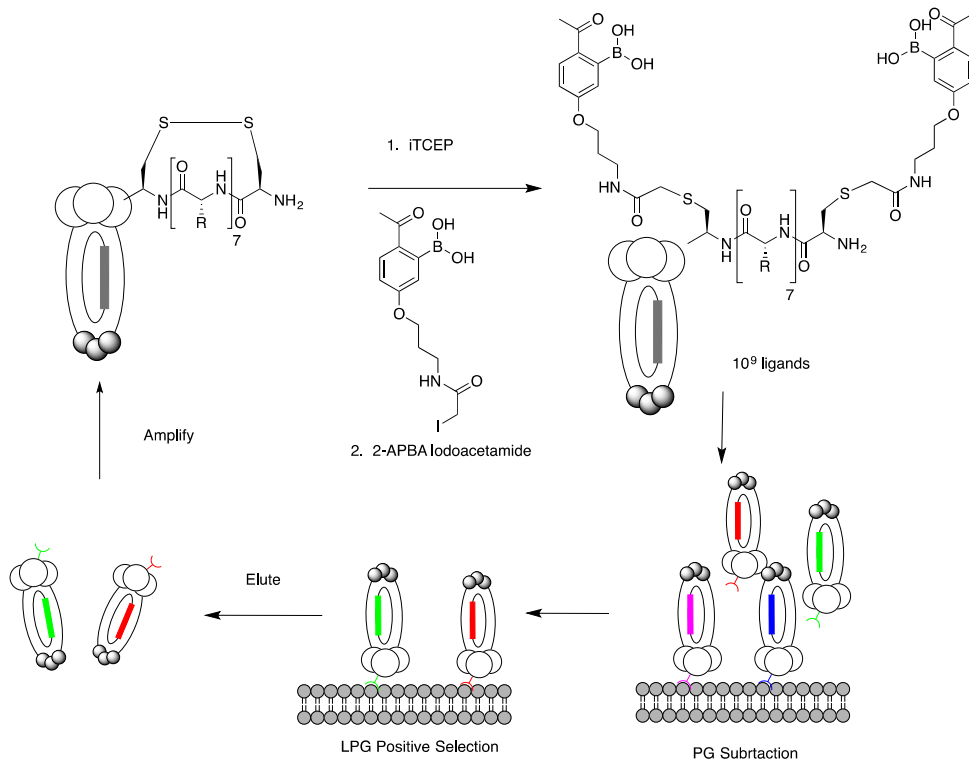


Figure 3-5 Screening process for modified phage display libraries against Lys-PG.

Following the third round of screening 20 plaques were randomly selected from the output population, DNA isolated and subjected to sequencing. Three colonies yielded blank sequences or phage with no C7C insert while four peptide sequences were observed repeatedly (**Table 3-1**).

Table 3-1 List of DNA and peptide sequences identified from Screen against Lys-PG.

Hit #	DNA Sequence	Peptide Sequence
1	GCACGAATGATTATTCTTCGGAGTACAAGC	ACTPKNNHSC
2	GCACGAATGATTATTCTTCGGAGTACAAGC	ACTPKNNHSC
3	GCACGTCATATCCCTATACTTCACACAAGC	ACVKYRDMTC
4	GCACCACGGAGCAACAATATTCTTACAAGC	ACKNIVAPWC
5	GCACCGATTAGACACATTCCGATCACAAGC	ACDRNVSNRC
6	GCACGAATGATTATTCTTCGGAGTACAAGC	ACTPKNNHSC
7	GCAAGTAGCCTCATGCTTAGAACTACAAGC	ACSSKHEATC
8	GCACTCCTTATTAATCATCCAATTACAAGC	ACNWMINKEC
9	GCACCACGGAGCAACAATATTCTTACAAGC	ACKNIVAPWC
10	GCACCGATTAGACACATTCCGATCACAAGC	ACDRNVSNRC
11	GCACGAATGATTATTCTTCGGAGTACAAGC	ACTPKNNHSC
12	GCACCGATTAGACACATTCCGATCACAAGC	ACDRNVSNRC
13	GCACAGATTAGACAGCATATTCAAACAAGC	ACLNMLSNLC
14	GCACGAATGATTATTCTTCGGAGTACAAGC	ACTPKNNHSC
15	GCAAGTAGCCTCATGCTTAGAACTACAAGC	ACSSKHEATC
16	GCACACATGATAACCCCTATCCCAACAAGC	ACWDRGYHVC
17	GCACGAATGATTATTCTTCGGAGTACAAGC	ACTPKNNHSC
18	GCACCACGGAGCAACAATATTCTTACAAGC	ACKNIVAPWC
19	GCAAGTAGCCTCATGCTTAGAACTACAAGC	ACSSKHEATC
20	GCACGAATGATTATTCTTCGGAGTACAAGC	ACTPKNNHSC

These repeating sequences were chosen for further analysis and solid phase peptide synthesis was performed on rink amide resin with an orthogonally protected Dap residue on the C-terminus separated by a triple glycine linker to allow for coupling of

fluorescein as well as an alanine on the N-terminus. After synthesis the peptide was cleaved off resin and free cysteines modified with APBA-IA.

Table 3-2 Peptides hits made for further characterization.

Name	Peptide Synthesized	Frequency
MAK5	AC _m TPKNNHSC _m GGGDap*	7
MAK6	AC _m KNIVAPWC _m GGGDap*	3
MAK7	AC _m DRNVSNRC _m GGGDap*	3
MAK8	AC _m SSKHEATC _m GGGDap*	3

C_m: APBA-IA modified Cys

* Labeled with FAM

3.4 Peptide Characterization

3.4.1 Flow Cytometry Analysis

Given that the ultimate goal of the study is to identify potent markers of bacterial pathogens, we directly assessed the peptide hits for their propensity to label *S. aureus* cells, which are known to express Lys-PG at unusually high concentrations.¹⁹ *S. aureus* cells were treated with the APBA modified peptides and unmodified cyclic peptide of MAK5-8. Fluorescence staining of the peptide-treated cells was first analyzed using flow cytometry (**Figure 3-6**). Plotting the cell median fluorescence intensity against peptide concentration yielded binding curves. Excitingly, three of the four peptide hits (MAK5-7) were found to give low micromolar potency for *S. aureus* cell staining, while MAK8 appears to be a false positive due to its minimal staining at all concentrations tested. Conversely, the corresponding cyclic peptides of MAK5-8 showed no detectable cell binding under the same conditions (**Figure 3-6**), highlighting the critical importance of the APBA moieties in staining the bacterial cells. These results collectively conclude that the

high potency of MAK5-7 originates from the cooperative action of the iminoboronate warheads and the central peptides, which enhance cell binding by forging additional interactions with the membrane.

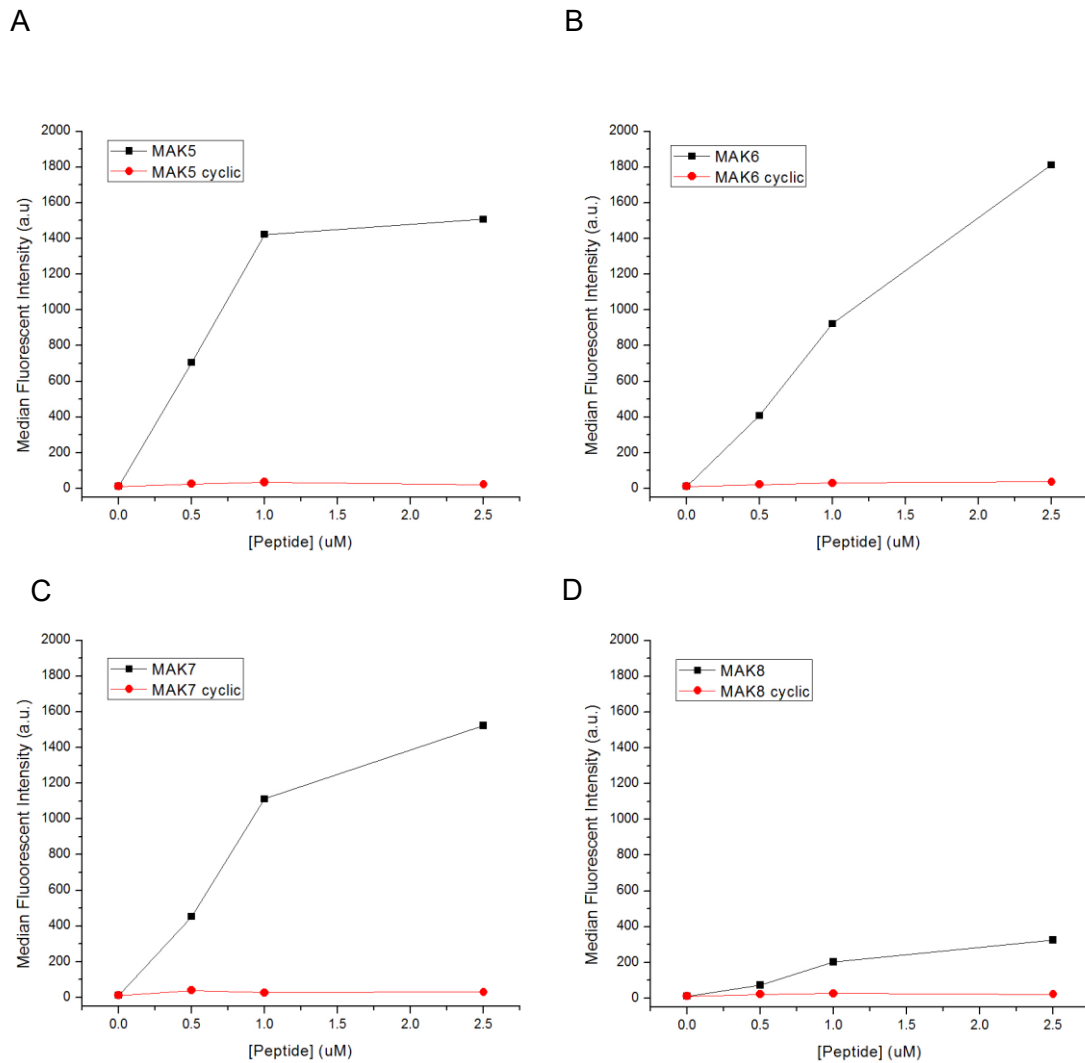


Figure 3-6 APBA modified peptides MAK5-8 and their unmodified C7C cyclic forms. Peptides were incubated with *S. aureus* and median fluorescent intensity measured by FACS.

3.4.2 Microscopy Analysis

Additional validation of the peptide hits was conducted by fluorescence microscopy. MAK7 was found to effectively stain *S. aureus* cells even at 1 μM concentration (**Figure 3-7**). Interestingly, the peptide elicited little staining of either *S. pyogenes* or *B. subtilis* under the same conditions. The observed selectivity is consistent with the fact that *S. aureus* expresses Lys-PG at larger quantities.^{23, 24}

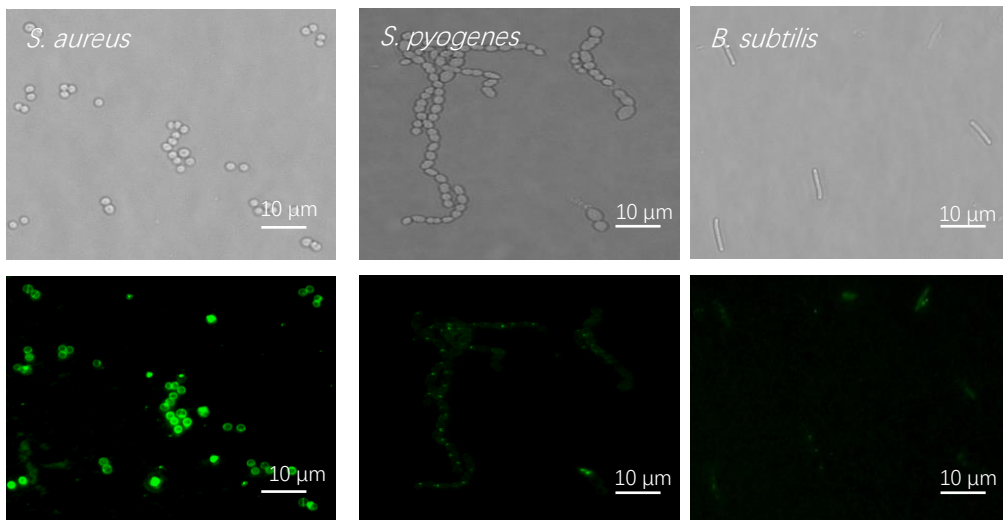


Figure 3-7 *S. aureus*, *S. pyogenes* and *B. subtilis*, incubated with MAK7 peptide at 1 μM and imaged at 100X.

3.4.3 Selectivity Over Mammalian Cells

Two of the peptide hits, MAK6 and MAK7, were studied further for their selectivity for *S. aureus* over mammalian cells. Toward this end, cultures of *S. aureus* and Jurkat cells were incubated with MAK6 and MAK7. Flow cytometry analysis was conducted on both strains as described previously.

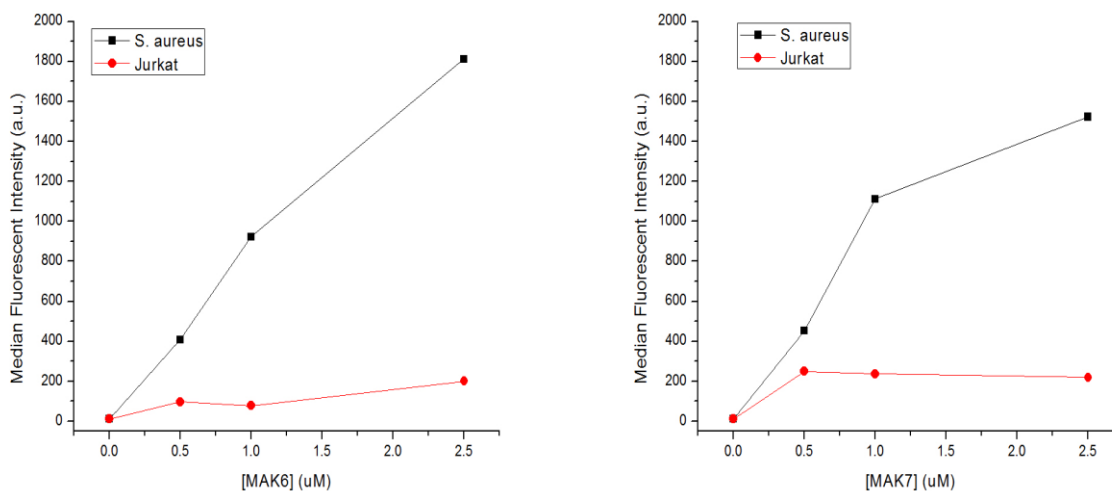


Figure 3-8 Co-culture FACS with peptides MAK6 (left) and MAK7(right) incubated at various concentrations with *S. aureus* and Jurkat cells analyzed by FACS.

The bacterial selectivity was quantitatively assessed via flow cytometry (**Figure 3-8**), which showed that the *S. aureus* cells were stained ten-fold brighter than the Jurkat cells. The *S. aureus* selectivity indicates that the peptide hits may serve as powerful tools for diagnosis of infections caused by this prevalent pathogen. Microscopic analysis of the co-cultures (**Figure 3-9**) showed effective labeling of *S. aureus* by both peptides, while the Jurkat cells displayed no detectable fluorescence, further demonstrating these peptides selectivity for *S. aureus*.

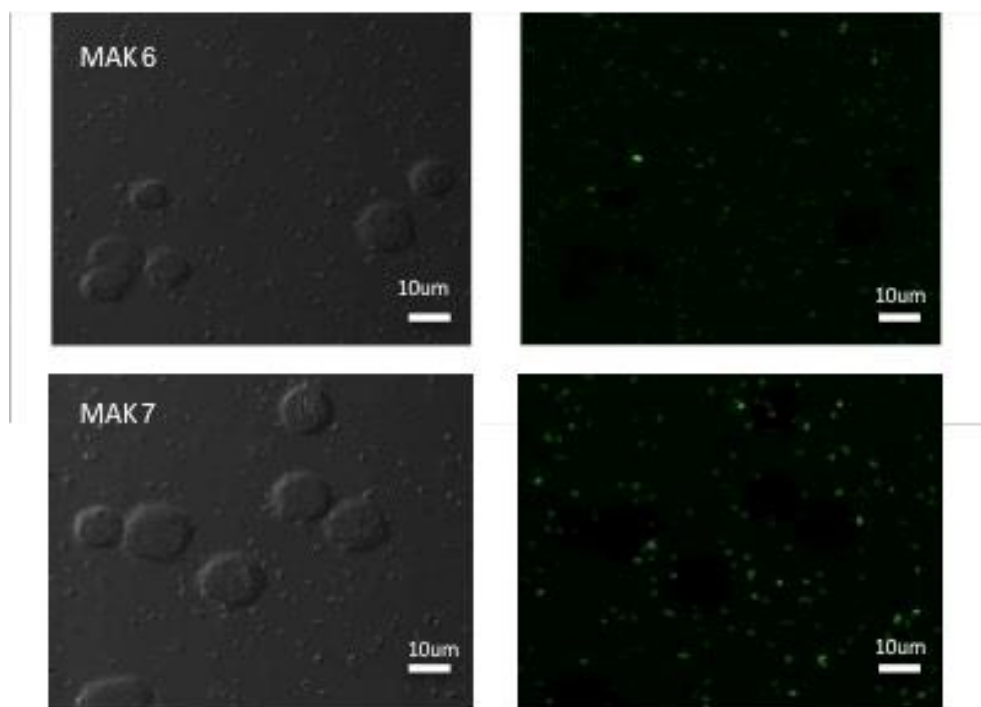


Figure 3-9 Confocal microscopic images of peptide stained co-cultures highlighting the bacterial selectivity of the peptides. Left: phase contrast; Right: FITC fluorescence. Peptide concentration: 1 μ M.

3.4.4 ELISA Characterization of Peptides

The peptide hits were further characterized via ELISA for Lys-PG selectivity. Lipids of desirable compositions were deposited into a high-binding plate and allowed to incubate with the peptides. After quick washing, the amount of bound peptide was assessed by using an anti-fluorescein antibody fused to HRP. Preferential binding of MAK6 and MAK7 to Lys-PG over PG was observed (**Figure 3-10A**). The amount of bound peptide increases with the increase of Lys-PG percentage in the lipid mixture. Consistent with the results of flow cytometry studies shown in (**Figure 3-6D**), MAK8 showed no binding to the lipids regardless of the presence of Lys-PG. Considering that both MAK6 and MAK7 display a net charge of +1, their preferential binding of Lys-PG over the anionic PG highlights the

power of the iminoboronate formation, which overwhelms the unfavorable charge-charge repulsion between the peptides and Lys-PG. A broader investigation of the lipid selectivity of MAK7 was performed by depositing lipid mixtures consisting of PG as a matrix lipid and a guest lipid at 50%. The false positive MAK8 elicited little binding to all lipid mixtures regardless of composition, enabling its use as a negative control. MAK7 affords significantly higher binding for the PG/Lys-PG containing Lys-PG than those with phosphatidylcholine (PC), cholesterol (CHL), or phosphatidylserine (PS) (**Figure 3-10B**). Contrastingly, the PG/PE (phosphatidylethanolamine) mixture elicited comparable peptide binding to that of PG/Lys-PG. The observed affinity of MAK7 to the PG/PE is perhaps not surprising given that the headgroup of PE lipid is known to form iminoboronates with APBA.¹⁵ Additionally, the presence of PE lipid can afford negative curvature membranes, which is known to promote binding of hydrophobic peptides.^{25, 26} However, the potent PE lipid binding of MAK7 appears to contradict the fact that MAK7 minimally stains *B. subtilis* and *S. pyogenes*, both known to have PE lipid in their membranes.

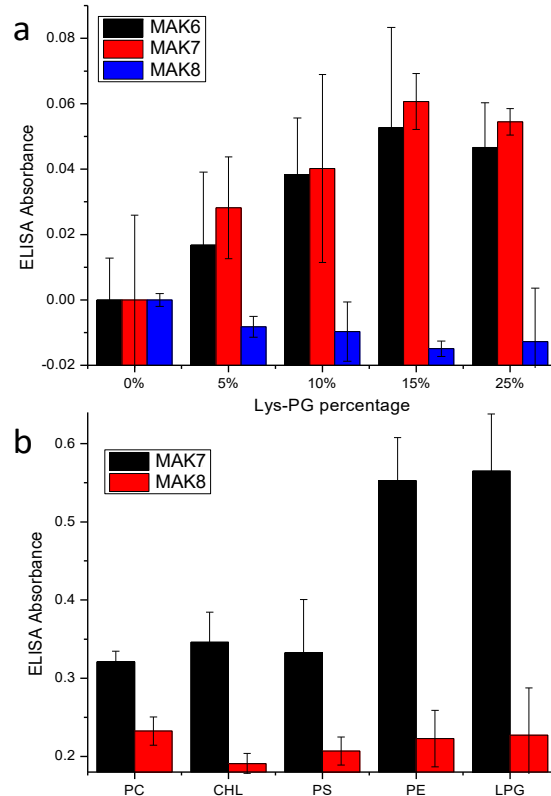


Figure 3-10 Assessing lipid selectivity of the peptide hits identified via phage display. (A) ELISA results showing that the lipid binding of MAK6 and MAK7 depends on Lys-PG concentration. (B) ELISA results demonstrating the lipid selectivity of the MAK7. MAK8, the false positive from phage display, serves as a negative control in both sets of experiments. Peptide concentration: 1 μ M.

3.5 Inhibition by Bovine Serum Albumin (BSA) and Second-Generation Peptides

3.5.1 BSA Inhibition Studies

Robust peptides should be potent and specific under various conditions, especially if they were to be used in diagnosing infections in a clinical setting. To replicate similar conditions to a patient sample, BSA was included and similar FACS experiments were conducted. Using the same concentrations of MAK7 as used previously *S. aureus* was stained with and without 1mg/mL BSA present. MAK7 was shown to lose 90% of its effective cell labeling with 1mg/mL BSA present.

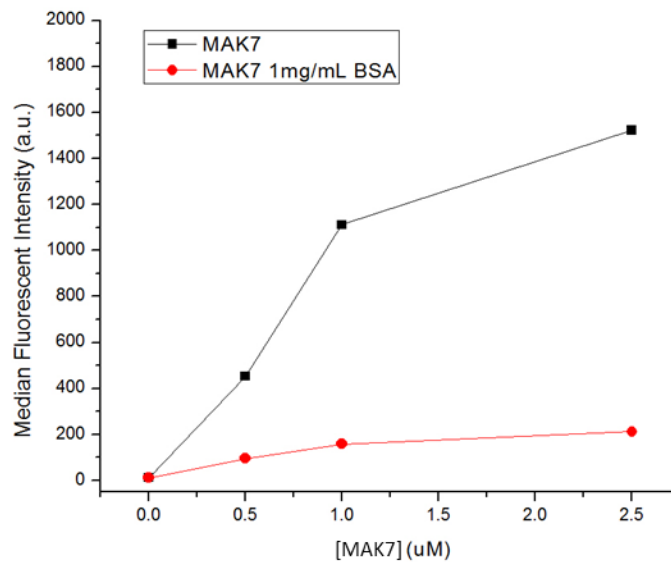


Figure 3-11 MAK7 with and without 1mg/mL BSA incorporated into PBS buffer.

This drop in BSA inhibition is perhaps not surprising due to the high amount of lysine present in BSA which can compete to bind with APBA. This data highlights the flaws in the initial screening approach. No BSA was included during the screening process and thus the peptides identified are not selective over this protein inhibition. A second screen would be appropriate to identify peptides that overcome this BSA inhibition.

3.5.2 Second Generation Peptides via Cell Screening with BSA Present

This section was done in collaboration with Kelly McCarthy.

The APBA modified phage display library was screened directly against *S. aureus* cells with 10mg/mL BSA present in order to identify *S. aureus* specific peptides that can overcome BSA inhibition. Specifically, KAM5 peptide showed strong binding with 1mg/mL

BSA present and that staining actually enhanced with higher concentrations of BSA in microscopy analysis.

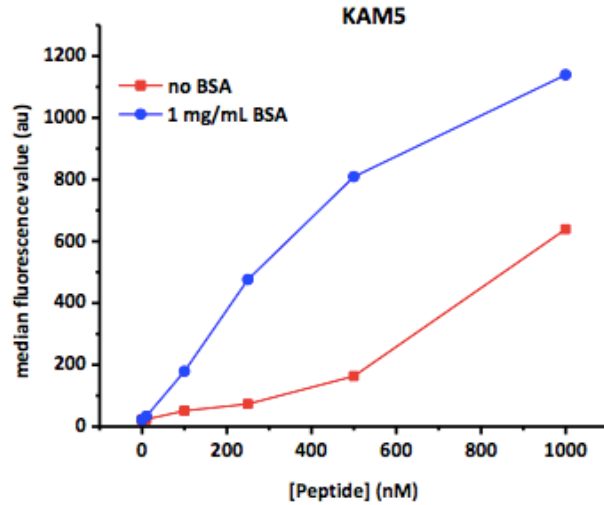


Figure 3-12 KAM5 AC_m VSPRSHEC_m GGGDap* with and without BSA present.

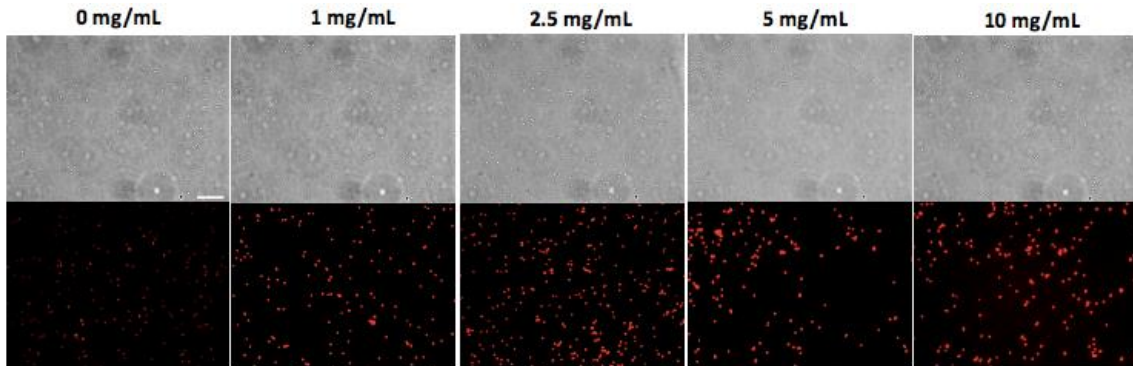


Figure 3-13 Increased binding of KAM5 with increased concentration of BSA present.

3.6 Conclusions and Discussion

Phage display, a powerful screening platform, has been typically limited to peptide libraries of canonical amino acids. Technological advances in genetics and protein engineering have explored the possibilities of phage display with designer functionalities. This contribution describes the first phage library modified with reversible covalent

binding moieties. Specifically, we have introduced a pair of APBA moieties to elicit target binding via reversible formation of iminoboronates. Screening of this library has yielded potent and selective binders of Lys-PG, which is highly abundant in the bacterial pathogen *S. aureus*. Several peptide hits were shown to bind *S. aureus* with low micromolar potency, while bypassing other bacteria as well as mammalian cells. We previously reported a rationally designed peptide probe for Lys-PG and *S. aureus*, which incorporates a APBA moiety to a polycationic peptide.¹⁵ The potency of the identified peptide hits significantly surpass this rationally designed peptide, highlighting the power of the phage display platform reported here. Due to the uniqueness of the APBA functionality great care is needed in designing the screening setup. Overcoming BSA inhibition will be key in the development of future peptides using similar APBA functionalities. In this chapter we demonstrate the power of this reversible covalent phage display library. Further development and implementation of new reversible covalent biomolecules will greatly expand the chemical space that can be covered by phage display.

3.7 Experimental Protocols

3.7.1 Materials and General Methods

The phospholipids were purchased from Avanti Polar Lipids (Alabaster, Al). PBS buffer, RPMI 1640 media and penicillin/streptomycin were purchased from Thermal Scientific. The gram-positive bacteria (*S. aureus* (ATCC 6538)) were purchased from Microbiologics as a lyophilized cell pellet. The Ph.D.-C7C library kit and the ER2738 *E. coli* strain were purchased from New England Biolabs. For sequencing, phage plaques were grown up in *E. coli* (ER2738) and the phage DNA was isolated using Qiagen miniprep kit.

Tetracycline was added to *E.coli* cultures at a final concentration of 20 µg/mL. Peptide synthesis was carried out on a Tribute peptide synthesizer from Protein Technologies. Mass spectrometry data was generated by using an Agilent 6230 LC TOF mass spectrometer. Fluorescence images were taken on a Zeiss Axio Observer A1 inverted microscope. Confocal images were collected on Leica SP5 confocal fluorescence microscope. Flow cytometry analyses were carried out on a BD FACSAria cell sorter housed in the Biology Department of Boston College.

3.7.2 Synthetic Scheme of 2-Acetylphenyl Boronic Acid Moiety: (2-acetyl-5-(3-(2-iodoacetamido)propoxy)phenyl)boronic acid

APBA-IA was provided by Dr. Kaicheng Li.

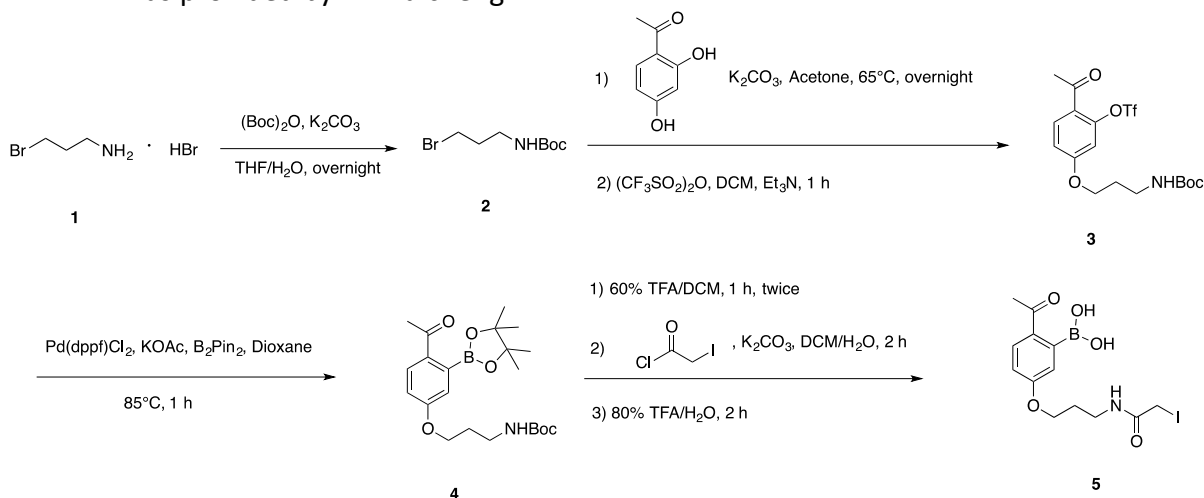


Figure 3-14 Synthetic scheme of APBA.

3.7.3 Synthesis of *Tert*-Butyl (3-bromopropyl)carbamate (**2**)

3-Bromopropylamine hydrobromide (7.00 g, 32.0 mmol) was dissolved in 60 mL 10% Na_2CO_3 solution and placed on ice for 5 min, to which Boc-anhydride (6.50 g, 29.8 mmol in 60 mL tetrahydrofuran) was added. The reaction was kept at room temperature overnight. THF in the reaction mixture was then evaporated. The residual solution was

acidified to pH 3 by 1 N HCl and the product was extracted with ethyl acetate (3× 150 mL). The organic layers were combined and washed with saturated brine (200 mL) and dried over sodium sulfate. Solvent removal yielded a white solid (6.40 g, 90% yield).

¹H NMR (500 MHz, Chloroform-*d*) δ 4.79 (br, 1H), 3.40 (t, *J* = 6.5 Hz, 2H), 3.22 (q, *J* = 6.4 Hz, 2H), 2.01 (m, *J* = 6.6 Hz, 2H), 1.39 (s, 9H).

¹³C NMR (126 MHz, Chloroform-*d*) δ 155.95, 79.29, 38.96, 32.70, 30.74, 28.34.

MS-ESI⁺: calculated for C₄H₉BrNO₂ [M-^tBu+H]⁺ 181.9817, found 181.9795.

3.7.4 Synthesis of 2-acetyl-5-(3-((*tert*-butoxycarbonyl)amino)propoxy)phenyl trifluoromethanesulfonate (3)

2 (3.00 g, 12.6 mmol) and 2,4-Dihydroxyacetophenone (2.13 g, 14.0 mmol) were dissolved in 30 mL of acetone. K₂CO₃ (7.74 g, 56.0 mmol) was added and the reaction was allowed to reflux at 65°C overnight. Acetone was then evaporated and the residue was dissolved in 100 mL water. The product was extracted with ethyl acetate (3× 100 mL). The organic layers were combined and washed with saturated brine (150 mL) and dried over sodium sulfate. Solvent removal yielded an off-white solid (3.78 g). 2.00 g of the crude product was directly dissolved in 40 mL dry dichloromethane. Triethylamine (2.17 g, 21.5 mmol) was added to the solution and the mixture was kept at -78°C for 5 min. Trifluoromethane sulfonic anhydride (3.52 g, 12.4 mmol) was added slowly during 5 min. The reaction was warmed up to room temperature and allowed to stir for 1 h. After that, the reaction was quenched with 40 mL saturated sodium bicarbonate. The mixture was stirred for 5 min and the product was extracted with DCM (3× 100 mL). The combined organic layer was washed with brine (100 mL) and dried over sodium sulfate. The solvent

was removed and the product was purified on a silica gel column using EtOAc/Hexane (1:4) to give the desired product as a light orange solid (2.29 g, 78% yield over two steps).

¹H NMR (600 MHz, Chloroform-*d*) δ 7.82 (d, J = 8.7 Hz, 1H), 6.96 – 6.91 (dd, 1H), 6.80 (d, J = 2.4 Hz, 1H), 4.71 (br, 1H), 4.08 (t, J = 6.1 Hz, 2H), 3.32 (q, J = 6.5 Hz, 2H), 2.58 (s, 3H), 2.01 (m, J = 6.3 Hz, 2H), 1.43 (s, 9H).

¹³C NMR (151 MHz, Chloroform-*d*) δ 197.63, 165.48, 158.64, 151.12, 135.37, 126.74, 121.26, 116.32, 111.97, 82.10, 69.29, 40.18, 32.11, 31.77, 31.00.

MS-ESI⁺: calculated for C₁₃H₁₅F₃NO₇S [M-^tBu+H]⁺ 386.0521, found 386.0494.

3.7.5 Synthesis of *tert*-butyl (3-(4-acetyl-3-(4,4,5,5-tetramethyl-1,3,2-dioxaborolan-2-yl)phenoxy)propyl)carbamate (4)

3 (1.00 g, 2.27 mmol), B₂Pin₂ (1.40 g, 5.51 mmol), Pd(dppf)Cl₂ (0.20 g, 0.27 mmol) and potassium acetate (0.8 g, 8.16 mmol) were dissolved in 20 mL of anhydrous dioxane, to which ~100 mg of 3 Å molecular sieves were added. The reaction was bubbled with argon for 15 min and allowed to stir for 1 h at 85 °C. The reaction was cooled down and 50 mL of water was added to the reaction. The product was extracted with ethyl acetate (3× 100 mL). The combined organic layer was washed with brine (100 mL) and dried over sodium sulfate. The solvent was removed and the product was purified on a silica gel column using EtOAc/Hexane (3:7) to give the desired product as a light-yellow viscous liquid (0.81 g, 85% yield).

¹H NMR (500 MHz, Chloroform-*d*) δ 7.69 (d, J = 8.6 Hz, 1H), 6.88 (d, J = 2.5 Hz, 1H), 6.77 (dd, J = 8.6, 2.6 Hz, 1H), 4.91 (br, 1H), 3.98 (t, J = 6.1 Hz, 2H), 3.21 (q, J = 6.5 Hz, 2H), 2.46 (s, 3H), 1.89 (m, J = 6.9 Hz, 2H), 1.36 (d, J = 1.6 Hz, 21H).

¹³C NMR (126 MHz, Chloroform-*d*) δ 198.26, 162.41, 155.99, 133.47, 130.68, 117.92, 113.83, 83.49, 83.48, 79.03, 65.80, 37.64, 29.39, 28.33, 24.86.

MS-ESI⁺: calculated for C₁₆H₂₃BNO₅ [M-Pin-H₂O+H]⁺ 320.1669, found 320.1857. calculated for C₁₈H₂₇BNO₆ [M-^tBu+H]⁺ 364.1931, found 364.2148.

3.7.6 Synthesis of (2-acetyl-5-(3-(2-iodoacetamido)propoxy)phenyl)boronic acid (5)

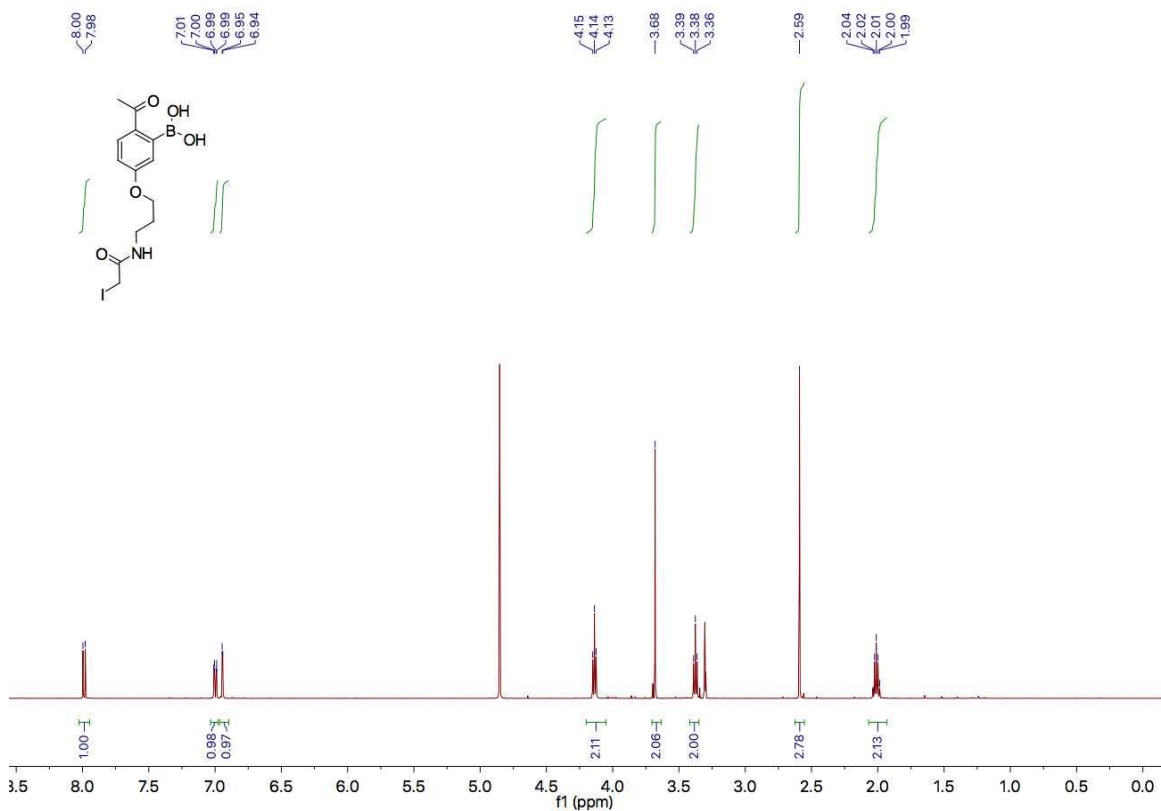
4 (250 mg, 0.60 mmol) was dissolved in 2 mL of DCM, to which was added 3 mL trifluoroacetic acid (TFA). The reaction was stirred at room temperature for 1 h. TFA and DCM were removed and the residue was treated with 60% TFA/DCM (5 mL) for another hour. After solvent removal, K₂CO₃ (500 mg, 2.89 mmol) was added to the residue. The mixture was dissolved in DCM/H₂O (2:1, 6 mL) and kept on ice for 20 min. Iodoacetyl chloride (533 mg, 2.62 mmol) was added slowly during 5 min to the reaction. The mixture was allowed to stir at room temperature for 2 h. The solution was acidified to pH 3 by 1 N HCl and the product was extracted with DCM (3 × 100 mL). The combined organic layer was washed with brine (100 mL) and dried over sodium sulfate. DCM was removed and the residue was treated with TFA/H₂O for 2 h. After solvent removal, the crude material was re-dissolved in 10 mL Acetonitrile/H₂O (2:3) solution and purified on reverse-phase HPLC (Waters Prep LC, Jupiter C18 Column). The product is a white solid after lyophilization (85 mg, 35% yield over three steps).

¹H NMR (500 MHz, Methanol-*d*₄) δ 7.99 (d, *J* = 8.6 Hz, 1H), 7.00 (dd, *J* = 8.6, 2.6 Hz, 1H), 6.94 (d, *J* = 2.5 Hz, 1H), 4.14 (t, *J* = 6.2 Hz, 2H), 3.68 (s, 2H), 3.38 (t, *J* = 6.7 Hz, 2H), 2.59 (s, 3H), 2.01 (m, *J* = 6.5 Hz, 2H).

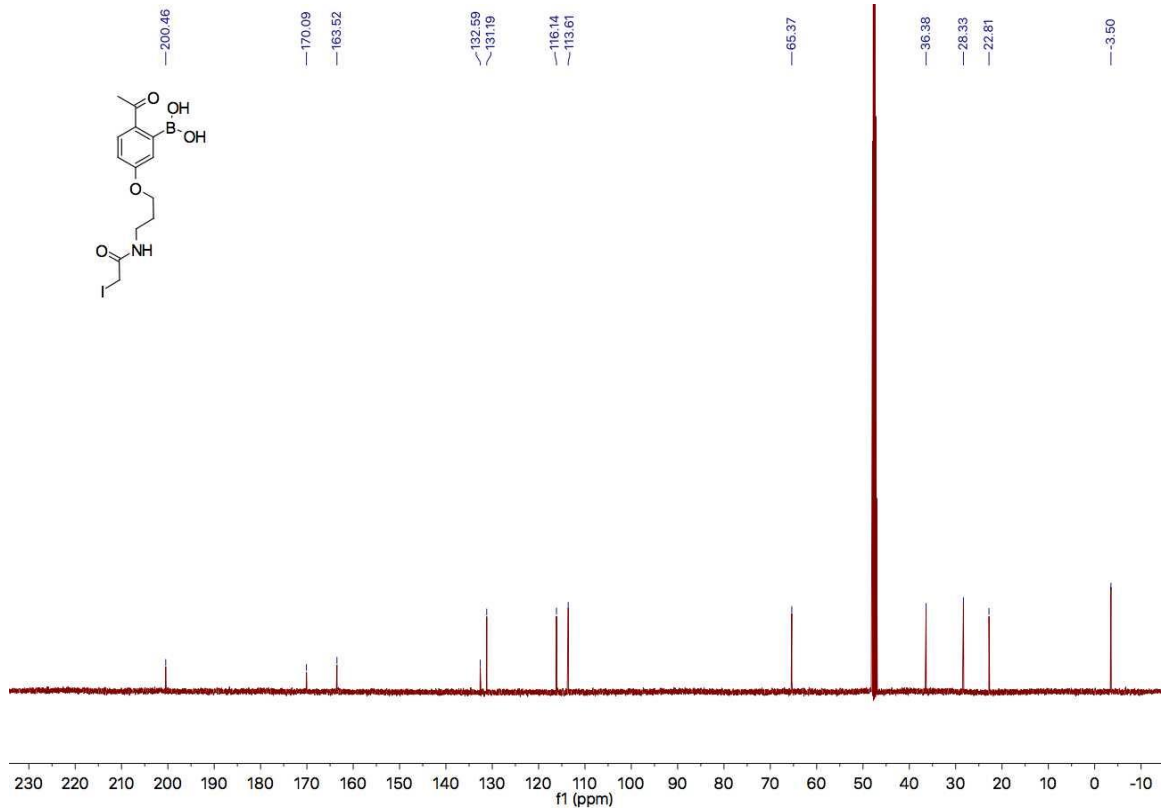
^{13}C NMR (126 MHz, Methanol- d_4) δ 200.46, 170.09, 163.52, 132.59, 131.19, 116.14, 113.61, 65.37, 36.38, 28.33, 22.81, -3.50.

MS-ESI $^+$: calculated for $\text{C}_{13}\text{H}_{16}\text{BINO}_4$ $[\text{M}-\text{H}_2\text{O}+\text{H}]^+$ 388.0217, found 388.0473.

^1H NMR



¹³C NMR



3.7.7 Bacterial Cell Culture and Staining

Bacterial cultures were grown overnight from a single colony in LB broth at 37 °C with agitation. An aliquot was diluted 200 times and allowed to grow for 3 hours until the culture reached mid logarithmic phase ($OD_{600} \sim 0.5$). For a typical labeling experiment, 1.0 mL of bacterial cell culture was spun down at 5,000 R.P.M. in a centrifuge tube (1.5 mL). The cells were washed once with 1.0 mL PBS (50 mM Na·Pi, pH=7.4), and then mixed with 100 μ L solution of peptide in PBS at desired concentrations.

3.7.8 Mammalian Cell Culture and Staining

Jurkat cells were grown and maintained in RPMI 1640 media with 10% FBS and 1% penicillin/streptomycin at 37 °C, 5% CO₂ and passed for less than 50 generations. The cell viability and density was checked and counted daily by using 0.2 μM trypan blue as a viability testing dye on a haemocytometer. Before staining with a peptide, the cells were cultured to a density of 1.5–2.0 × 10⁶ cells per mL in a Corning cell culture flask (with vent cap). Small molecule staining was carried out by a similar protocol as used for the bacterial cells except the speed of centrifugation (Jurkat cells were spun down at 200 r.c.f. (relative centrifugal force)). The co-culture samples were prepared as previously described for both cell lines and then mixed together and allowed to incubate for 30 min before analysis.

3.7.9 Phage Display and Affinity Selection

The phage particles were subjected to iTCEP reduction for 48 hours at 4 °C in PBS (pH 8.5). After 48 hours APBA-IA was added to a final concentration of 2 mM and allowed to react for 2 hours. The iTCEP was spun down and the phage were collected and precipitated to remove excess APBA-IA with PEG/NaCl. The precipitated phage particles were resuspended in 100 μL PBS (pH 7.4) for panning.

Affinity selection was performed by first depositing 1 μg/well of lipid into a 96-well plate. Negative selection was performed against PG, while positive selection wells were composed of 1:1 mixture PG:Lys-PG. Lipid mixtures were dissolved in ethanol and allowed to incubate in wells overnight. Wells were then blocked for 1 hour with a 5 mg/mL BSA solution in PBS buffer (pH 7.4). 10 μL of phage at a concentration 10¹³ pfu/mL was

diluted 10 times to a final concentration of 10^{12} pfu/mL in a total volume of 100 μ L. The phage solution was incubated first in the negative selection well for 1 hour. Then the unbound phage was transferred to the positive selection well for an additional hour. The supernatant was removed and the wells were washed 8 times with PBS containing 0.05% TWEEN 20. 100 μ L of 0.2M Glycine-HCl (pH 2.2) and 1 mg/mL BSA was added to elute off the bound phage and then neutralized with 1M Tris-HCl (pH 9.1). The recovered phage was then amplified for 4.5 hours and subsequently labeled for the next round of panning. A total of three rounds of panning were done, following the third round 20 plaques were grown up in a 5 mL culture containing ER2738 cells overnight. The phage DNA was then minipreped according to Qiagen protocols and subjected to sequencing. The DNA was analyzed to look for repeating sequences. Recurring sequences were selected for peptide synthesis.

3.7.10 Streptavidin Capture Assay

For confirmation of APBA-IA labeling on phage, streptavidin agarose resin (25 μ L/sample) was washed with PBS (pH 7.4) and blocked with 10 mg/mL BSA via incubation for 1 hr. The APBA-IA labeled library was subjected to subsequent labeling with Biotin-IA (2 mM) for 2 hr followed by dilution to minimize small molecule concentration. Biotin-IA labeled and APBA-IA/Biotin-IA labeled phage (200 μ L, $\sim 1 \times 10^{10}$ pfu/mL) were subjected to the streptavidin resin for 1 hr. Non-reduced and reduced phage, without small molecule labeling, were also analyzed. Unbound phage was removed from resin and the phage titer was calculated. The titer was compared to that of phage not subjected to streptavidin to generate a percent capture. The average percent capture and standard

deviation of three trials was plotted. Wild-type phage, with no library insert, was subjected to the same analysis for comparison.

3.7.11 Solid Phase Peptide Synthesis

Peptides were synthesized on 0.05 mmol scale using a Tribute peptide synthesizer from Protein Technologies. Using the Rink Amide resin, all peptides were made with an alloc-protected Dap on the C-terminus followed by a triple glycine spacer, the desired C7C peptide sequence, and an N-terminal alanine as displayed on phage. Dap was selectively deprotected on resin using 60 mg of Pd(PPh₃)₄ with 0.2 ml phenylsilane in DCM over 1 hour. Fluorophore labeling of Dap was accomplished with HBTU activated 5(6)-carboxy fluorescein in presence of 0.4 M NMM in DMF. Peptides underwent a final Fmoc deprotection and cleavage from resin, then purified by RP-HPLC. The purified peptides were allowed to go through air oxidation to give disulfide-cyclized peptides. Alternatively, the purified peptides were reduced with 1 equivalent of TCEP in DMF and then labeled with 2-APBA with 3 equivalents of APBA-IA for 2 hours. The labeled peptides were purified via RP-HPLC. The purity and integrity of the all peptides were confirmed by LC-MS.

Table 3-3 Calculated and observed mass of the disulfide-cyclized peptides.

Name	Sequence	Calculated Mass	Experimental Mass
MAK5	ACTPKNNHSCGGDap	1689.63 [M] ⁺	1689.61[M] ⁺
MAK6	ACKNIVAPWCGGDap	1719.70 [M] ⁺	1719.69 [M] ⁺
MAK7	ACDRNVSNRCCGGDap	1752.67 [M] ⁺	1752.65 [M] ⁺
MAK8	ACSSKHEATCGGDap	826.31 [M + 2H] ²⁺	825.80 [M + 2H] ²⁺

Table 3-4 Calculated and observed mass of the 2-APBA labeled peptides.

Name	Sequence	Calculated Mass	Experimental Mass
MAK5	AC*TPKNNHSC*GGGDap	1121.91[M+2H] ²⁺	1121.91 [M+2H] ²⁺
MAK6	AC*KNIVAPWC*GGGDap	1128.45 [M + 2H] ²⁺	1128.46 [M + 2H] ²⁺
MAK7	AC*DRNVSNRC*GGGDap	1144.45 [M – H ₂ O+2H] ²⁺	1144.93 [M – H ₂ O+2H] ²⁺
MAK8	AC*SSKHEATC*GGGDap	1094.40 [M – H ₂ O+2H] ²⁺	1093.90 [M – H ₂ O+2H] ²⁺

C* indicates cysteines modified with 2APBA-IA moieties.

3.7.12 Microscopy and FACS Analysis

For fluorescence microscopy, 5 μ L of the bacterial cell suspension was dropped on a glass slide (Fisherfinest premium, 75 \times 25 \times 1 mm³). A coverslip (Fisherbrand, 22 \times 22 \times 0.15 mm³) was pressed down on the cell droplet to give a single layer of cells on the glass slides. White light and fluorescence images were taken on a Zeiss Axio Observer A1 inverted microscope equipped with a filter cube (488 nm excitation, 515–520 nm emission) suitable for detection of FAM fluorescence. A Plan-NeoFluar \times 100 oil objective from Zeiss was used to visualize the bacterial cells. Confocal microscopy slides were prepared in a similar manner with a co-culture of *S. aureus* and Jurkat cells. Samples were excited with an Argon laser 15% power (excitation 488nm, emission 496-564nm) while monitoring with a 63x oil objective. All images were captured with the exposure time of 500 ms. All fluorescence images were processed following a fixed protocol with the software Fiji ImageJ. For flow cytometry, the samples were prepared and stained following the same protocol described for microscopy. The samples were analyzed on a BD FACS Aria cell sorter (BD Biosciences). Data analysis was performed with FlowJo (Tree

Star, Inc.), from which the median fluorescence intensities of the stained cells were extracted and plotted against peptide concentration. The plots were fit to a hyperbolic curve for determination of EC50 values.

3.7.13 Fluorescent SDS-PAGE

Phage samples were labeled as previously described with Biotin or 2APBA. Samples were precipitated to remove excess reagent and then incubated with 2mM SCZ-FITC for 1 hour. Phage samples were then precipitated to remove excess fluorophore, and heat denatured. Samples were run on 15% SDS PAGE gel for 50 min and allowed the lower M.W. pVIII protein to run off the gel. The gel was imaged at 495nm using BioRad ChemiDoc MP Imaging System.

3.7.14 ELISA Assay on Peptide Binding to Pure Lipids

Lipids were deposited in high binding 96 well plates overnight in appropriate concentrations. Wells were blocked with 5mg/ml BSA in PBS pH 7.4 for 1 hour. Wells were slapped out and peptide labeled with fluorescein was added at a concentration of 1 μ M in 100 μ L and allowed to incubate for an additional hour. The plates were washed 4 times with PBS pH 7.4 0.05% tween then incubated with HRP conjugated anti-fluorescein antibody for 1 hour. Wells were washed again six times before incubation with 1-Step ultra TMB-ELISA substrate solution for 30min, allowing for sufficient color to develop. Absorbance of wells was then measured at 650nm.

3.8 References

1. Smith, G. P., and Petrenko, V. A. (1997) Phage Display, *Chemical Reviews* 97, 391-410.
2. Sidhu, S. S., and Koide, S. (2007) Phage display for engineering and analyzing protein interaction interfaces, *Curr Opin Struct Biol* 17, 481-487.
3. Chen, G., Koellhoffer, J. F., Zak, S. E., Frei, J. C., Liu, N., Long, H., Ye, W., Nagar, K., Pan, G., Chandran, K., Dye, J. M., Sidhu, S. S., and Lai, J. R. (2014) Synthetic Antibodies with a Human Framework That Protect Mice from Lethal Sudan Ebolavirus Challenge, *ACS chemical biology* 9, 2263-2273.
4. Liu, C. C., Mack, A. V., Tsao, M. L., Mills, J. H., Lee, H. S., Choe, H., Farzan, M., Schultz, P. G., and Smider, V. V. (2008) Protein evolution with an expanded genetic code, *Proceedings of the National Academy of Sciences of the United States of America* 105, 17688-17693.
5. Day, J. W., Kim, C. H., Smider, V. V., and Schultz, P. G. (2013) Identification of metal ion binding peptides containing unnatural amino acids by phage display, *Bioorg Med Chem Lett* 23, 2598-2600.
6. Mohan, K., and Weiss, G. A. (2016) Chemically Modifying Viruses for Diverse Applications, *ACS chemical biology* 11, 1167-1179.
7. Ng, S., Jafari, M. R., and Derda, R. (2012) Bacteriophages and Viruses as a Support for Organic Synthesis and Combinatorial Chemistry, *ACS chemical biology* 7, 123-138.
8. Ng, S., Jafari, M. R., Matochko, W. L., and Derda, R. (2012) Quantitative synthesis of genetically encoded glycopeptide libraries displayed on M13 phage, *ACS chemical biology* 7, 1482-1487.
9. Ng, S., Lin, E., Kitov, P. I., Tjhung, K. F., Gerlits, O. O., Deng, L., Kasper, B., Sood, A., Paschal, B. M., Zhang, P., Ling, C. C., Klassen, J. S., Noren, C. J., Mahal, L. K., Woods, R. J., Coates, L., and Derda, R. (2015) Genetically encoded fragment-based discovery of glycopeptide ligands for carbohydrate-binding proteins, *Journal of the American Chemical Society* 137, 5248-5251.

10. Heinis, C., Rutherford, T., Freund, S., and Winter, G. (2009) Phage-encoded combinatorial chemical libraries based on bicyclic peptides, *Nat Chem Biol* 5, 502-507.
11. Jafari, M. R., Deng, L., Kitov, P. I., Ng, S., Matochko, W. L., Tjhung, K. F., Zeberoff, A., Elias, A., Klassen, J. S., and Derda, R. (2014) Discovery of light-responsive ligands through screening of a light-responsive genetically encoded library, *ACS chemical biology* 9, 443-450.
12. Bandyopadhyay, A., and Gao, J. (2016) Targeting biomolecules with reversible covalent chemistry, *Curr Opin Chem Biol* 34, 110-116.
13. Miller, R. M., and Taunton, J. (2014) Targeting protein kinases with selective and semipromiscuous covalent inhibitors, *Methods Enzymol* 548, 93-116.
14. Cal, P. M., Vicente, J. B., Pires, E., Coelho, A. V., Veiros, L. F., Cordeiro, C., and Gois, P. M. (2012) Iminoboronates: A New Strategy for Reversible Protein Modification, *Journal of the American Chemical Society* 134, 10299-10305.
15. Bandyopadhyay, A., McCarthy, K. A., Kelly, M. A., and Gao, J. (2015) Targeting bacteria via iminoboronate chemistry of amine-presenting lipids, *Nat Commun* 6.
16. Akcay, G., Belmonte, M. A., Aquila, B., Chuaqui, C., Hird, A. W., Lamb, M. L., Rawlins, P. B., Su, N., Tentarelli, S., Grimster, N. P., and Su, Q. (2016) Inhibition of Mcl-1 through covalent modification of a noncatalytic lysine side chain, *Nat Chem Biol* 12, 931-936.
17. Bandyopadhyay, A., Cambray, S., and Gao, J. (2017) Fast Diazaborine Formation of Semicarbazide Enables Facile Labeling of Bacterial Pathogens, *Journal of the American Chemical Society* 139, 871-878.
18. Kocaoglu, O., and Carlson, E. E. (2016) Progress and prospects for small-molecule probes of bacterial imaging, *Nat Chem Biol* 12, 472-478.
19. Liu, C. C.; Mack, A. V.; Brustad, E. M.; Mills, J. H.; Groff, D.; Smider, V. V.; Schultz, P. G. (2009) Evolution of Proteins with Genetically Encoded "Chemical Warheads". *J Am Chem Soc*, 131, 9616-9617.

20. Tharp, J. M.; Hampton, J. T.; Reed, C. A.; Ehnbohm, A.; Chen, P.-H. C.; Morse, J. S.; Kurra, Y.; Pérez, L. M.; Xu, S.; Liu, W. R. (2020) An amber obligate active site-directed ligand evolution technique for phage display. *Nature communications*, 11, 1392.
21. Adaligil, E.; Patil, K.; Rodenstein, M.; Kumar, K. (2019) Discovery of Peptide Antibiotics Composed of d-Amino Acids. *ACS Chem Biol*, 14, 1498-1506.
22. Slavetinsky, C., Kuhn, S., and Peschel, A. (2016) Bacterial aminoacyl phospholipids - Biosynthesis and role in basic cellular processes and pathogenicity, *Biochimica et biophysica acta*.
23. Peschel, A., Jack, R. W., Otto, M., Collins, L. V., Staubitz, P., Nicholson, G., Kalbacher, H., Nieuwenhuizen, W. F., Jung, G., Tarkowski, A., van Kessel, K. P., and van Strijp, J. A. (2001) *Staphylococcus aureus* resistance to human defensins and evasion of neutrophil killing via the novel virulence factor MprF is based on modification of membrane lipids with l-lysine, *J Exp Med* 193, 1067-1076.
24. Thapa, N., Kim, S., So, I. S., Lee, B. H., Kwon, I. C., Choi, K., and Kim, I. S. (2008) Discovery of a phosphatidylserine-recognizing peptide and its utility in molecular imaging of tumour apoptosis, *J Cell Mol Med* 12, 1649-1660.
25. Ju, T., Niu, W., and Guo, J. (2016) Evolution of Src Homology 2 (SH2) Domain to Recognize Sulfotyrosine, *ACS chemical biology* 11, 2551-2557.
26. Roy, H. (2009) Tuning the properties of the bacterial membrane with aminoacylated phosphatidylglycerol, *IUBMB Life* 61, 940-953.
27. Ernst, C. M., and Peschel, A. (2011) Broad-spectrum antimicrobial peptide resistance by MprF-mediated aminoacylation and flipping of phospholipids, *Mol Microbiol* 80, 290-299.
28. Yang, L., Gordon, V. D., Trinkle, D. R., Schmidt, N. W., Davis, M. A., DeVries, C., Som, A., Cronan, J. E., Jr., Tew, G. N., and Wong, G. C. (2008) Mechanism of a prototypical synthetic membrane-active antimicrobial: Efficient hole-punching via interaction with negative intrinsic curvature lipids, *Proceedings of the National Academy of Sciences of the United States of America* 105, 20595-20600.

29. Morton, L. A., Yang, H., Saludes, J. P., Fiorini, Z., Beninson, L., Chapman, E. R., Fleshner, M., Xue, D., and Yin, H. (2013) MARCKS-ED peptide as a curvature and lipid sensor, *ACS chemical biology* 8, 218-225.

Chapter 4

Peptide Probes of Colistin Resistance Discovered via Chemically Enhanced Phage Display

4.1 Introduction

4.1.1 Colistin Resistance

Antibiotic resistant bacterial pathogens have become a global threat to public health. Resistance to essentially all current antibiotics has been reported, and diverse mechanisms of resistance have been reported in recent years and are continuously being discovered.¹ According to the Center for Disease Control, over 2 million antibiotic resistance infections are reported each year, leading to approximately 23,000 deaths in the United States alone. There are numerous bacterial pathogens emerging that harness multi-drug resistance and require immediate attention. Of particular importance are the “ESKAPE pathogens” (*Enterococcus faecium*, *Staphylococcus aureus*, *Klebsiella pneumoniae*, *Acinetobacter baumannii*, *Pseudomonas aeruginosa* and *Enterobacter* species) which exhibit prominent levels of antibiotic resistance and often escape eradication by antibiotics.² These species of bacteria are responsible for the majority of infections among society and have become increasingly prevalent in health care settings. The resistant strains of these bacteria are becoming progressively difficult to treat, with effective therapeutic options declining. As a result, many doctors are forced to treat patients with antibiotics of last resort, despite their significant toxicity to healthy human cells. For example, colistin, an old antibiotic that had been shelved for several decades, is now increasingly used to treat multidrug resistant gram-negative infections,³ including *E. coli*, *K. pneumoniae*, *A. baumannii*, and various *Enterobacter* species. As a consequence of its increased use, colistin resistance is increasingly reported from hospitals.⁴⁻⁶ Currently, the only way to assess colistin resistance is through lab culturing, which is time

consuming and often plagued by contaminations. Rapid and reliable detection of colistin resistant pathogens is highly desirable for enacting effective treatment plans in a timely manner.

The bactericidal mechanism of colistin, although still not fully clear, is believed to involve binding of the polycationic peptide to the lipid A portion of lipopolysaccharides (LPS) and insertion of the hydrophobic tail to lipid membrane.⁷ As expected, a major mechanism of colistin resistance involves modification of LPS or LOS (lipooligosaccharide for select bacterial species) via regulated installation of phosphoethanolamine or 4-aminoarabinose onto the lipid A core (**Figure 4-1**).^{8,9} The structurally altered LPS/LOS can no longer bind colistin, therefore affording resistance of the bacteria. A more extreme mechanism of resistance was recently reported that involves complete shut-down of LOS biosynthesis and replacing the exterior leaflet of the outer membrane with lipoproteins.^{10,11} However, the level of pathological significance remains unclear for this unusual mechanism.^{12,13}

We envisioned that the surface modifications responsible for colistin resistance can be targeted to enable rapid diagnosis of colistin-resistant infections. Towards this goal, we resorted once again to phage display, a powerful technology for screening peptide libraries.¹⁴⁻¹⁶ Several attempts¹⁷ were documented that use phage displayed peptide libraries to uncover molecular probes for specific bacterial strains. However, these attempts have yielded limited success, at best revealing probes of modest potency (millimolar K_d 's).¹⁸ The lack of success in these earlier endeavors reveals the limitation of natural peptides (composed of natural amino acids) in terms of binding bacterial cell

surfaces, which largely comprise hydrophilic molecules in contrast to proteins with hydrophobic pockets. Looking to expand upon our previous efforts we again employed the APBA-dimer library, which incorporates a pair of APBA moieties as warheads to “bind” biological amines via dynamic iminoboronate formation (**Figure 4-1**).^{24,25} Screening of this covalent binding library yielded sub to low micromolar binders of *S. aureus* as well as a lipooligosaccharide depleted (LOS-) strain of *Acinetobacter baumannii*. In this chapter, we examine the APBA-dimer library for its potential to recognize bacterial strains that harbor LPS modifications, and hence exhibit colistin resistance (**Figure 4-1**). The resulting peptide probes, with proper fluorophore installed, selectively stain colistin-resistant strains of bacteria over corresponding non-resistant controls. Interestingly, the relative fluorescence intensity of the stained bacteria cells appears to correlate with their level of colistin resistance, indicating the potential use of these peptide probes for diagnosis of colistin resistance.

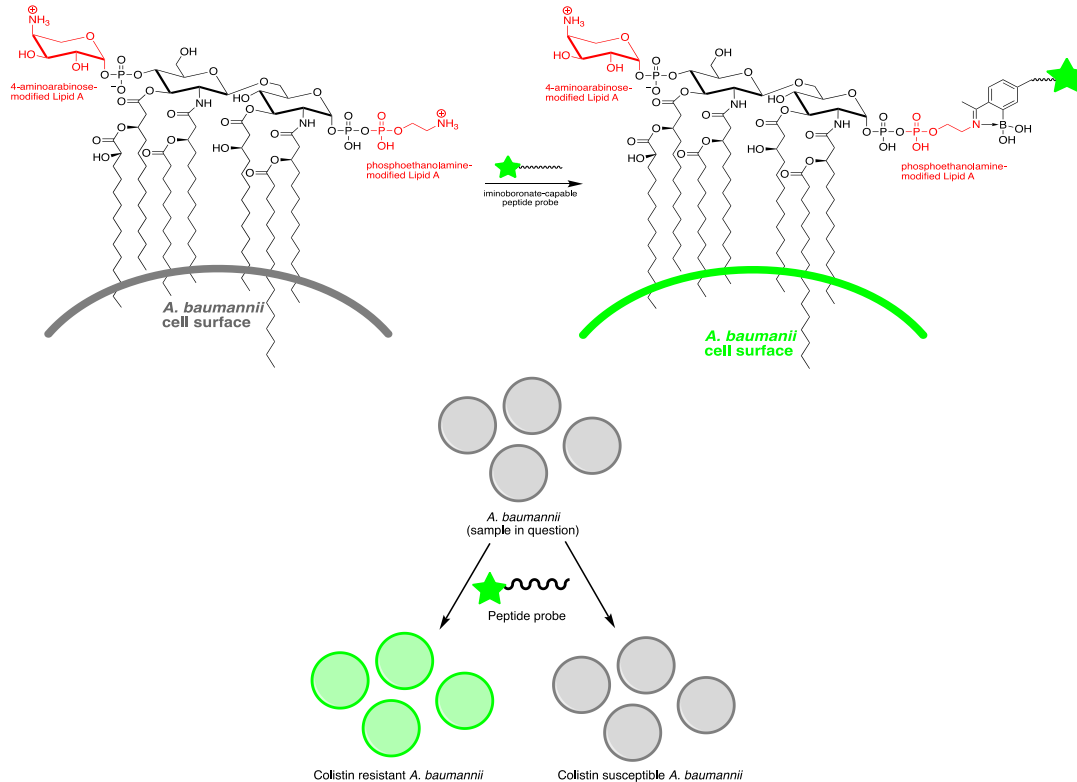


Figure 4-1 Illustration of surface modifications of colistin resistant bacteria. Surface modifications of *A. baumannii* are used as an example. The modified structures display amino groups that can be targeted with iminoboronate-capable peptides, which hold promise to distinguish colistin-resistant versus colistin-sensitive bacteria as illustrated on the bottom.

4.2 Identification of Probes for *Mcr-1* Positive *E. coli*

4.2.1 Panning Against *Mcr-1* Positive *E. coli*

A major and particularly worrisome mechanism of colistin resistance originates from a plasmid-borne *mcr-1* gene,⁵ which encodes for a phosphoethanolamine (PE) transferase. Since its initial discovery in 2016, plasmids carrying the *mcr-1* gene have been reported for many strains of bacterial pathogens. The Centers for Disease Control and Prevention (CDC) has curated a panel of colistin resistant bacteria with many harboring a *mcr-1* plasmids (<https://wwwn.cdc.gov/arisolatebank/Panel/PanelDetail?ID=10>). We

obtained several strains of *mcr-1* positive bacteria from CDC (**Table 4-1**) and panned our APBA-dimer library against an *E. coli* strain (493) for our initial trial (**Figure 4-2**).

Table 4-1 List of bacterial strains used in this work.

Number	Strain Name	Strain	<i>Mcr-1</i> indicator	Colistin MIC µg/mL
1	BL21	<i>E. coli</i>	-	<0.25 [°]
2	348	<i>E. coli</i>	-	<0.25*
3	350	<i>E. coli</i>	+	4*
4	493	<i>E. coli</i>	+	8*
5	494	<i>E. coli</i>	+	8*
6	495	<i>E. coli</i>	+	4*
7	347	<i>K. pneumoniae</i>	-	<0.25*
8	4352	<i>K. pneumoniae</i>	-	<0.25 ^π
9	497	<i>K. pneumoniae</i>	+	8*
10	EGA408	<i>A. baumannii</i>	-	8 ^φ
11	17978	<i>A. baumannii</i>	-	0.5 ^φ

*Strains and MICs obtained from the CDC. Details can be found at the following website: <https://wwwn.cdc.gov/arisolatebank/Panel/PanelDetail?ID=10>

[°] Previously reported¹ ^πPreviously reported²

^φ Determined by broth micro-dilution assay

Library modification was conducted as reported previously by attaching two APBA reversible covalent moieties at the two N-terminal cysteines of the C7C peptide. Once the APBA dimer library was confirmed it was used for serial rounds of panning against *mcr-1* positive *E. coli* strain 493. Each round of panning was initiated with an input population of 10¹⁰ pfu followed by extensive washing to eliminate non-binders. The screens were performed in the presence of 10 mg/ml BSA to exclude non-specific binders. The bound phage were subjected to acid to elute the phage from the bacteria as acidification triggers dissociation of iminoboronates and disrupts any other interactions that may occur

between the peptide and target.²⁶ The typical output populations were around 10^3 to 10^5 pfu, similar to the previously reported screen against *S. aureus* with an APBA dimer library.²⁴ From each output population, a small sample of plaques were sequenced and analyzed for sequence convergence. Sequence convergence was observed after three rounds of panning and the results from rounds 2 and 3 summarized in **Table 4-2**. Recurring peptide sequences denoted, MAK30-32, (**Table 4-2, 4-3**) were synthesized via solid phase peptide synthesis for further analysis.

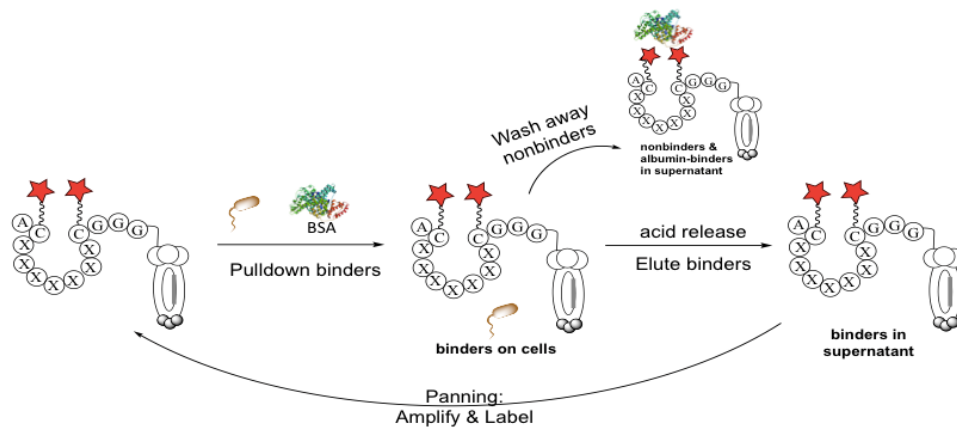


Figure 4-2 Schematic illustration of phage panning against live bacterial cells. Stars denote APBA-IA modification. Three rounds of screening were carried out against cell lines resistant to colistin.

Table 4-2 Sequencing results for the output populations of *E. coli* (493 strain) screening.

Round 2				
Hit	DNA Sequence	Peptide	Repeats	Name
1	GCTTGTAAATGATACGAGTAATAATGCTTGC	ACNDTSNNAC	1	
2	GCTTGTATGACTAATACGCCTGTTCTTGC	ACMTNTPVPC	1	
3	GCTTGTCTGGAGAGTATGTAGACGTATTGC	ACLESM*TYC	1	
4	GCTTGTGTTGAGGATGATAGGGTTTCGTGC	ACVEDDRVSC	1	
5	GCTTGTACGCCTCGTTCGGCGAATTATTGC	ACTPRSANYC	1	
6	GCTTGTAAATAATCATGGGTATTGGTGGTGC	ACNNHGYWWC	1	
7	GCTTGTATGGGAATTCGCCGCTGACGTGC	ACYGNSPLTC	1	
8	GCTTGTATTTCGCAATTCCGCCTGATGTGC	ACYSQFRLMC	1	
9	N/A	Blank	2	
Round 3				
Hit	DNA Sequence	Peptide	Repeats	Name
1	GCTTGTGATCCGAATCGGATGGATAGGTGC	ACDPNRMDRC	4	MAK30
2	GCTTGTATGACTAATACGCCTGTTCTTGC	ACMTNTPVPC	2	MAK31
3	GCTTGTAGGGCGCATGAGCAGTCTCTGTGC	ACRAHEQSLC	2	MAK32
4	GCTTGTATGGGTATTCATAATTTGTATTGC	ACMGIHNLYC	1	
5	GCTTGTGGGACGAATCCGATTAAGAAGTGC	ACGTNPIKKC	1	
6	GCTTGTAAAGAATTATTCGCAGCCGATTTGC	ACKNYSQPIC	1	
7	N/A	Blank	4	

SPPS was performed on a rink amide resin incorporating an orthogonally protected Dap residue followed by a triple glycine linker and the core C7C peptide. Selective deprotection of the Dap residue on resin allows facile installation of a fluorophore to facilitate analysis. After global deprotection and cleavage from resin, the

peptides were modified with APBA-IA. The purity and identity of the final peptides were assessed via LC-MS analysis (**Table 4-3**).

Table 4-3 Sequence and mass-spec data of peptide hits.

Name	Sequence	Calculated m/z	Observed m/z
MAK30	AC _m DPNRMDRC _m GGGDap*	1156.92 [M-2H ₂ O+2H] ²⁺	1157.30
MAK31	AC _m MTNTPVPC _m GGGDap*	1093.91 [M-H ₂ O+2H] ²⁺	1094.79
MAK32	AC _m RAHEQSLC _m GGGDap*	1134.44 [M+2H-H ₂ O] ²⁺	1134.81

C_m indicates cysteines modified with 2APBA-IA moieties.

4.3 Characterization of the Peptide Hits for Detecting Colistin Resistance

4.3.1 Flow Cytometry Analysis of Peptide Hits

These peptides were first characterized by flow cytometry analysis. MAK30-32 were incubated at increasing concentrations from 0 μM to 2 μM concentrations with the *mcr-1* positive 493 strain to generate binding curves. Additionally, the *mcr-1* negative *E. coli* 348 strain was used as a control to initially probe the specificity of these peptides to the *mcr-1* positive strain 493 that was selected for during screening. All three peptides showed significant binding to the *mcr-1* positive *E. coli* strain 493 over the *mcr-1* negative *E. coli* strain 348. The trend was reproducible and showed maximum binding at 2μM concentration of peptide.

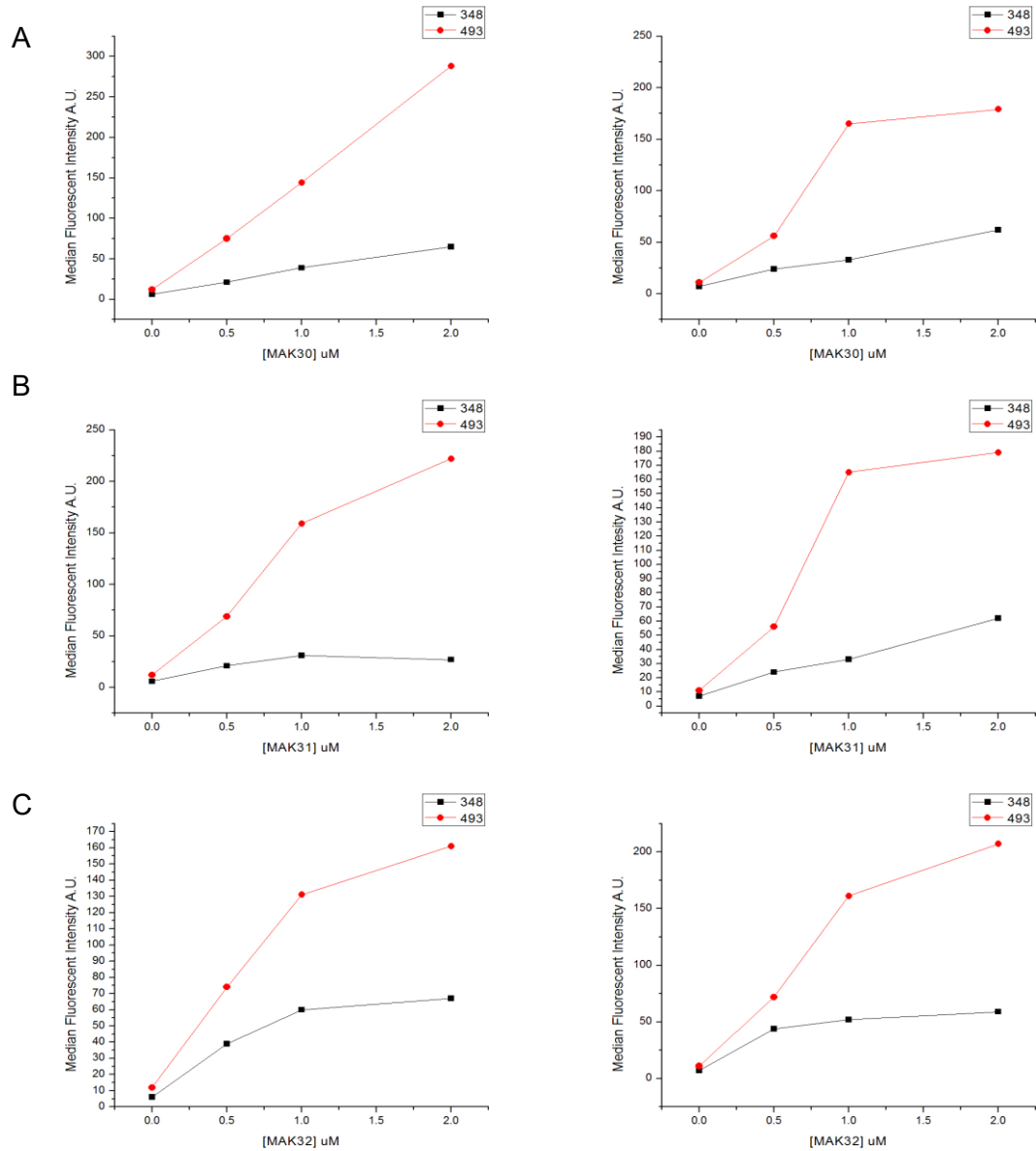


Figure 4-3 Flow cytometry analysis of MAK30 (A) MAK31 (B) and MAK32 (C) against *mcr-1* (-) and *mcr-1* (+) *E. coli* strains. Median fluorescent intensity was measured as a function of increasing concentration of the peptide. Two replicate data sets are presented to show the consistency of our experimental results.

An additional negative control was tested to gain mechanistic insights of MAK30. Fluorescein alone elicited no cell staining for either strain of *E. coli*, indicating that the

bacterial staining of MAK30 is dictated by the peptide rather than the fluorophore used (Figure 4-4).

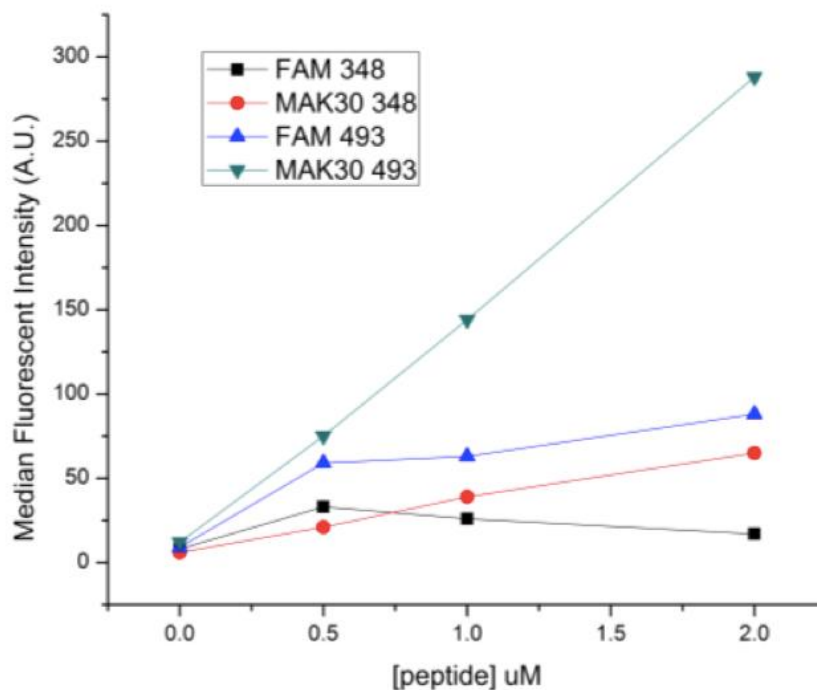


Figure 4-4 MAK30 and fluorescein alone tested against 493 and 348 to show the specificity and potency of MAK30 to *E. coli* strain 493.

4.3.2 Scope of MAK30 for Detecting Colistin Resistant Pathogens

The peptide hit MAK30 was then assessed for its ability to bind the target *E. coli* strain (493) using fluorescence microscopy. The microscopic images show that MAK30 elicits strong fluorescence staining of the 493 *E. coli* cells at 1 μ M concentration (Figure 4-5). Further comparative studies showed the presence or absence of BSA has little effect on the bacterial staining capabilities of MAK30 (Figure 4-5). The lack of BSA inhibition can be attributed to the design of our screen conditions where BSA was included as an internal competitor. Interestingly, under the same experimental conditions, MAK30 affords no

staining of the 348 strain of *E. coli*, which does not carry the *mcr-1* gene and is colistin susceptible (**Figure 4-5**).

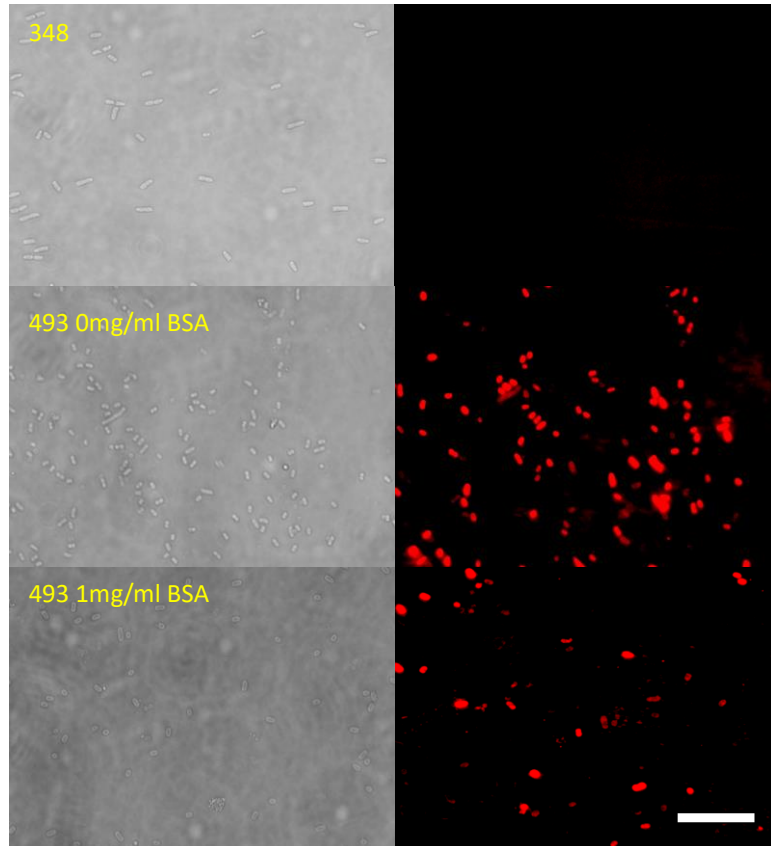


Figure 4-5 Microscopy analyses showing MAK30 selectively labels the target bacterial strain. Microscopic images show MAK30 labels the *mcr-1* (+) strain (493) in presence and absence of BSA, but not the *mcr-1* (-) strain (348). Scale bar: 10 μm ; MAK30: 1 μM ; BSA: 1 mg/ml.

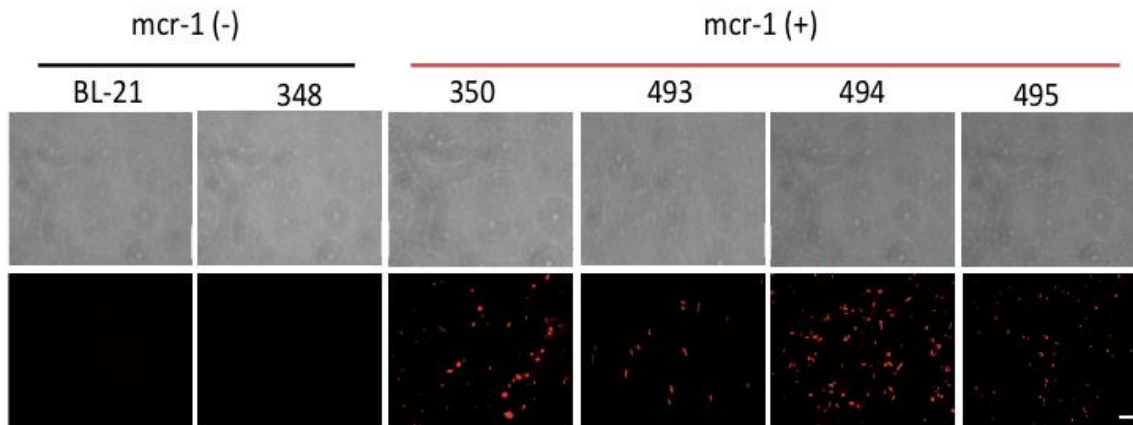


Figure 4-6 MAK30 is a pan-*mcr-1* (+) strain selective probe for *E. coli*. (a) Microscopic analysis of MAK30 staining of a panel of *mcr-1* (+) *E. coli* strains as well as two negative controls. Scale bar: 10 μ m; MAK30: 1 μ M; BSA: 1 mg/ml.

To examine the scope of MAK30 for detecting colistin resistant pathogens, we performed parallel analysis of MAK30 against a larger panel of colistin-sensitive and colistin-resistant *E. coli* strains (**Figure 4-6, Table 4-1**). Specifically, various strains of *E. coli* were treated with MAK30 (1 μ M) and then subjected to microscopy as well as flow cytometry analyses. To our satisfaction, all *E. coli* strains that harbor a *mcr-1* plasmid displayed strong fluorescence staining by MAK30 according to the results of fluorescence microscopy. In contrast, the two *mcr-1* negative strains tested showed no noticeable fluorescence staining (**Figure 4-6**). This finding is further supported with flow cytometry analysis, in which the *mcr-1* positive strains consistently gave higher mean fluorescence intensity than the *mcr-1* negative strains (**Figure 4-7**), although a significant variation of mean cell fluorescence was observed among the *mcr-1* positive strains.

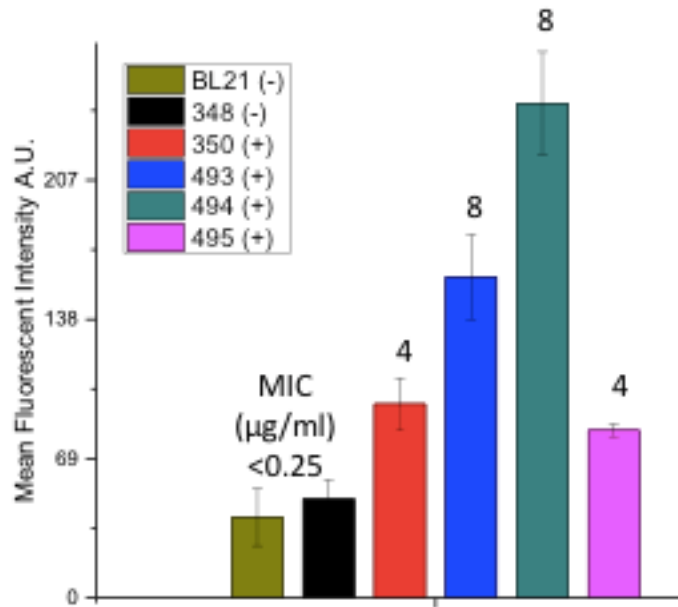


Figure 4-7 Flow cytometry analysis of MAK30 against a variety of *E. coli* strains with and without *mcr-1*. Their respective resistance to colistin listed above each.

Additional microscopy studies to understand the unique *mcr-1* binding capabilities of MAK30 were conducted. KAM5, a previously reported peptide probe of *S. aureus*, was imaged in the same manner as MAK30 and afforded no staining of the *E. coli* cells, which showcases the importance of the MAK30 peptide sequence for *E. coli* binding (**Figure 4-8**).

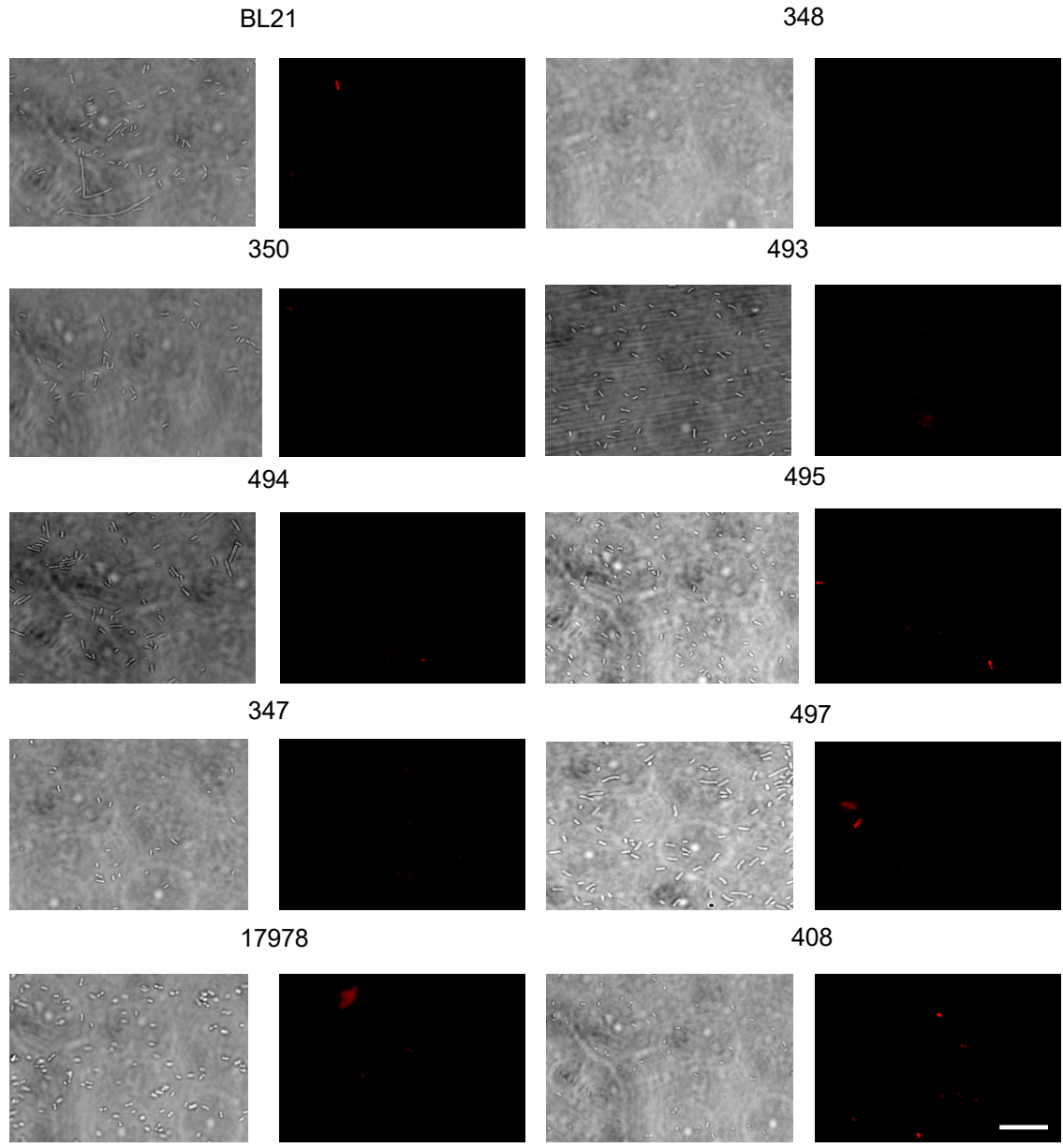


Figure 4-8 Microscopy analysis of KAM5, a previously identified peptide for *S. aureus*. The lack of staining of this APBA dimer peptide for any of these bacterial strains demonstrates the sequence importance of the MAK30 for staining colistin resistant bacterial strains.

Finally, the MAK30 precursor peptide that does not have the APBA warheads failed to stain the *E. coli* cells as well, highlighting the functional significance of the

covalent binding motifs (**Figure 4-9**). Collectively this data demonstrates the potency and specificity of these peptides for *mcr-1* containing strains.

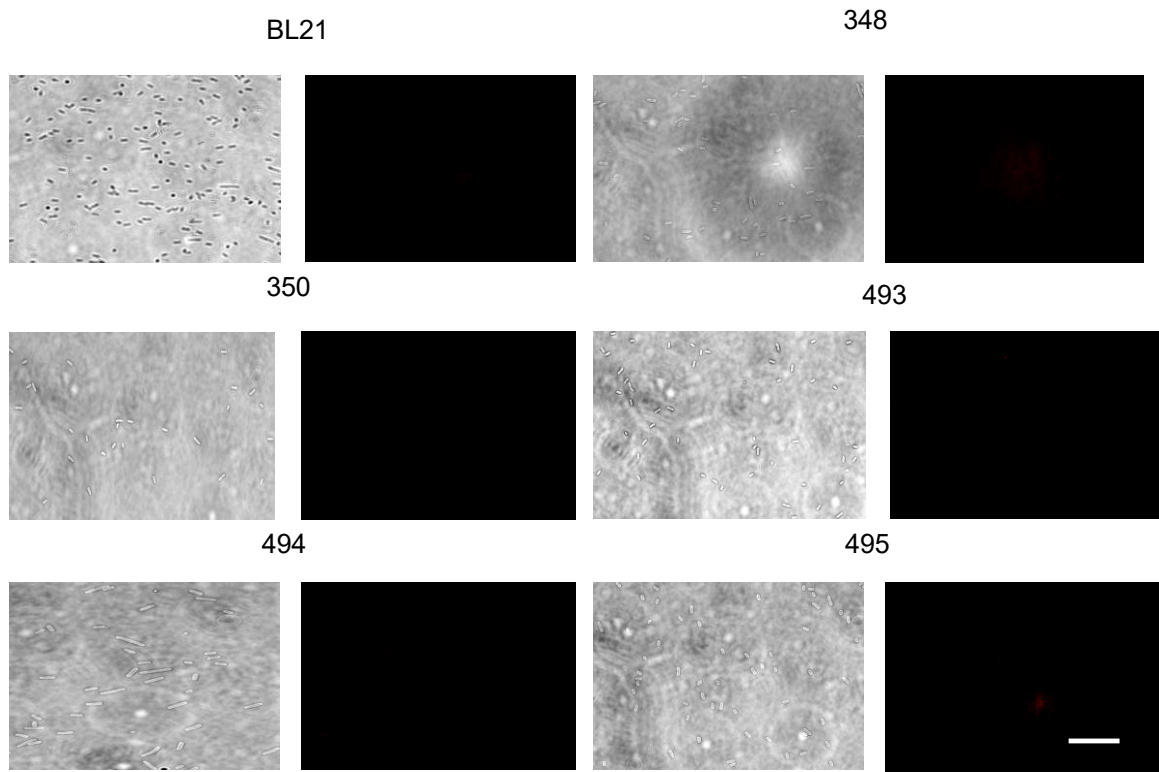


Figure 4-9 Microscopy images of linear MAK30 precursor peptide (no APBA warheads) demonstrating the necessity of the APBA moieties in bacterial binding of these peptides. Scale bar: 10 μm .

These findings nicely corroborate the flow cytometry analysis, in which MAK30 clearly distinguished the *mcr-1* positive 493 strain from the *mcr-1* negative *E. coli* 348 cells and further explores its potential for other *mcr-1* carrying strains. The lack of binding without APBA demonstrates the necessity to each aspect of these APBA peptides.

4.3.3 Lipopolysaccharide Analysis

The consistent favorable staining of the *mcr-1* positive strains by MAK30 suggests that the peptide is targeting a product of the *mcr-1* gene. As mentioned earlier, the *mcr-1* gene is known to encode a phosphoethanolamine (PE) transferase responsible for PE modification of lipopolysaccharide (LPS). To probe the extent of LPS modification, we performed lipid extraction and analysis for all these *E coli* strains. With reference to the lipid signature peaks as documented in literature,²⁷ we identified the mass spec peaks for lipid A with and without PE modification respectively (**Figure 4-10** and **Figure 4-11**).

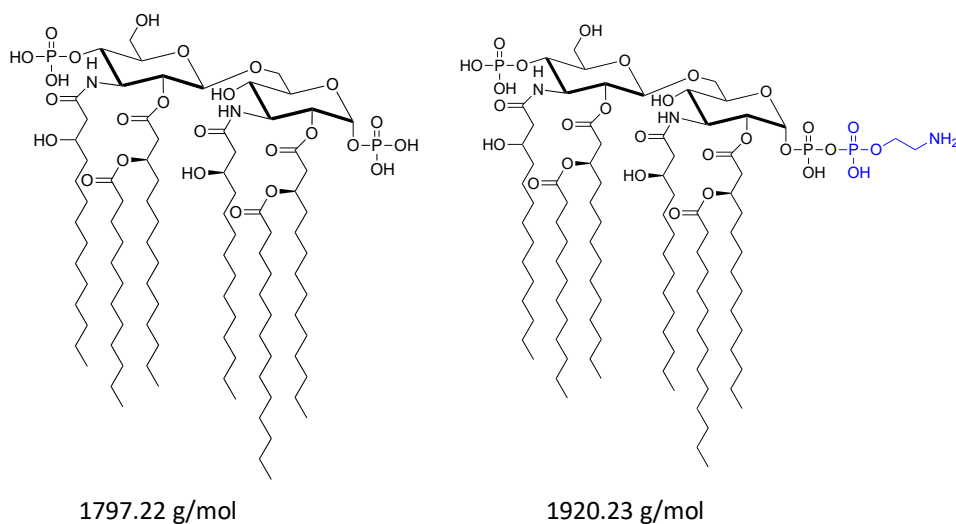


Figure 4-10 Lipopolysaccharide (LPS) with and without the addition of PE highlighted in blue. PE generates a definitive 123 da shift in mass spec samples.

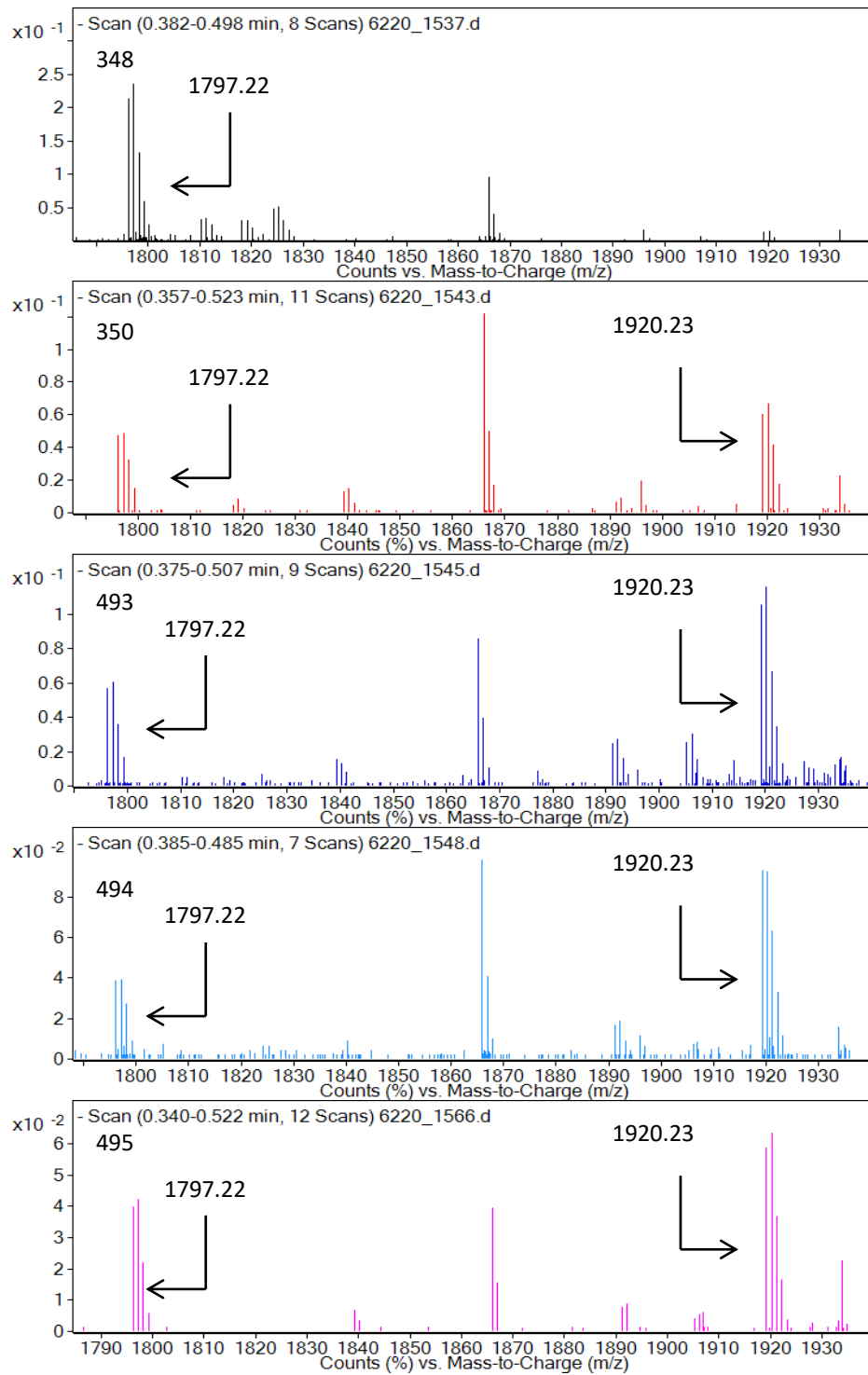


Figure 4-11 Mass-spec analysis of bacterial lipids showing *mcr-1* induced PE modification of LPS in *mcr-1* (+) stains of *E. coli*.

Quantification of the mass spec peak intensities allowed us to estimate the extent of PE modification and the results are summarized in **Figure 4-12**. Considering that the modified and unmodified lipid A may have different ionization potentials, we emphasize the numbers shown in **Figure 4-12** should be considered as **apparent** percentages of PE modification. Nevertheless, these numbers should inform the **relative** extent of PE modifications across these *E. coli* strains. As expected, the *mcr-1* (-) strain (348) showed little to no lipid A modification with PE, while the PE modified lipid A appeared as the major species (60-70%) in the *mcr-1* (+) strains (**Figure 4-12**).

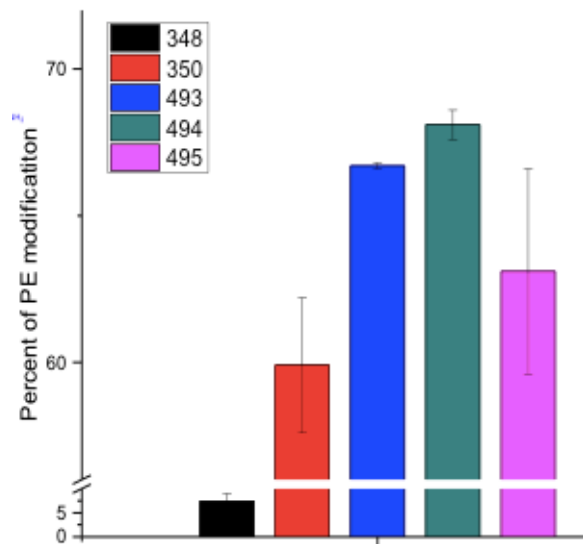


Figure 4-12 Bar graph showing the apparent percentages of lipid A modification with PE estimated from mass-spec results. This bar graph displays a similar pattern as (**Figure 4-7**), indicating MAK30 targets PE modified lipids in *mcr-1* (+) *E. coli*.

Interestingly, the apparent extent of PE modification of the *E. coli* strains exhibits a similar pattern to the MAK30-induced fluorescence staining, suggesting that MAK30 binds to the *mcr-1* (+) cells by targeting the PE modified lipids. Furthermore, we note that

the MAK30-induced fluorescence staining positively correlates with the reported colistin MIC values (marked on top of individual bars in **Figure 4-7**) for these *E. coli* strains. This is consistent with prior literature reports that PE modification can give rise to colistin resistance. Nevertheless, our results collectively showcase the potential of MAK30 in predicting the extent of colistin resistance in *E. coli*.

4.4 Targeting Additional Colistin Resistant Strains

4.4.1 Identifying Probes Against Colistin-Resistant *A. baumannii* and *K. pneumoniae*

This section was done in collaboration with Dr. Samantha Cambray and Dr. Kelly McCarthy

To test the generality of our approach to targeting colistin-resistant pathogens, we have set out to identify peptide probes for a colistin-resistant strain of *Klebsiella pneumoniae* and *Acinetobacter baumannii*, respectively. The 497 strain of *K. pneumoniae* is a *mcr-1* (+) strain, which we obtained from the CDC Antibiotic Resistance isolate bank. This *Klebsiella* strain was reported to give colistin MIC of 8 µg/ml and our lipid extraction analysis revealed a high degree of PE modification of its LPS (**Table 4-1, Figure 4-14B**). Applying a similar panning protocol used for *E. coli* resulted in several recurring sequences after three rounds of panning. Three peptide hits (SEC18-20) were synthesized in their fluorophore-labeled forms and subjected to cell biological validation experiments (**Table 4-4**).

Table 4-4 SEC18-20.

Name	Sequence	Calculated m/z	Observed m/z
SEC18	AC _m SERQHLQC _m GGGDap*	1162.95 [M-H ₂ O+2H] ²⁺	1163.43
SEC19	AC _m RSHDSAMC _m GGGDap*	1107.38 [M-2H ₂ O+2H] ²⁺	1107.37
SEC20	AC _m LATKGSIC _m GGGDap*	1059.43[M-H ₂ O+2H] ²⁺	1058.91

C_m: APBA-IA modified cysteine; *: 5,6 carboxyfluorescein modified.

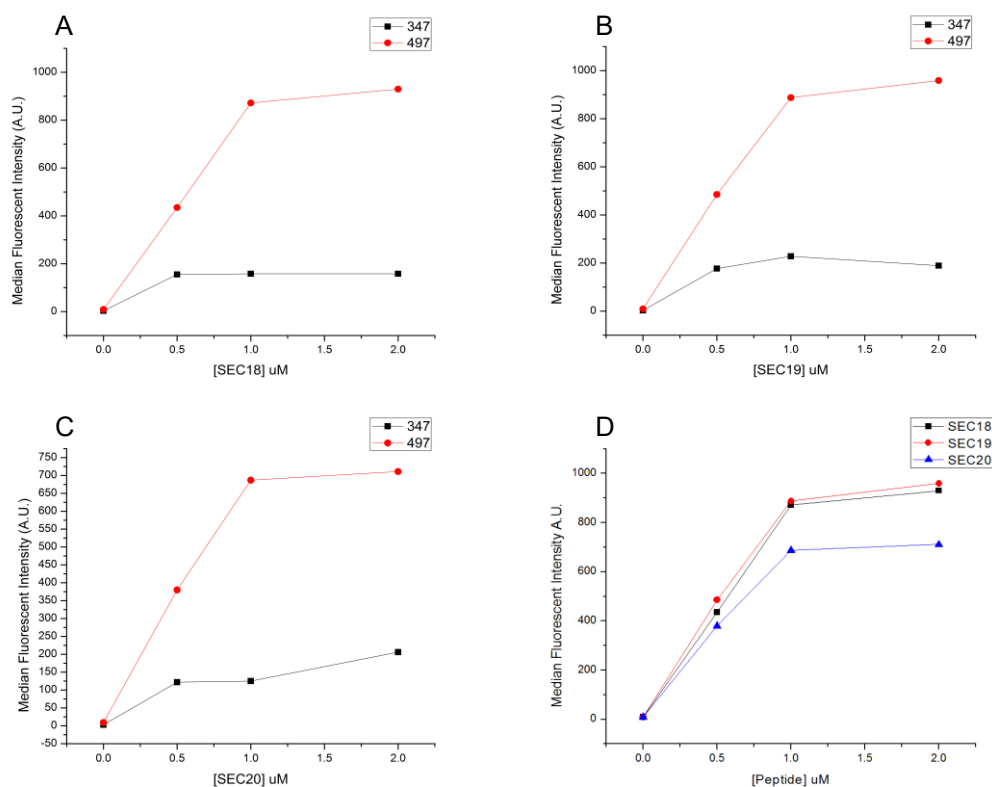


Figure 4-13 *K. pneumoniae* binding curves of SEC18 (A), SEC19 (B), and SEC20 (C). The data were generated via flow cytometry. All three peptides show selective binding of the *mcr-1* (+) strain (497 strain) over the *mcr-1* (-) control (347 strain). Part (D) compares the relative potency of the three peptides for staining the 497 strain of *K. pneumoniae*.

Gratifyingly, SEC18 and SEC19 elicited strong fluorescence staining of the bacterium, while SEC20 was found to be slightly less potent (**Figure 4-13**). Importantly, the fluorescence labeling of *Klebsiella* appeared to be highly specific to the 497 strain as

no fluorescence was observed for two control strains that are *mcr-1* (-) and susceptible to colistin killing at < 0.25 ug/ml concentrations (**Figure 4-14A**).

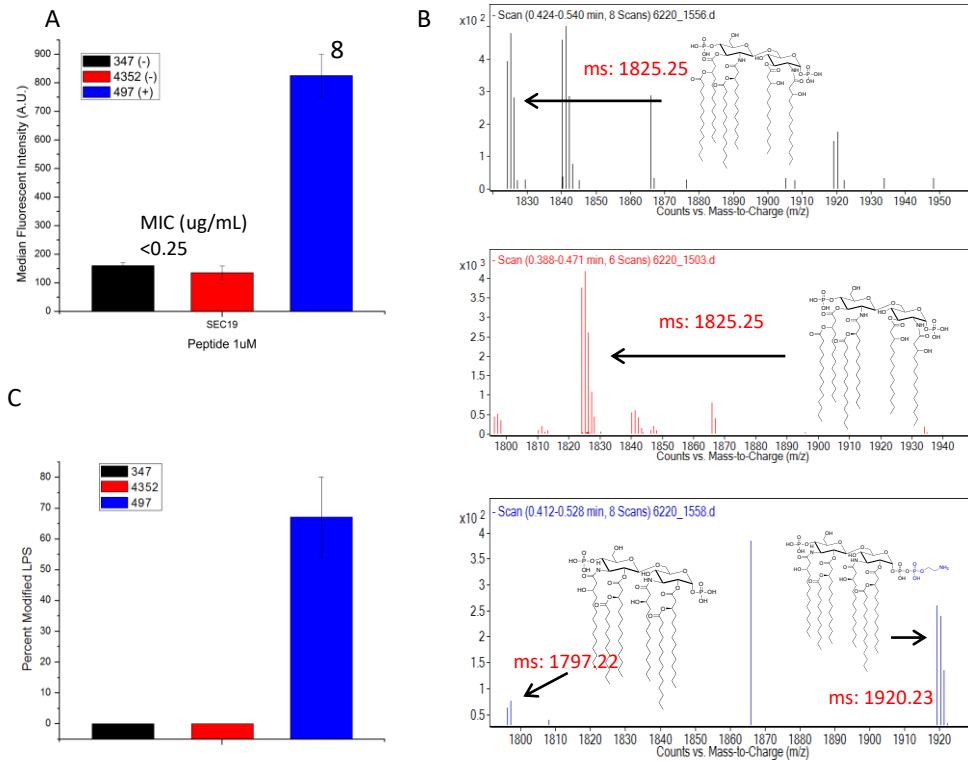


Figure 4-14 Mass spec LPS analysis of *K. pneumoniae*. (A) Bar graph of mean fluorescence intensity to compare SEC19 staining of various *K. pneumoniae* bacterial strains. The results show a positive correlation between the fluorescence intensities and the reported MICs values for this panel of bacteria. (B) Mass-spec analysis of bacterial lipids showing *mcr-1* induced PE modification of LPS in colistin resistant strain of *K. pneumoniae*. The *K. pneumoniae* strains are non-isogenic which leads to slight differences in LPS structures. The structures featured here have been reported previously. (C) Bar graph showing the apparent percentages of lipid A modification with PE estimated from mass-spec results. This bar graph displays a similar pattern as (A), indicating SEC19 targets PE modified lipids in *K. pneumoniae*.

In addition to *Klebsiella*, we further extended our study to colistin-resistant *A. baumannii*. As the CDC collection does not have *mcr-1* (+) *A. baumannii*, we used a lab-evolved colistin-resistant strain of *A. baumannii* for this study. Specifically, the EGA408 (408) strain was obtained in a lab evolution experiment and gave a MIC value of 8 µg/ml

towards colistin. Whole genome sequencing revealed a T235I mutation in PmrB, a two-component sensor histidine kinase. The PmrA/PmrB two-component system is a major regulator of LPS modifications in gram-negative bacteria²⁸ and the T235I mutation has been previously indicated to afford colistin resistance.^{29,30} We have performed lipid analysis as described earlier for other bacterial species. The results (**Figure 4-16**) clearly shows the presence of phosphoethanolamine modified lipid, which is absent from the parent strain.

Table 4-5 SEC5 & KAM20-21.

Name	Sequence	Calculate m/z	Observed m/z
SEC5	AC _m KPLHSRSC _m GGGDap*	1126.46[M-H ₂ O+2H] ²⁺	1126.95
KAM20	AC _m TNANH ₂ YFC _m GGGDap*	1147.51 [M-H ₂ O+2H] ²⁺	1147.91
KAM21	AC _m YSSPSHFC _m GGGDap*	1126.48 [M-H ₂ O+2H] ²⁺	1126.88

C_m: APBA-IA modified cysteine; *: 5,6 carboxyfluorescein modified.

Two parallel screens were performed against this colistin-resistant strain of *A. baumannii*, which revealed three recurring peptide sequences (**Table 4-5**). The three peptide hits were chemically synthesized with a fluorophore label as described for earlier peptides (**Table 4-3, 4-4**). Flow cytometry analysis shows that these peptide hits (SEC5, KAM20, and KAM21) selectively stained the target colistin-resistant strain (EGA408) over the parent strain that is colistin-susceptible (**Figure 4-15**). According to the concentration profiles generated via flow cytometry (**Figure 4-15**), SEC5 appears to be most potent for EGA408 staining giving an EC₅₀ of ~0.5 μM, similar to the potency of peptide probes for other bacterial species.

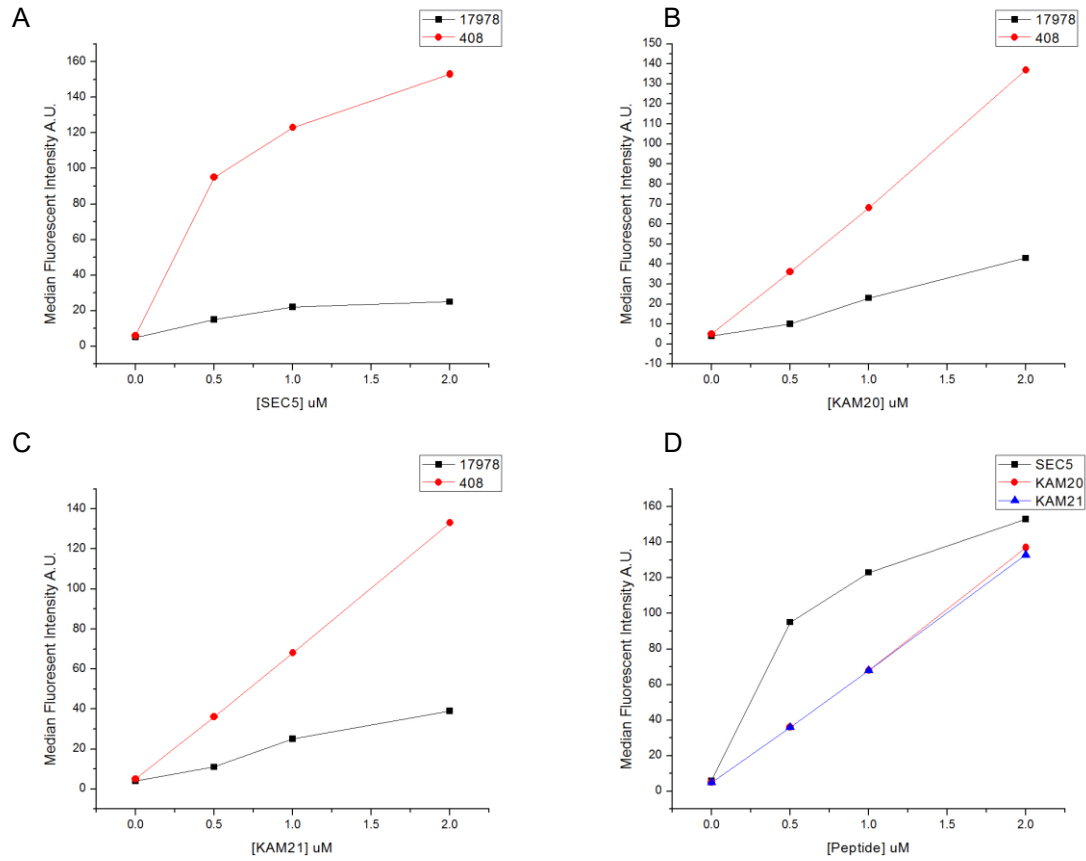


Figure 4-15 Flow cytometry analysis of *A. baumannii* staining by (A) SEC5, (B) KAM20, and (C) KAM21. Median fluorescent intensity was measured and plotted against the concentration of peptides. Part (D) overlays the concentration profiles of the three peptides, revealing the superior potency of SEC5 for staining the colistin-resistant strain of *A. baumannii*.

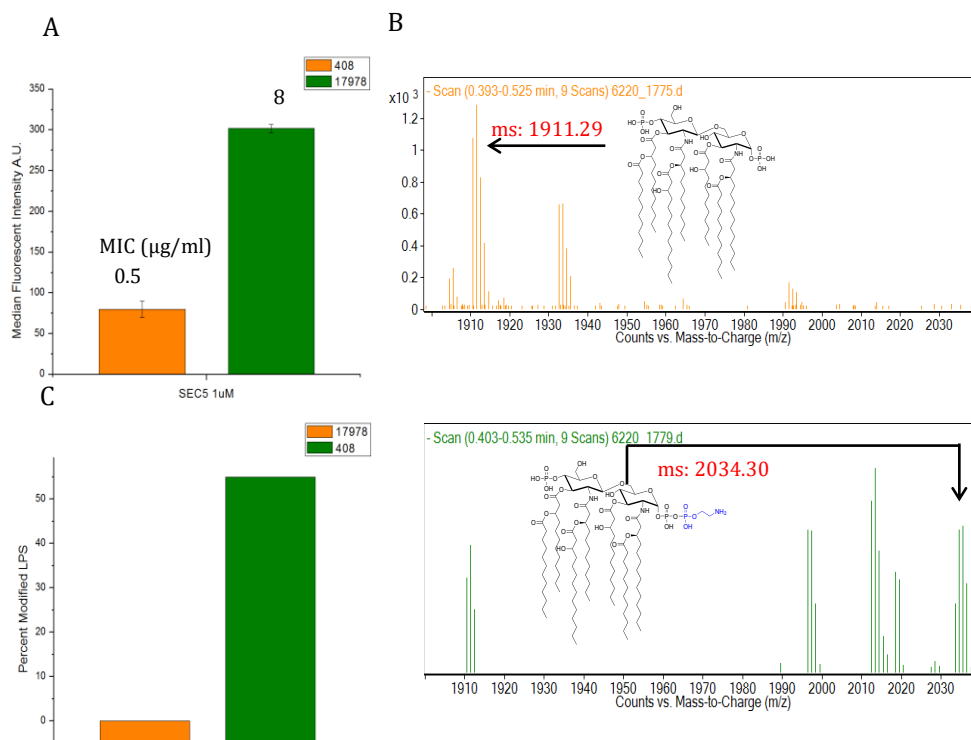


Figure 4-16 LPS modification in colistin resistant *A. baumannii*. (A) Bar graph of mean fluorescence intensity to compare SEC5 staining of the two bacterial strains. The results show a positive correlation between the fluorescence intensities and the reported MICs values for this pair of bacteria. (B) Mass-spec analysis of bacterial lipids showing PE modified LPS in the colistin resistant strain of *A. baumannii*. (C) Bar graph showing the apparent percentages of lipid A modification with PE estimated from mass-spec results. This bar graph displays a similar pattern as (A), indicating SEC5 targets PE modified lipids in *A. baumannii*.

4.4.2 Cross Examination of Peptide Probes Against Different Bacterial Species

The results shown above consistently showcase the potential of our APBA-dimer peptides for differentiating colistin-resistant and colistin-susceptible bacterial pathogens. Importantly, our lipid analysis results suggest that PE modification is the underlying reason for the peptides' selective binding to colistin-resistant strains. To gain further insights on binding mechanisms as well as to probe the potential of using these peptides

for diagnostics, we examined two exemplary peptides, namely SEC5 from *A. baumannii* screen and SEC18 from *K. pneumoniae* screen, against a broader panel of bacterial species. Specifically, the peptides were tested for staining a number of colistin-sensitive and colistin-resistant bacteria and the extent of fluorescence staining was quantified via flow cytometry analysis. Excitingly, both peptides elicited significantly stronger fluorescence for the colistin-resistant strains in comparison to the colistin-susceptible group, indicating the peptides' potential to detect colistin resistance without the need of species-specific controls. This result is also consistent with the hypothesis that our peptide probes target the lipid modifications shared by the colistin-resistant strains. Interestingly, SEC18 and SEC5 afforded nearly identical patterns in terms of the relative fluorescence brightness across the bacterial strains (**Figure 4-14, 4-16**). This is somewhat surprising as these two peptides were identified from different screens against *K. pneumoniae* and *A. baumannii* respectively. Further, we note that for both peptides, the 497 strain of *K. pneumoniae* displayed the strongest fluorescence staining, with a mean-cell-fluorescence two to three times stronger than the other two *mcr-1* (+) strains. This observation suggests that, in addition to the LPS modifications, some species-specific features also contribute to the binding of our peptide probes. Further elucidation of these species-specific features would deepen our understanding of microbiology, and importantly allow development of species-specific diagnostic tools of colistin resistance.

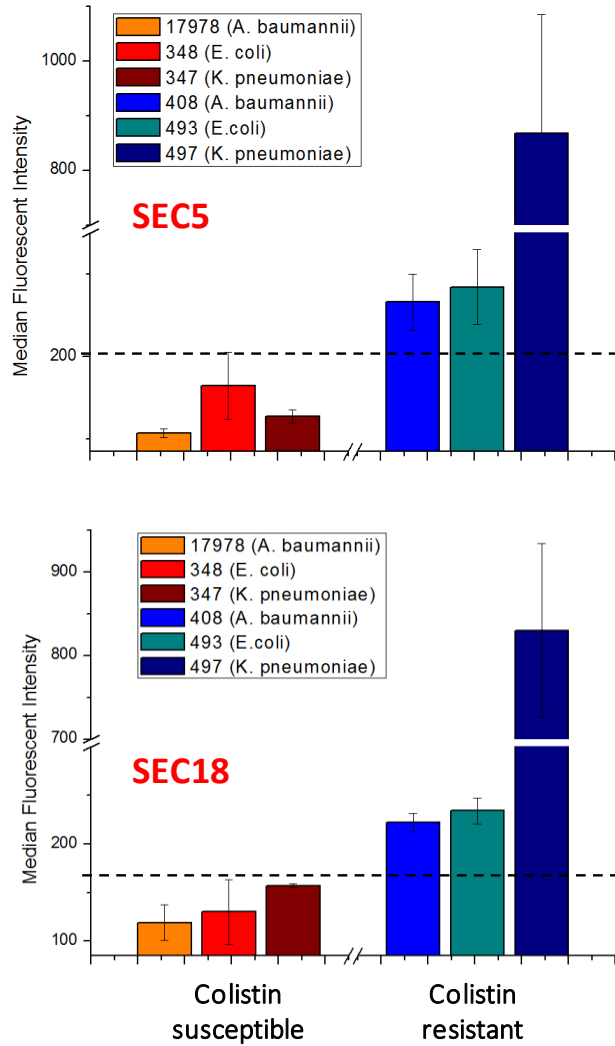


Figure 4-17 Cross examination of SEC5 and SEC18 against various bacterial species. The plots depict the median fluorescence intensities of the bacterial strains stained with 1 μ M SEC5 (a) and SEC18 (b) respectively. The samples were prepared in triplicates and analyzed using flow cytometry. The dotted lines represent the upper limit of fluorescence staining observed for the colistin-susceptible bacteria. Collectively, the data of this figure demonstrate that both peptide probes elicit consistently higher fluorescence staining of the colistin-resistant strains in comparison to the colistin-susceptible group.

4.5 Combination Therapies

4.5.1 Peptides in Combination with Antibiotics

Mcr-1 confers resistance to gram-negative bacteria by adding PE to lipid A and in doing so prevents colistin from perturbing the cell membrane leading to cell death. It is hypothesized that the positive charge on PE repels the highly positively charged colistin however, certain studies have shown that colistin is still able to bind to these cells. With these peptides presumably “capping” the amine on PE it is intriguing to consider that these peptides might restore the activity of colistin when used in combination. Eliminating the positive surface charge might allow colistin to once again perturb these membranes. Combination therapies with colistin have been previously successful with such drugs as rifampicin.³² These drugs typically only work on gram-positive cells as they are not able to penetrate the outer layer of gram-negative bacteria but with colistin perturbing the membrane they can penetrate the cell reaching their intracellular targets.³² This is true even in the cases of colistin resistant bacteria. With this in mind, MAK30 was tested in combination with colistin and a panel of other antibiotics to test the peptides ability to restore the antimicrobial activity against these resistant strains.

Cell killing assays were conducted for MAK30 with several antibiotics including, colistin, rifampicin, and clarithromycin. Colistin in combination with rifampicin was shown previously to be effective in killing *mcr-1* containing cells dropping the colistin MIC's from 8 µg/mL to 0.1 µg/mL. Repeated here it is clear that colistin when used in combination with rifampicin can overcome colistin resistance achieving 100% cell killing as low as 1 µg/mL colistin (**Figure 4-14**). Following this MAK30 was tested with the same antibiotics

at 1 and 10 μM peptide concentration. Unfortunately, MAK30 failed to elicit any meaningful changes in cell killing of the three antibiotics it was tested with.

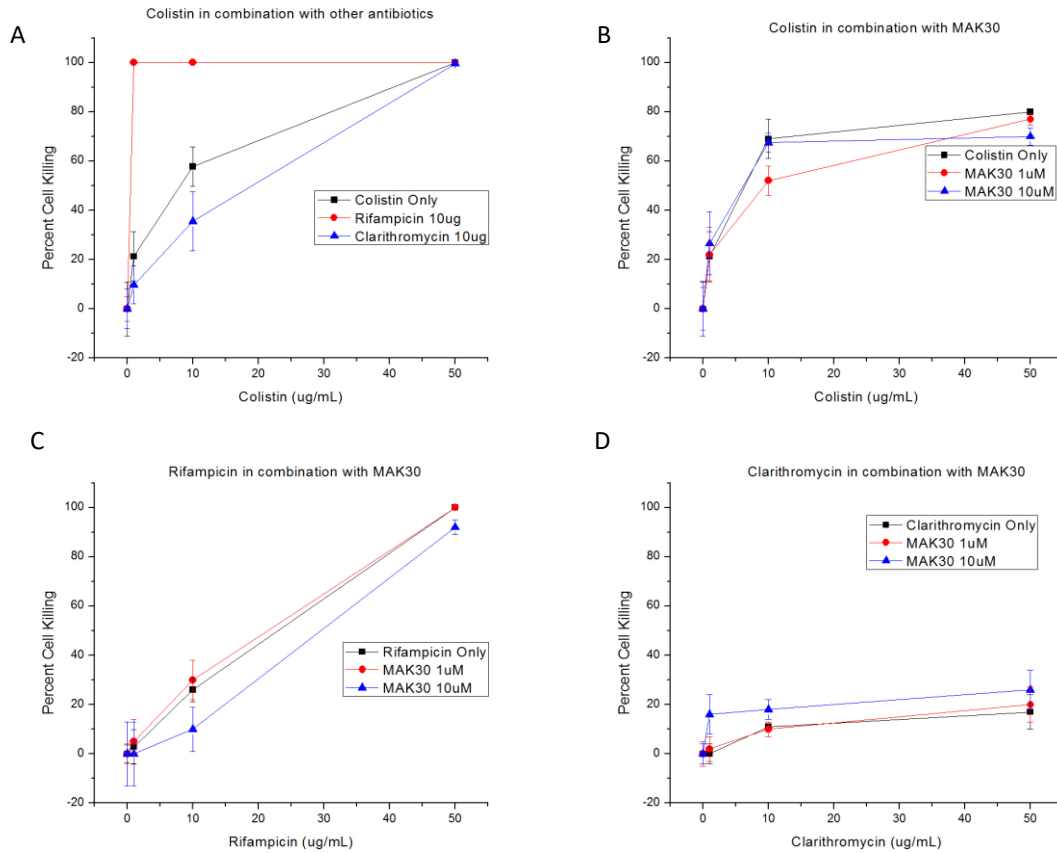


Figure 4-18 Cell killing curves were generated for rifampicin and clarithromycin in combination with colistin (A). Colistin and rifampicin showed significant synergy in cell killing while clarithromycin had no noticeable effect. MAK30 had no noticeable effect in combination with colistin (B), rifampicin (C), or clarithromycin (D).

4.6 Conclusions and Discussion

This contribution describes the discovery and characterization of a series of peptide probes that show selective binding to colistin-resistant bacterial pathogens. Utilizing an innovative phage display platform, which incorporates a pair of dynamic covalent warheads (APBA) for binding cell surface amines, we show that APBA-dimer peptides can be readily identified to differentiate colistin-resistant and colistin-sensitive bacterial pathogens. With proper fluorophore labeling, the peptide probes are found to stain colistin-resistant bacteria at sub-to-low micromolar concentrations, while minimal fluorescence is observed for the colistin-susceptible controls. Importantly, the peptides' capability to stain bacterial cells is unaffected by the presence of BSA, which projects promise for their use as diagnostic tools of colistin resistance. The low micromolar potency of the APBA-dimer peptides is remarkable as previous efforts that panned non-chemically modified phage libraries against live bacteria yielded only millimolar binders at the best.¹⁷ This much enhanced potency of the APBA-dimer peptides highlights the benefit of chemical modification, more specifically the use of dynamic covalent binding motifs,³¹ in the development of functional peptides.

It is interesting to note that the peptide probes, regardless of which screen they are identified from, elicited a similar pattern in terms of fluorescence staining of several bacterial species. In particular, the 497 strain of *K. pneumoniae* appears to be the most attractive to both SEC18 and SEC5, even though SEC5 is a peptide identified for a screen against *A. baumannii*. Furthermore, while SEC18 did show preferential binding to its target bacterial strain (497 *K. pneumoniae*), SEC5 afforded comparable fluorescence

staining to the 493 strain *E. coli* as to its target strain *A. baumannii* (EGA408). This lack of discrimination of these bacterial species sharply contrasts the robust selectivity of these peptides for colistin-resistant bacteria, which suggest that our peptide probes recognize certain shared features of colistin-resistant bacterial pathogens. As indicated by earlier publications^{27,29} as well as our own lipid analysis data (**Figures 4-11, 4-14, 4-16**) lipid modification in the form of phosphoethanolamine (PE) addition presents a universal mechanism for colistin resistance. Our data presented in this contribution documents a robust correlation between the extent of PE modification and the fluorescence intensity caused by peptide binding. Collectively, our findings can be best rationalized with the notion that the peptide probes recognize colistin-resistant bacteria via the PE modified lipids, although more mechanistic studies are needed to fully validate this hypothesis. Although our peptide probes elicited effective staining for all colistin-resistant bacterial strains, the 497 strain of *K. pneumoniae* appears unique as it consistently gives stronger fluorescence than other colistin-resistant species. We reason that this stronger staining of the 497 strain may arise from additional features of its cell surface. Further elucidation on this point may yield peptide probes that not only detect colistin-resistance, but also reveal species information of the pathogenic bacteria.

Unfortunately, MAK30 was unsuccessful in combination therapies with the antibiotics tested. Though MAK30 showed significant binding at 1 μ M concentrations in both microscopy and FACS experiments it failed to make an impact in cell killing assays at even 10 μ M concentrations. It is possible that the reversible covalent nature of MAK30 was not enough to perturb the membrane in any way to synergize with any of the

antibiotics tested. The conditions under which these peptides were identified made no attempt to select for membrane perturbing peptides so perhaps it is not surprising that MAK30 was unsuccessful.

4.7 Experimental Protocols

4.7.1 Materials and Instrumentation

The Ph.D.-C7C Phage Display Peptide Library Kit and the *E. coli* K12 ER2738 strain for phage amplification were purchased from New England Biolabs. All ER2738 cultures were grown in the presence of 20 µg/mL tetracycline. Chemical reagents for peptide synthesis were purchased from various vendors and used as received. Human serum was purchased from Fisher Scientific and diluted in RPMI medium. *Mcr-1* positive strains, 350, 493, 494, 495, and 497 as well as *mcr-1* negative strains 348, and 347 were obtained from the Center for Disease Control (<https://www.cdc.gov/arisolatebank/Panel/PanelDetail?ID=10>). Wild type *A. baumannii* 17978 and mutant strain EGA-408 were obtained from the laboratory of Professor Tim van Opijnen

4.7.2 Peptide Synthesis

Solid phase peptide synthesis was performed on a rink amide resin using Fmoc chemistry. An alloc-protected diaminopropionic acid residue was installed at the C-terminus for on-resin coupling of a fluorophore, followed by a triple glycine linker and the peptide hit sequence at the N-terminus. 5(6)-carboxyfluorescein or 5(6)-tetramethylrhodamine were conjugated to the peptide on resin by first removing the alloc protecting group with tetrakis(triphenylphosphine)palladium(0) and phenylsilane in

DCM followed by subsequent HBTU-mediated amide bond coupling in 0.4 M NMM/DMF. The peptides were cleaved off resin and globally deprotected with reagent B (88% TFA, 5% H₂O, 2% triisopropylsilane, 5% phenol). Crude peptides were obtained via ether precipitation and purified by RP-HPLC. For cysteine alkylation, each peptide hit was treated with 3 equivalents of APBA-IA in the presence of TCEP (2 eq) in 2 M NMM/DMF for 3 hours and purified via RP-HPLC. All peptides were characterized with LC-MS to confirm their identities and excellent purities (>95%).

4.7.3 APBA-Dimer Library Panning Against Whole Cells.

The synthesis of the APBA-dimer library was described previously.³ All strains were grown to an OD₆₀₀ ≈ 1.0 (~1 × 10⁹ cfu/mL) in LB medium. The cells (1 mL) were washed with chilled PBS containing 0.05% Tween (PBST) twice and resuspended in PBS (pH 7.4) with 10 mg/mL BSA present. The APBA-labeled phage library (~1 × 10¹⁰ pfu) was added to the cell suspension and allowed to incubate on ice for 1 h. The cells were washed three times with PBST and three times with PBS to remove unbound phage. Cell-bound phage were incubated with 200 μL elution buffer (Glycine-HCl, pH 2.2, 1 mg/mL) for 15 min followed by centrifugation of the cells. The supernatant was removed and neutralized with 150 μL Tris-HCl (pH 9.1). All Eppendorf tubes utilized in the panning procedure were blocked with 10 mg/mL BSA before use. Centrifugation of cells was performed at 5000 rcf for 5 min. The eluted bound phage solution was added to early log phase ER2738 and amplified for 4.5 h followed by precipitation to isolate the amplified phage. The amplified phage were labeled with APBA-IA and subjected to the next round of panning. The phage titer was calculated before and after each round of panning to determine the input and

output population. Individual phage colonies from each round of panning were amplified in ER2738. Phage DNA was isolated using a Qiagen miniprep kit and sent for sequencing analysis by Eton Bioscience, Inc.

4.7.4 Fluorescence Microscopy

Each bacterial strain was grown to an $OD_{600} \approx 1.0$, washed and diluted with PBS (pH 7.4). The cells ($\sim 1 \times 10^9$ cfu/mL) were incubated with various concentrations of TAMRA- labeled peptide with BSA or human serum in PBS for 1 h. White light and fluorescent images were obtained on the Zeiss microscope equipped with filter set 20 HE (excitation: BP 546/12, emission: BP 607/80) suitable for detection of TAMRA fluorescence. Images were captured using the 100X oil immersion objective with a 1 s exposure time. All images were processed consistently using ImageJ software.

4.7.5 Flow Cytometry Analysis

Each bacterial strain was grown to an $OD_{600} \approx 0.5$, washed and diluted with PBS (pH 7.4). The cells ($\sim 1 \times 10^7$ cfu/mL) were incubated with various concentrations of FAM-labeled peptide with 1 mg/mL BSA in PBS. After incubation for 1 h, samples were subjected to flow cytometry analysis. Data obtained were analyzed via BD FACSDiva software and median fluorescent values were computed from the generated histograms. All flow cytometry experiments were repeated and generated consistent results .

4.7.6 Mass Spec Analysis of LPS

Lipid A was extracted from cell pellets using an ammonium hydroxide-isobutyric acid-based procedure. Briefly, approximately 5 ml of cell culture was pelleted and resuspended in 400 μ l of 70% isobutyric acid and 1 M ammonium hydroxide (5:3

[vol/vol]). Samples were incubated for 1 hr at 100°C and centrifuged at 2,000 × *g* for 15 min. Supernatants were collected, added to nanopure water (1:1 [vol/vol]), snap-frozen on dry ice, and lyophilized overnight. The resultant material was washed twice with 1 ml methanol, and lipid A was extracted using 100 µl of a mixture of chloroform, methanol, and water (3:1:0.25 [vol/vol/vol]). Quantification of LPS isolates for all *E. coli*, *K. pneumoniae*, and *A. baumannii* strains was done using an Agilent 6220 TOF mass spectrometer. Samples were run in duplicates and relative intensities of modified and unmodified LPS were compared to determine percent PE modified.

4.7.7 Cell Killing Assay

A single colony of *E. coli* (493) was selected from an LB agar plate and grown overnight in LB broth, incubating at 37°C with agitation. In the morning, a small aliquot was taken and diluted 100 times in fresh broth. The OD600 was monitored until it reached ~0.6. This culture was centrifuged (4000 rpm, 5 min) and washed with PBS buffer (pH 7.4) two times. The final cell solution was diluted to ~5 × 10⁵ cfu/mL in fresh media. In a sterile 96-well plate, 200 µL of cell suspension was added to each well. To each well, 125µM peptide in DMSO (2 µL) were added in triplicate. The plate was incubated for two hours at 37°C. Aliquots of each sample (10 µL) was diluted into fresh buffer (990 µL) and mixed before being spread on LB agar plates. The plates were allowed to incubate at 37°C overnight. Individual colonies were counted on each plate and triplicates were averaged for each data point. To calculate a percent viability, the average number of colonies for each peptide was divided by the average number of colonies for blank samples and

multiplying by 100. Percent killing was then considered to be the percent viability subtracted from 100.

4.8 References

1. Blair, J. M.; Webber, M. A.; Baylay, A. J.; Ogbolu, D. O.; Piddock, L. J. (2015) Molecular mechanisms of antibiotic resistance. *Nat Rev Microbiol*, 13, 42-51.
2. Peterson, L. R. (2009) Bad Bugs, No Drugs: No ESCAPE Revisited. *Clinical Infectious Diseases*, 49, 992-993.
3. Li, J.; Nation, R. L.; Turnidge, J. D.; Milne, R. W.; Coulthard, K.; Rayner, C. R.; Paterson, D. L. (2006) Colistin: the re-emerging antibiotic for multidrug-resistant Gram-negative bacterial infections. *Lancet Infect Dis*, 6, 589-601.
4. Rossi, F.; Girardello, R.; Cury, A. P.; Di Gioia, T. S. R.; Almeida, J. N. d.; Duarte, A. J. d. S. (2017) Emergence of colistin resistance in the largest university hospital complex of São Paulo, Brazil, over five years. *The Brazilian Journal of Infectious Diseases*, 21, 98-101.
5. Liu, Y. Y.; Wang, Y.; Walsh, T. R.; Yi, L. X.; Zhang, R.; Spencer, J.; Doi, Y.; Tian, G.; Dong, B.; Huang, X.; Yu, L. F.; Gu, D.; Ren, H.; Chen, X.; Lv, L.; He, D.; Zhou, H.; Liang, Z.; Liu, J. H.; Shen, J. (2016) Emergence of plasmid-mediated colistin resistance mechanism MCR-1 in animals and human beings in China: a microbiological and molecular biological study. *Lancet Infect Dis*, 16, 161-8.
6. Cheng, Y. H.; Lin, T. L.; Pan, Y. J.; Wang, Y. P.; Lin, Y. T.; Wang, J. T. (2015) Colistin resistance mechanisms in *Klebsiella pneumoniae* strains from Taiwan. *Antimicrob Agents Chemother*, 59, 2909-13.
7. Velkov, T.; Thompson, P. E.; Nation, R. L.; Li, J. (2010) Structure--activity relationships of polymyxin antibiotics. *J Med Chem*, 53, 1898-916.
8. Steinbuch, K. B.; Fridman, M. (2016) Mechanisms of resistance to membrane-disrupting antibiotics in Gram-positive and Gram-negative bacteria. *Medchemcomm*, 7, 86-102.

9. Needham, B. D.; Trent, M. S. (2013) Fortifying the barrier: the impact of lipid A remodelling on bacterial pathogenesis. *Nature Reviews Microbiology*, 11, 467.
10. Moffatt, J. H.; Harper, M.; Harrison, P.; Hale, J. D.; Vinogradov, E.; Seemann, T.; Henry, R.; Crane, B.; St Michael, F.; Cox, A. D.; Adler, B.; Nation, R. L.; Li, J.; Boyce, J. D. (2010) Colistin resistance in *Acinetobacter baumannii* is mediated by complete loss of lipopolysaccharide production. *Antimicrob Agents Chemother*, 54, 4971-7.
11. Boll, J. M.; Crofts, A. A.; Peters, K.; Cattoir, V.; Vollmer, W.; Davies, B. W.; Trent, M. S. (2016) A penicillin-binding protein inhibits selection of colistin-resistant, lipooligosaccharide-deficient *Acinetobacter baumannii*. *Proc Natl Acad Sci U S A*, 113, E6228-E6237.
12. Powers, M. J.; Trent, M. S. (2018) Expanding the paradigm for the outer membrane: *Acinetobacter baumannii* in the absence of endotoxin. *Molecular Microbiology*, 107, 47-56.
13. Simpson, B. W.; Trent, M. S. (2019) Pushing the envelope: LPS modifications and their consequences. *Nat Rev Microbiol*, 17, 403-416.
14. Smith, G. P.; Petrenko, V. A. (1997) Phage Display. *Chemical Reviews*, 97, 391-410.
15. Hamzeh-Mivehroud, M.; Alizadeh, A. A.; Morris, M. B.; Church, W. B.; Dastmalchi, S. (2013) Phage display as a technology delivering on the promise of peptide drug discovery. *Drug Discov Today*, 18, 1144-57.
16. Sidhu, S. S.; Koide, S. (2007) Phage display for engineering and analyzing protein interaction interfaces. *Current Opinion in Structural Biology*, 17, 481-487.
17. (Huang, J. X.; Bishop-Hurley, S. L.; Cooper, M. A. (2012) Development of anti-infectives using phage display: biological agents against bacteria, viruses, and parasites. *Antimicrob Agents Chemother*, 56, 4569-82.
18. Gasanov, U.; Koina, C.; Beagley, K. W.; Aitken, R. J.; Hansbro, P. M. (2006) Identification of the insulin-like growth factor II receptor as a novel receptor for binding and invasion by *Listeria monocytogenes*. *Infect Immun*, 74, 566-77.

19. Heinis, C.; Rutherford, T.; Freund, S.; Winter, G. (2009) Phage-encoded combinatorial chemical libraries based on bicyclic peptides. *Nat Chem Biol*, 5, 502-7.
20. Ng, S.; Jafari, M. R.; Matochko, W. L.; Derda, R. (2012) Quantitative synthesis of genetically encoded glycopeptide libraries displayed on M13 phage. *ACS Chem Biol*, 7, 1482-7.
21. Liu, C. C.; Mack, A. V.; Brustad, E. M.; Mills, J. H.; Groff, D.; Smider, V. V.; Schultz, P. G. (2009) Evolution of Proteins with Genetically Encoded "Chemical Warheads". *J Am Chem Soc*, 131, 9616-9617.
22. Tharp, J. M.; Hampton, J. T.; Reed, C. A.; Ehnbohm, A.; Chen, P.-H. C.; Morse, J. S.; Kurra, Y.; Pérez, L. M.; Xu, S.; Liu, W. R. (2020) An amber obligate active site-directed ligand evolution technique for phage display. *Nature communications*, 11, 1392.
23. Adaligil, E.; Patil, K.; Rodenstein, M.; Kumar, K. (2019) Discovery of Peptide Antibiotics Composed of d-Amino Acids. *ACS Chem Biol*, 14, 1498-1506.
24. McCarthy, K. A.; Kelly, M. A.; Li, K.; Cambray, S.; Hosseini, A. S.; van Opijnen, T.; Gao, J. (2018) Phage Display of Dynamic Covalent Binding Motifs Enables Facile Development of Targeted Antibiotics. *J Am Chem Soc*, 140, 6137-6145.
25. Bandyopadhyay, A.; McCarthy, K. A.; Kelly, M. A.; Gao, J. (2015) Targeting bacteria via iminoboronate chemistry of amine-presenting lipids. *Nature communications*, 6, 6561.
26. Bandyopadhyay, A.; Gao, J. (2016) Iminoboronate-Based Peptide Cyclization That Responds to pH, Oxidation, and Small Molecule Modulators. *J Am Chem Soc*, 138, 2098-2101.
27. Liu, Y. Y.; Chandler, C. E.; Leung, L. M.; McElheny, C. L.; Mettus, R. T.; Shanks, R. M. Q.; Liu, J. H.; Goodlett, D. R.; Ernst, R. K.; Doi, Y. (2017) Structural Modification of Lipopolysaccharide Conferred by *mcr-1* in Gram-Negative ESKAPE Pathogens. *Antimicrob Agents Chemother*, 61.

28. Chen, H. D.; Groisman, E. A. (2013) The biology of the PmrA/PmrB two-component system: the major regulator of lipopolysaccharide modifications. *Annu Rev Microbiol*, 67, 83-112.
29. Beceiro, A.; Llobet, E.; Aranda, J.; Bengoechea, J. A.; Doumith, M.; Hornsey, M.; Dhanji, H.; Chart, H.; Bou, G.; Livermore, D. M.; Woodford, N. (2011) Phosphoethanolamine modification of lipid A in colistin-resistant variants of *Acinetobacter baumannii* mediated by the pmrAB two-component regulatory system. *Antimicrob Agents Chemother*, 55, 3370-9.
30. Arroyo, L. A.; Herrera, C. M.; Fernandez, L.; Hankins, J. V.; Trent, M. S.; Hancock, R. E. (2011) The pmrCAB operon mediates polymyxin resistance in *Acinetobacter baumannii* ATCC 17978 and clinical isolates through phosphoethanolamine modification of lipid A. *Antimicrob Agents Chemother*, 55, 3743-51.
31. Bandyopadhyay, A.; Gao, J. (2016) Targeting biomolecules with reversible covalent chemistry. *Curr Opin Chem Biol*, 34, 110-116.
32. MacNair, C. R., Stokes, J. M., Carfrae, L. A., Fiebig-Comyn, A. A., Coombes, B. K., Mulvey, M. R., & Brown, E. D. (2018). Overcoming mcr-1 mediated colistin resistance with colistin in combination with other antibiotics. *Nature communications*, 9(1), 1-8.

Chapter 5

Conclusions: Unique Targets Require Innovative Screening Strategies

Conventional targets for drug and probe development are typically large proteins with a clear binding pocket for a small molecule inhibitor to bind. However, when looking to develop probes for unique targets such as the ones previously discussed in this work, innovative and alternative approaches must be used to generate success. It is no longer changing and modifying a small molecule to fit a specific binding pocket in a large protein, but instead developing selective probes around a small unchanging target.

PS containing membranes was the first unique target that started this process. Nature has been able to successfully target PS by evolving large proteins capable of selectively binding to PS, such as annexin and lactadherin.^{1,2} But these large proteins have a number of disadvantages and limitations for therapeutic applications. For example, they are unstable, difficult to produce and scale up, and expensive to manufacture. These disadvantages could be overcome with small, stable peptides. Prior work in the Gao lab resulted in the successful design of small peptide probes that mimicked the lactadherin-binding pocket. This peptide was effective due to its rigid cyclic structure and conformationally preorganized residues.³

In the present work, a new approach to discover novel potent probes utilizing high throughput screening methods was undertaken. The short cyclic C7C library of phage display was reasoned to be an ideal choice for screening against PS as its naturally cyclic structure could be taken advantage of in a similar manner to cLac. The peptides identified by screening against PS were moderately successful. They were able to bind to PS containing liposomes but failed to recognize PS in mammalian membranes. This strategy of high throughput screening of a simple cyclic library was able to yield target specific

probes but lacked the necessary potency to be effective under biologically relevant conditions. Future work would improve selection conditions to increase potency of peptide probes.

An ideal candidate to increase potency of our peptide probes was the APBA chemistry being developed in our lab. This chemistry could be used in combination with our phage display libraries to target amine-presenting lipids such as Lys-PG, which is expressed on the surface of pathogenic *S. aureus*.⁴ APBA and its derivatives could readily conjugate at low millimolar concentrations with evidence of additional potency through multivalent interactions. Furthermore, conjugation of APBA to cationic peptide Hlys demonstrated the potential for synergistic binding capabilities with Hly-AB1.⁵ The cationic peptide portion was able to direct binding to a specific target with the APBA moiety increasing potency. Even in this synergistic manner Hly-AB1 required relatively high concentrations of 100 μ M or higher to bind. This all led to the generation of the novel APBA dimer phage display library. This library effectively combined the high throughput screening platform capable of identifying peptides for a specific target with the potency of multivalent APBA head groups. The new APBA dimer phage display library was screened against Lys-PG and successfully identified peptides specific and potent for gram-positive bacteria *S. aureus*. The yielded peptide binders were ~100 fold more potent than Hlys-AB1 with binding affinities as low as 1 μ M. The peptides identified in this screen were selected against lipids deposited in wells but remained potent enough to be effective on whole cells overcoming the previous downfalls of the aforementioned PS screen.

Continued interrogation of these peptides showed minimal interaction with other gram-positive bacteria like *B. subtilis* or *S. pyogenes* demonstrating their specificity. However, the peptides did lose 90% of their binding ability in the presence of BSA. This was a problem as if the peptides were to be used in a clinically relevant setting, they would need to be effective with competing proteins present in the media. Although these peptides ultimately failed at being specific enough for biologically relevant purposes, it forced us to rethink our experimental setup. Future work would involve overcoming BSA inhibition. This could be accomplished by optimizing the screening conditions to identify optimized binders.

The second generation of Lys-PG targeting peptides (KAM5) was able to overcome the previous pitfalls identified in MAK7. Rather than screening in 96 well plates the screen was carried out directly against whole cells. This proved to be effective at identifying binders for cell lines of interest as opposed to a specific lipid. In addition to whole screening, 10mg/mL BSA was incorporated in the media during the screening process. By incorporating BSA during the screening process it eliminated peptides that bind preferentially to BSA over the target of interest. This optimized protocol identified KAM5, a peptide that increased binding to *S. aureus* cells with the addition of BSA to the media. KAM5 highlights the importance of setting up the appropriate screening conditions to yield potent specific peptides.

While screening directly against live cells is effective, it does have a major limitation. There is a serious lack of knowledge of the target the peptides are binding to. We can only speculate as to the target of these peptides potentially being Lys-PG. Probing

the binding mechanism of KAM5 could prove to be beneficial and elucidate the mechanistic interactions of the peptide. One method to explore this mechanism would be to generate Mprf-knockout strains that don't have the ability to produce Lys-PG. Lys-PG would be indirectly confirmed as the target of KAM5 if a reduction in staining is observed. Target identification would be an important aspect to explore, as it would elucidate the peptides potential for application to other strains. KAM5 could then potentially be used for all strains expressing Lys-PG giving KAM5 a broader scope for application.

Identifying strain specific peptide probes is only one application of the APBA dimer library. The previous screening applications have shown this library to be a powerful tool in peptide discovery demonstrating its versatility in identifying other meaningful targets. Our attention switched from gram-positive bacteria to gram-negative with the goal to target ESKAPE pathogens specifically colistin resistant bacteria.

Colistin resistance from *mcr-1* is a growing concern due to its rapid spread.⁶ The addition of PE to lipid A on the outer surface of the cell presents an ideal candidate for our amine-targeting library. The previously optimized screening strategy was used for screening against *mcr-1* positive strains. Separately, peptides were identified for *E. coli*, *K. pneumoniae*, and *A. baumannii*, all strains that showed some level of colistin resistance. Exploring this further, these peptides were tested for their ability to broadly bind to *mcr-1* containing strains. Of the strains tested MAK30 showed significantly more affinity to four *mcr-1* positive strains compared to the two *mcr-1* negative strains. Similarly, SEC19 showed selectivity for *K. pneumoniae* strains that were *mcr-1* positive and SEC5 showed

selectivity for PmrAB mutated strains. Binding affinity of these peptides appeared to be correlated with MIC's of the strains. Brighter binding was observed in strains with higher MIC values and those with sub $\mu\text{g/mL}$ MIC's showed minimal peptide binding even at high concentrations of MAK30. To probe this relationship further mass spec analysis of LPS isolates was conducted. PE modified LPS isolates produced the same trend correlating PE modifications of LPS, colistin resistance, and MAK30 binding. Correlating peptide binding to colistin resistance could be a useful tool in diagnosing and treating gram-negative infections. By establishing a minimum threshold of peptide binding that would act as an indication of colistin resistance, an *mcr-1* positive infection could be readily diagnosed using these peptides.

As with the previously identified probes, there are limitations to what these peptides can achieve. It was hypothesized that these *mcr-1* probes might be able to restore the activity of colistin. Capping the amine on PE might allow the highly positively charged colistin to once again perturb the membrane but unfortunately that was not possible. Future selections could utilize this knowledge to set up screens to find cell membrane perturbing peptides that work in combination with colistin.

As with every selection it is important to look back and reevaluate the selection process, in doing so we can improve the next selection. The first selection used a relatively simple cyclic library for a unique and difficult target. Improving the library to a covalent dimer library allowed for potent probes however, they still had trouble with BSA. Improving the selection conditions overcame BSA inhibition. This enhanced phage platform was then ideally suited to identify probes to the rising global pandemic of *mcr-*

1 colistin resistance. The continued refinement of this selection process implies there is no limit to what these APBA libraries can achieve.

It is intriguing to consider the numerous modifications that could be easily attached to the C7C library. This potent dimer library proved to be an excellent tool for peptide discovery, but other reversible covalent libraries could potentially be made. The original screen against PS utilized the C7C library taking advantage of its cyclic rigid structure. Combining the advantages of a cyclic library with a reversible covalent moiety has the potential to identify peptides for new, unique targets. These novel libraries are currently being explored in our lab and show significant promise.

In conclusion, the work described in this dissertation clearly demonstrates the power and utility of these APBA libraries. Enhanced reversible covalent screening is a unique strategy capable of producing potent peptide probes. With the rise of antibiotic resistant ESKAPE pathogens these unique strategies will become key in combating and overcoming these diseases. *Mcr-1* was first reported in 2016 and to date the probes listed in this work are the only probes capable of detecting these colistin resistant strains. This dearth in probes has led to many unanswered questions regarding the extent of PE modification in these cell lines. Hopefully with the peptides reported here more research can be done to explore *mcr-1* positive cell lines.

5.1 References

1. Zhang, G., Gurtu, V., Kain, S. R., & Yan, G. (1997). Early detection of apoptosis using a fluorescent conjugate of annexin V. *Biotechniques*, 23(3), 525-531.
2. Shi, J., Heegaard, C. W., Rasmussen, J. T., & Gilbert, G. E. (2004). Lactadherin binds selectively to membranes containing phosphatidyl-L-serine and increased curvature. *Biochimica et Biophysica Acta (BBA)-Biomembranes*, 1667(1), 82-90.
3. Zheng, H., Wang, F., Wang, Q., & Gao, J. (2011). Cofactor-free detection of phosphatidylserine with cyclic peptides mimicking lactadherin. *Journal of the American Chemical Society*, 133(39), 15280-15283.
4. Killee, E., Pokorny, A., Yeaman, M. R., & Bayer, A. S. (2010). Lysyl-phosphatidylglycerol attenuates membrane perturbation rather than surface association of the cationic antimicrobial peptide 6W-RP-1 in a model membrane system: implications for daptomycin resistance. *Antimicrobial agents and chemotherapy*, 54(10), 4476-4479.
5. Bandyopadhyay, A., McCarthy, K. A., Kelly, M. A., & Gao, J. (2015). Targeting bacteria via iminoboronate chemistry of amine-presenting lipids. *Nature communications*, 6(1), 1-9.
6. Wang, R., van Dorp, L., Shaw, L. P., Bradley, P., Wang, Q., Wang, X., ... & Dorai-Schneiders, T. (2018). The global distribution and spread of the mobilized colistin resistance gene mcr-1. *Nature communications*, 9(1), 1-9.

Additional Data

Chapter 6

Targeting Proteins with APBA Libraries

6.1 Introduction

6.1.1 Expanding the Scope to Proteins

Phage display is a well-characterized screening platform that has long been used to identify ligands for a number of different targets.¹ One of the more traditional targets of phage display is proteins. Many proteins present an ideal target for phage display due to their rigid structure and defined binding pockets.² Numerous peptides have been identified by phage display to have nanomolar to micromolar affinities for their targets of interest, often bound to the well-defined binding pocket.²

To expand the scope of the previously reported³ APBA dimer phage display library, a novel mono APBA cyclic library was created using similar methodology; the new library leveraged a small molecule APBA derivative containing two chloroacetamide groups. With two chloroacetamide reactive handles, the small molecule would staple the C7C peptide, restoring its rigid preorganized structure, and imparting the unique reversible covalent functionality to these libraries. We surmised that traditional protein targeting could benefit from our enhanced, reversible covalent screening platforms. Specifically, we envisioned that these libraries, the APBA linear dimer and the APBA cyclic monomer, would not be limited to the binding pocket of proteins, but rather, could efficiently bind between exposed lysines throughout the protein. Using these APBA reversible covalent strategies, we sought to identify novel binders for well-characterized proteins of interest.

One particular protein of interest, human lysozyme presents ideal binding opportunities for an APBA peptide. Human lysozyme is a 14.4 kDa protein that plays an important role in the human body's defense against bacterial infections.⁴ The primary

action of human lysozyme is to cleave the 1-4 glycosidic bond of N-acetylglucosamine (NAG) and N-acetylmuramic acid (NAM) polysaccharide, which is present on the peptidoglycan of gram-positive bacterial cells.⁵ This cleavage compromises the integrity of the bacterial cell wall, ultimately leading to lysis of the bacteria. Structurally, human lysozyme has a fairly simple composition; it consists of seven helices and a short, three-stranded beta sheet, but more importantly it contains a modest lysine content.⁶ The five relatively exposed lysine residues highlighted in red (**Figure 6-1**) offer optimal binding opportunities for an APBA containing peptide.

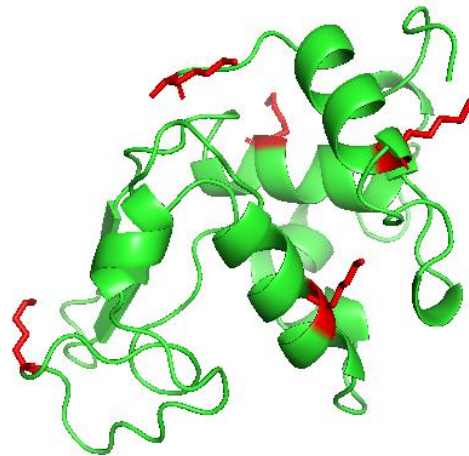


Figure 6-1 3D structure of human lysozyme protein with lysine residues highlighted in red.⁷

Sortase A (SrtA), a transpeptidase from *S. aureus*, was identified as an additional screening target. This enzyme is involved in cell wall generation in gram-positive bacteria. SrtA cleaves proteins in the LPXT-G motif, and then catalyzes the formation of an amide bond between the new C-terminal threonine and the cell wall pentaglycine cross-bridge.⁸ The structure of SrtA has a unique fold, with the core of the protein being an eight-strand beta barrel that has 19 lysine residues located throughout the protein.⁹ These lysines are

easily accessible on the surface of SrtA, and anticipated to provide plenty of free amines for coordination with APBA libraries.

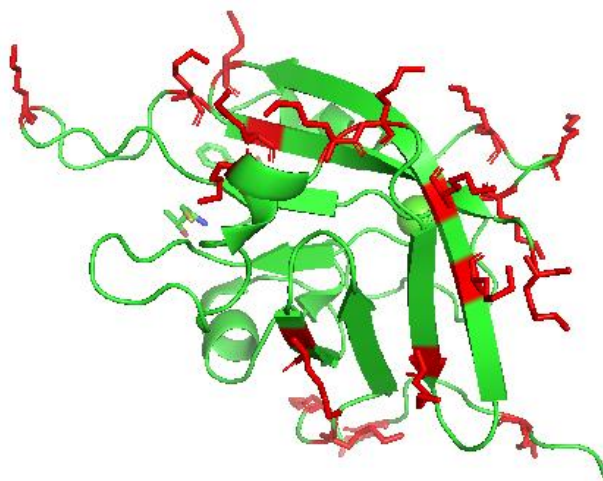


Figure 6-2 3D structure of Sortase A protein with lysine residues highlighted in red.⁹

6.2 Targeting Proteins

6.2.1 Screening APBA Libraries Against Protein Targets

Three libraries were used for screening against the identified protein targets of interest. As a control, the unmodified C7C library was used in parallel with the mono APBA cyclic library and APBA dimer library. Considering the novelty in screening reversible covalent libraries against protein targets, two different strategies were employed: physical deposition into 96 well plates, and immobilization on resin. For the physical deposition approach, human lysozyme was deposited into 96 well plates for three rounds of panning with all three libraries. Alternatively, for the immobilization strategy, SrtA was modified with biotin-NHS to selectively label the N-terminus. SrtA now with an installed biotin handle, could be captured by streptavidin resin for screening and peptide characterization purposes. Previous screens of the dimer library and the unmodified

library were performed by Wenjian Wang, thus, only the mono APBA cyclic library was screened here.

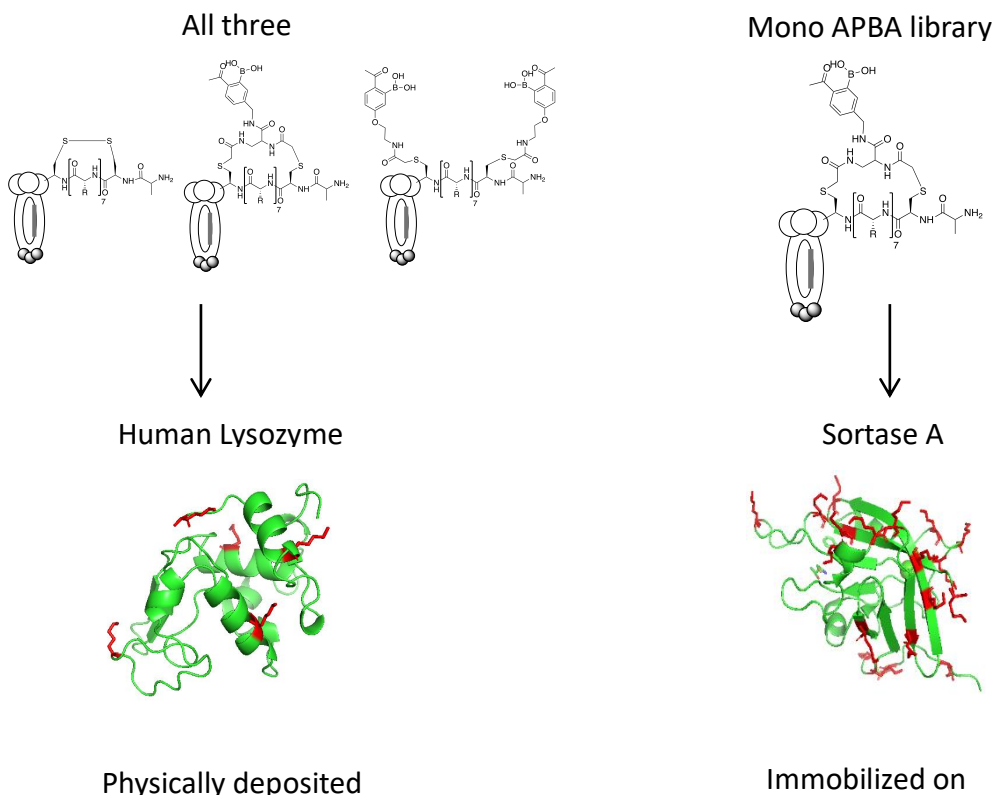


Figure 6-3 Summary of screens performed and the manner of immobilization of each protein target.

6.2.2 Creating Novel Mono APBA Cyclic Libraries

The APBA dimer library proved to be successful in identifying potent binders. Expanding on reversible covalent libraries, we sought to generate a novel mono APBA cyclic library capable of reversible covalent interactions with a preorganized rigid structure. With a rigid structure, peptides would have a reduced entropic cost to binding, and could potentially have greater binding affinities to various targets of interest. To this aim, we created a novel mono APBA small molecule containing two chloroacetamide

groups for reacting with free cysteines (**Figure 6-4A**). This molecule would generate the cyclic peptide structure while also providing reversible covalent interactions. As was necessary for the dimer APBA library, evidence was needed to ensure phage were labeled with the APBA staple. To confirm, we repeated the pulse chase experiment, as previously described, with an additional step to ensure a 1:1 reaction between the peptide displayed on the PIII protein and the APBA staple (**Figure 6-4C**) —if the peptide and staple react in a 1:2 manner, meaning a separate small molecule were present at each cysteine (**Figure 6-4D**), it would not form a cyclic structure, leaving two free chloroacetamides on the peptide. A biotin cysteamine (**Figure 6-4B**) was made to ensure peptide cyclization occurred and no free chloroacetamides remained on phage-displayed peptides. The free thiol in biotin cysteamine caps any unreacted chloroacetamides, allowing for pull down during the streptavidin capture assay. Combining this method with the previous techniques for the pulse chase assay, would allow us to quantify the extent of peptide stapled correctly on phage.

As illustrated by the pull-down assay (**Figure 6-4E**), only the positive control labeled by biotin iodoacetamide showed significant capture by streptavidin resin; all other samples showed minimal capture, indicating peptides on phage were successfully stapled with the APBA linker. This data confirmed that the phage library was suitable for screening purposes.

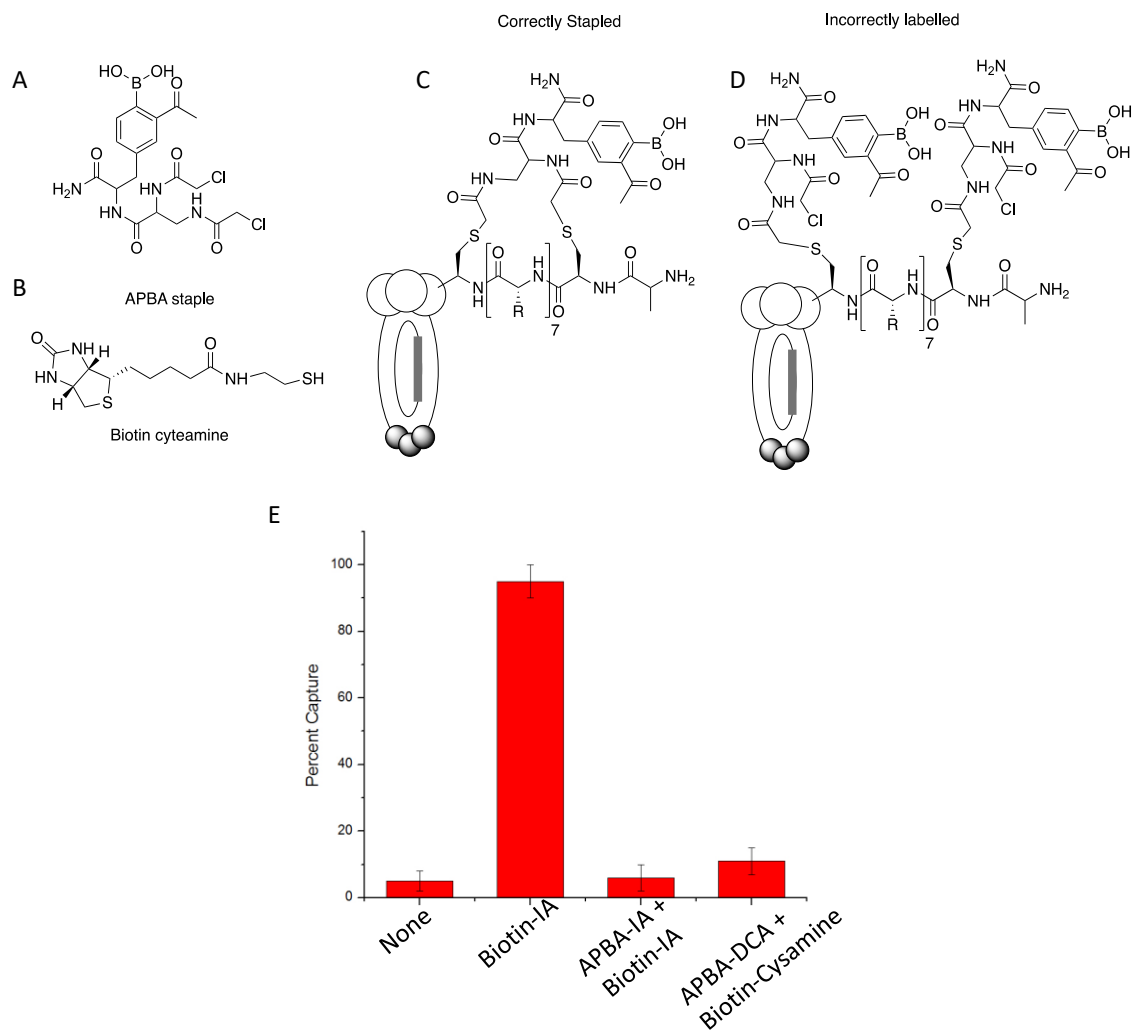


Figure 6-4 Confirmation of Mono APBA library. APBA-DCA (staple) used for creating mono APBA cyclic library (A) and Biotin cysteamine (B) for confirming proper cyclization of peptide library. Correctly stapled peptide library (C) will contain one APBA-DCA reacted with both cysteines whereas the incorrectly modified library (D) would contain two APBA-DCA molecules attached at the free cysteines. Free dichloroacetamide residues in (D) will react with biotin cysteamine (B) and be captured by streptavidin. The results of the streptavidin capture assay (E) show high capture with positive control Biotin-IA but minimal capture with APBA-IA+Biotin-IA or APBA-DCA+Biotin cysteamine, indicating the library is correctly stapled (C).

6.2.3 Human Lysozyme Screen and Peptide Characterization

To perform human lysozyme screening, three rounds of affinity selection were executed in the presence of 10mg/mL BSA with an input population of $\sim 10^{11}$ plaque forming units (pfu) with extensive washing to eliminate nonbinders. Sequences were isolated after rounds 2 and 3 of panning to identify repeating sequences for peptide characterization. As summarized in **Table 6-1**, the unmodified library produced one peptide, appearing twice in round 2, and the APBA dimer library showed sequence convergence with one sequence (highlighted green) appearing in both rounds 2 and 3.

Table 6-1 Sequences identified for human lysozyme.

Round 2		
C7C unmodified	Mono APBA	APBA Dimer
ACSAASGSLC (2)	ACPVSLNRTC	ACTTSHMDNC (2)
ACFKANYGGC	ACDTRTGWSC	ACNPTEPAFC
ACHTPLSRTC	ACDKSKTTLC	ACRDPIRTTC
Blank (2)	ACPGPRLHC	ACAAPMHRSC
	ACFWGPHDRC	
Round 3		
C7C unmodified	Mono APBA	APBA Dimer
ACIFPFLWNC	ACQMDTRTSC	ACTTSHMDNC (6)
ACAKIGDKIC	ACDQRDDRFC	ACAPNNRLQC
ACHTLQSHMC	ACTDVVRSSC	ACHWKHDLYC
ACNIRPDKYC	ACYPYLSQC	ACHANGKISC
Blank (6)	ACWFH*SVVC	ACASTSCPGC
	ACLGERHQQC	ACNLNPNNSC
	ACTLSPADAC	ACSGAAISVC
	ACAPNNRLQC	ACLSPHSWWC
	ACSGDQLWHC	ACVDPHPRTC
	ACQIKGAIYC	ACPHPSTNAC
	Blank (8)	ACTPGIHHWC

Sequences highlighted in green appeared multiple times for a single screen.

Peptides identified in the unmodified C7C screen and the APBA dimer screen were made via solid phase peptide synthesis, as described previously. Peptides included a triple glycine linker, followed by an alloc-protected Dap residue that was selectively deprotected and labeled with FAM for analysis purposes (**Table 6-2**). For the peptide identified in the C7C unmodified screen, MAK20 was oxidized in PBS pH 7.4 buffer to form the cyclic structure, as would have been present during the screening process. MAK21 was modified with APBA-IA to generate the dimer APBA peptide. In addition to the APBA dimer, MAK21 was reacted with a simple iodoacetamide, denoted as MAK21-IA; this peptide was used as a control to demonstrate the importance of APBA-IA functionality in binding to human lysozyme.

Table 6-2 Peptide sequences for human lysozyme made via SPPS.

Name	Sequence	Calculated Mass m/z	Obs. Mass m/z
MAK20	ACSAASGSLCGGGDap	1483.53 [M+H] ¹⁺	1483.51
MAK21	AC _m TTSHMDNC _m GGGDap	1064.86 [M-2H ₂ O+2H] ²⁺	1064.49
MAK21-IA	AC _{IA} TTSHMDNC _{IA} GGGDap	906.81 [M+2H] ²⁺	906.78

_m indicates the peptide was modified with APBA-IA moieties

_{IA} indicates the peptide was modified with a simple iodoacetamide without any reversible covalent head group

Peptides were then tested for their ability to bind to human lysozyme in two distinct manners: ELISA assay and microscopy. Replicating the conditions used for screening, human lysozyme was deposited into wells and incubated with each peptide at 1μM and 10μM concentrations. After washing away any weak binding interactions, an HRP-conjugated anti-fluorescein antibody was added to detect any remaining peptide

bound to human lysozyme. Interestingly, MAK21 at both 1 μ M and 10 μ M showed significant binding to the protein, while MAK21-IA and MAK20 showed minimal ELISA signal (Figure 6-5A).

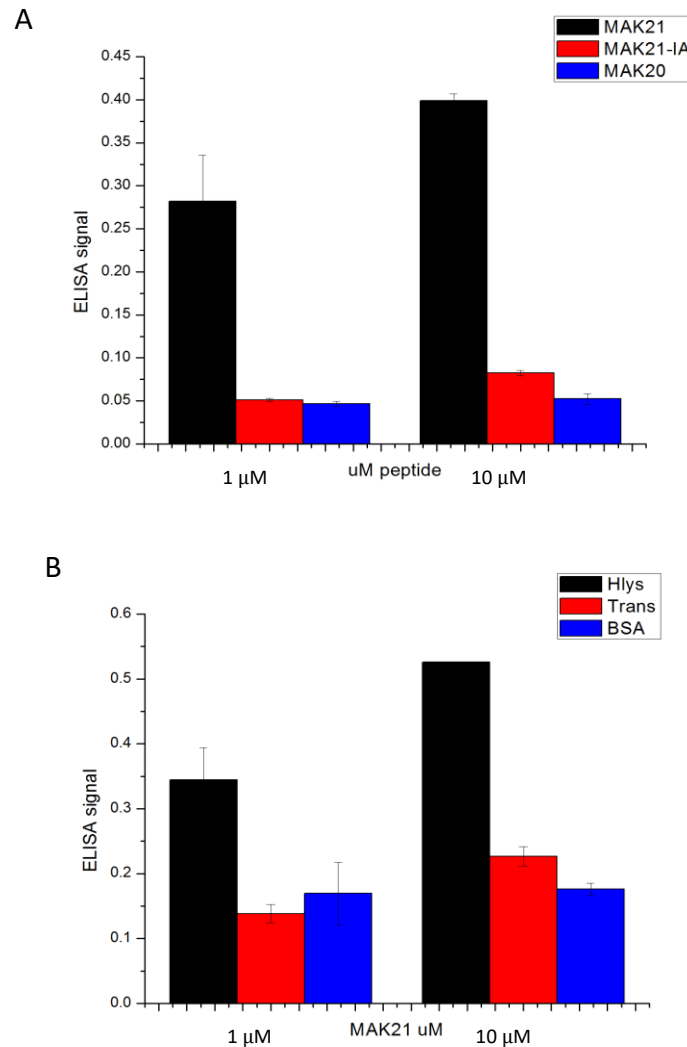


Figure 6-5 ELISA human lysozyme peptides (A) ELISA assay of peptides at 1 μ M and 10 μ M concentrations for human lysozyme deposited into wells. (B) MAK21 against 3 different proteins human lysozyme, transferrin, and BSA showing the specificity of MAK21 for human lysozyme.

Wanting to probe MAK21 further, the peptide was tested for its specificity for human lysozyme. To this end, human lysozyme, transferrin, and BSA were all deposited

into separate wells for further ELISA analysis. MAK21 was then incubated with each protein, testing its binding ability. The ELISA results indicated that MAK21 preferentially bound to wells containing human lysozyme over wells with BSA and transferrin. These results suggest MAK21 is specific for human lysozyme.

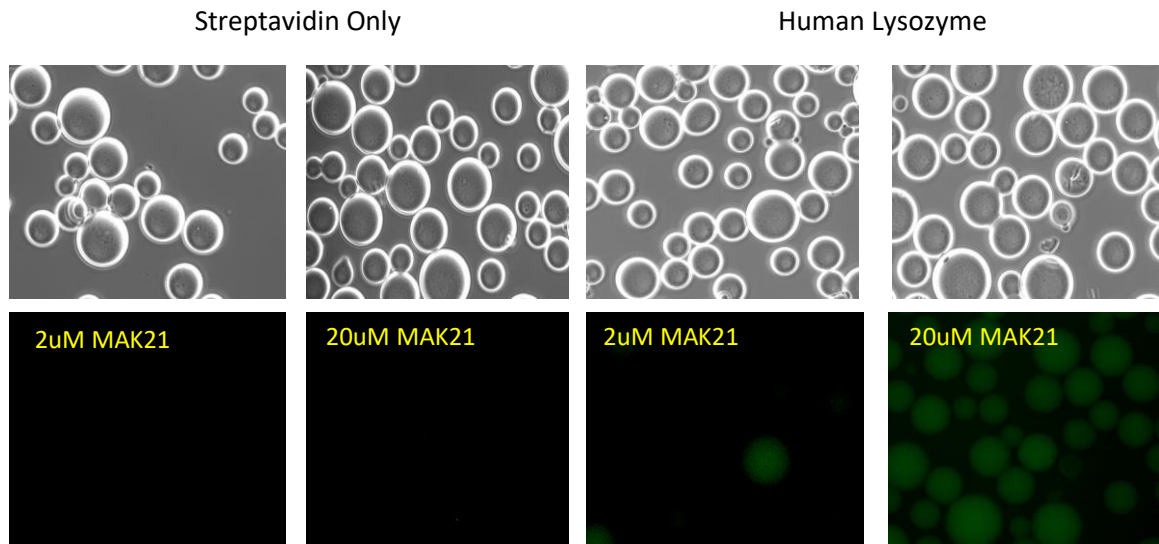


Figure 6-6 Images of MAK21 incubated with streptavidin beads and human lysozyme captured on beads. MAK21 was incubated at 2 μM and 20 μM (and then diluted 10 times) concentrations before imaging.

In addition to an ELISA assay, MAK21 was evaluated for its ability to bind to human lysozyme immobilized on streptavidin resin using microscopy. Human lysozyme was reacted with biotin-NHS to yield a biotin-labeled protein. This protein was then captured with streptavidin resin and incubated with MAK21 at 2 μM and 20 μM concentrations for imaging by fluorescent microscopy. 2 μM concentrations approached the limits of fluorescent microscopy due to the saturation of the image by background fluorescence. At 2 μM of MAK21, minimal binding was observed to human lysozyme containing beads. To increase binding, MAK21 was incubated at 20 μM for one (1) hour before diluting ten

(10) times for imaging. This marginally increased binding, indicating that MAK21 may not have a robust binding affinity for human lysozyme under all conditions.

6.2.4 Sortase A Screen and Peptide Characterization

For screening and characterization, SrtA was expressed in BL21 cells and purified by a nickel column. Subsequently, the protein was modified with biotin-NHS and confirmed by LC-MS. Three rounds affinity selection were performed against SrtA immobilized on streptavidin resin with the mono APBA cyclic library. After the second and third round, plaques were isolated for sequencing and convergence identification. A summary of the hits isolated can be seen in **Table 6-3**. As previously performed, peptides included a triple glycine linker, followed by an alloc-protected Dap residue that was selectively deprotected and labeled with FAM all peptides were modified with the cyclic linker, creating mono APBA cyclic peptides.

Table 6-3 Sequences identified for SrtA.

Peptide Sequences	Rd 2	Rd 3	Name
ACFDSRLNPC	1	3	MAK35
ACYGNSPLTC		2	MAK36
ACNNHGYWWC		3	MAK37
ACHMRQGMAC	1		
ACGGNKPPVC	1		
ACVSKWPALC	1		
ACMYTPSIKC	1		
ACLLGTVQTC	1		
ACQPMAPKNC	1		
ACPDLHVKVC	1		
ACQQANQEHC	1		
ACRGPAGSIC	1		
ACYTYQASPC	1		
ACDGRPDRAC	1		
ACKGTSMRTC	1		
ACGTNPIKCC		1	
ACKNYSQPIC		1	
ACDGRPDRAC		1	
ACMGIHNLIC		1	
Blank	7	8	

Table 6-4 Peptide sequences for SrtA made via SPPS.

Name	Sequence	Calculated Mass m/z	Obs Mass m/z
MAK35	AC _{mc} FDSRLNPC _{mc} GGGDap	1070.41 [M-H ₂ O+2H] ²⁺	1070.20
MAK36	AC _{mc} YGNSPLTC _{mc} GGGDap	2042.74 [M-H ₂ O+H] ¹⁺	2042.21
MAK37	AC _{mc} NNHGYWWC _{mc} GGGDap	1134.40 [M-H ₂ O+2H] ²⁺	1133.89

mc indicates the peptide was modified with cyclic APBA-IA staple

These peptides were analyzed for their ability to bind to SrtA immobilized on resin by fluorescent microscopy. A dimer peptide (WW6) isolated by Wenjian Wang was previously found to bind to SrtA, and used in these experiments as a positive control.

Peptides were incubated at 20 μ M, and then diluted ten (10) times for fluorescent imaging. The positive control, WW6, showed intense binding to SrtA coated resin. Of the three cyclic peptides, MAK37 showed the brightest staining, while MAK35 and MAK36 were noticeably dimmer. It is not surprising that the positive control had a greater affinity for SrtA, as it is able to take advantage of multivalent interactions. Alternatively, the cyclic peptides still demonstrated noticeable binding to SrtA, and thus, should be further characterized for their specificity and binding affinities under varying conditions. Fluorescent microscopy is limited in its comparative analysis of peptide binding: additional assays will need to be conducted to generate binding curves of these peptides and quantitatively assess their potential as a SrtA binder.

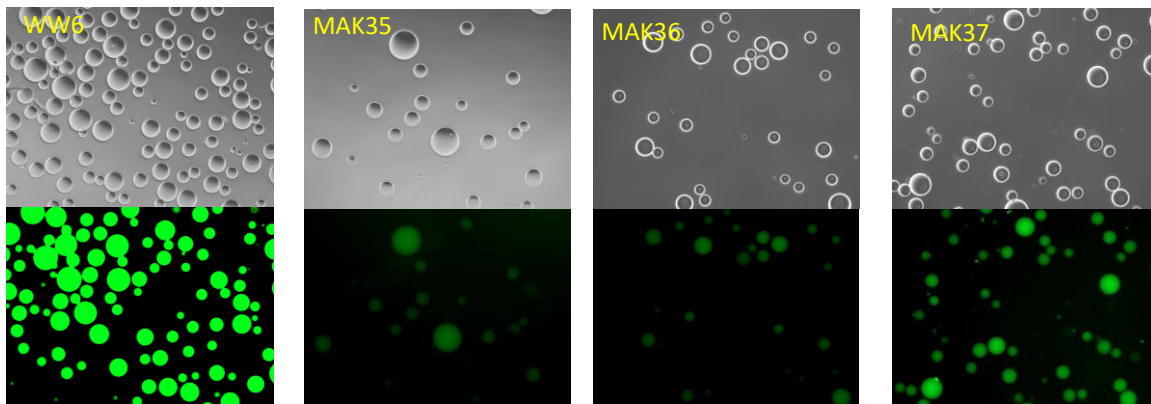


Figure 6-7 Fluorescent microscopy imaging of positive control WW6 and MAK35-37 peptides for SrtA protein immobilized on streptavidin resin.

6.3 Conclusions and Discussion

Of the three screens against human lysozyme, only the unmodified C7C library and the dimer APBA library were successful in identifying converging peptide sequences. MAK20 was unsuccessful in generating any signal in ELISA assays and was likely a false positive. That said, the initial characterization of MAK21 identified in the dimer APBA

screen for human lysozyme shows some promise. MAK21 showed preferential binding to human lysozyme over transferrin and BSA in ELISA assays, however, it needed relatively high concentrations (20 μ M) to show any binding in fluorescent microscopy analysis. The requirement of these higher concentrations indicates that MAK21 is likely not as potent of a ligand when compared to previously identified APBA peptides. Generation of binding curves through additional experiments would shed light on the potential of MAK21 as a peptide binder to human lysozyme.

The SrtA screen using the mono APBA cyclic library was successful in identifying converging peptide sequences. Nonetheless, peptides identified in the SrtA screen showed diminished intensity when compared to the linear dimer WW6 peptide. Further analysis and characterization of these peptides is needed to assess their potential as SrtA binders.

The cyclic APBA library demonstrated in these experiments expands on APBA reversible covalent libraries. The pulse chase assay confirmed that APBA cyclic libraries can be generated in phage display platforms with upwards of 70% efficiency in labeling. Though the library did not produce any recurring sequences for human lysozyme, it did identify peptides in SrtA screens. Further study is needed in order to fully characterize the peptide probes identified here, but the library, as a screening platform, has shown potential. It is intriguing to consider the potential for library development following this mono APBA cyclic library; specifically, the combination of the multivalent approach of the dimer library with the rigid, cyclic peptide would be interesting. Others in the Gao lab are currently developing di-APBA cyclic libraries that have the potential to overtake both the

linear dimer and cyclic monomer APBA libraries for producing high affinity peptide binders.

6.4 Experimental Protocols

6.4.1 General Methods and Procedures

Human lysozyme protein was obtained from fisher scientific. SortaseA plasmid was obtained from Addgene pET28a-SrtAdelta59. The plasmid was isolated from cells and then transformed into BL-21 cells for large-scale expression. APBA dichloroacetamide (APBA-DCA) was obtained from Jhuma. The Ph.D.-C7C library, SPPS, and microscopy studies were carried out as described previously (Chapter 3).

6.4.2 Library Screening

Library screening was conducted as previously described in chapter 2 for physical deposition with the notable exception of BSA blocking for 1 hr and its incorporation at every step of the panning process. 25ug of biotin labeled SrtA was incubated with 10uL of streptavidin resin for 45 min in PBS buffer pH 7.4. Resin was washed twice and then blocked with 10mg/mL BSA for 1 hr. Libraries were labeled as previously described (Chapter 3) and were also blocked for 1 hr. Following this the library was incubated with the SrtA resin for 1 hr with subsequent washing and elution of phage from target protein. Phage were amplified for additional rounds of screening and plaques picked for sequencing.

6.4.3 Pulse Chase Assay

For APBA-IA labeling protocol see chapter 3 procedures. For confirmation of APBA-DCA labeling on phage, streptavidin agarose resin (25 μ L/sample) was washed with

PBS (pH 7.4) and blocked with 10 mg/mL BSA via incubation for 1 hr. APBA-DCA labeled library was split with one population subjected to subsequent labeling with Biotin-IA (2 mM) for 2 hr and the other subjected to Biotin cysteamine (4mM) for 2 hr followed by dilution to minimize small molecule concentration. Biotin-IA labeled, APBA-DCA/Biotin-IA labeled and APBA-DCA/Biotin cysteamine phage (200 μ L, $\sim 1 \times 10^{10}$ pfu/mL) were subjected to the streptavidin resin for 1 hr. Non-reduced and reduced phage, without small molecule labeling, were also analyzed. Unbound phage was removed from resin and the phage titer was calculated. The titer was compared to that of phage not subjected to streptavidin to generate a percent capture. The average percent capture and standard deviation of three trials was plotted. Wild-type phage, with no library insert, was subjected to the same analysis for comparison.

6.4.4 Protein Labeling with Biotin-NHS

3 equivalents of Biotin-NHS were added to protein of interest for 16hr or overnight at pH 9.5.¹⁰ Following this, proteins were purified via buffer exchange and a small portion were run on LC-MS to confirm single site modification. LC-MS data was deconvoluted and protein masses were compared to their unmodified masses. A summary of masses identified can be seen in **Table 6-5**.

Table 6-5 Protein labeling with Biotin-NHS.

Number	Sample	Calculated Mass	Deconvoluted Mass
1	SrtA	19047	19048
2	SrtA-Biotin	19274	19273
3	Human Lys	14692	14692
4	Human Lys-Biotin	14918	14918

6.4.5 ELISA Assay

Human lysozyme, transferrin and BSA were deposited in wells overnight at 4°C with gentle shaking. Following this, wells were washed once with PBST and then peptides added at appropriate concentrations for 1 hr incubation. Next wells were washed with PBST 8 times followed by incubation of anti-fluorescein antibody conjugated to HRP for 30 min. After antibody incubation, wells were washed an additional three times to remove excess antibody. 100µL of ELISA-TMB were added to each well using a multichannel to ensure TMB was added at the same time for PC and PS wells. Color was allowed to develop for 20-45 min before absorbance measurements on a plate reader at 600nm.

6.5 References

1. Katz, B. A. (1995). Binding to protein targets of peptidic leads discovered by phage display: crystal structures of streptavidin-bound linear and cyclic peptide ligands containing the HPQ sequence. *Biochemistry*, *34*(47), 15421-15429.
2. Pande, J., Szewczyk, M. M., & Grover, A. K. (2010). Phage display: concept, innovations, applications and future. *Biotechnology advances*, *28*(6), 849-858.
3. McCarthy, K. A., Kelly, M. A., Li, K., Cambray, S., Hosseini, A. S., van Opijnen, T., & Gao, J. (2018). Phage display of dynamic covalent binding motifs enables facile development of targeted antibiotics. *Journal of the American Chemical Society*, *140*(19), 6137-6145.
4. Huang, J., Wu, L., Yalda, D., Adkins, Y., Kelleher, S. L., Crane, M., ... & Huang, N. (2002). Expression of functional recombinant human lysozyme in transgenic rice cell culture. *Transgenic research*, *11*(3), 229-239.
5. Manchenko, G. (1994). Lysozyme. *Handbook of Detection of Enzymes on Electrophoretic Gels*, 98.
6. Osserman, E. F., Cole, S. J., Swan, I. D., & Blake, C. C. (1969). Preliminary crystallographic data on human lysozyme. *Journal of molecular biology*, *46*(1), 211-212.
7. Muraki, M., Harata, K., Sugita, N., & Sato, K. I. (1996). Origin of carbohydrate recognition specificity of human lysozyme revealed by affinity labeling. *Biochemistry*, *35*(42), 13562-13567.
8. Ton-That, H., Liu, G., Mazmanian, S. K., Faull, K. F., & Schneewind, O. (1999). Purification and characterization of sortase, the transpeptidase that cleaves surface proteins of *Staphylococcus aureus* at the LPXTG motif. *Proceedings of the National Academy of Sciences*, *96*(22), 12424-12429.
9. Zong, Y., Bice, T. W., Ton-That, H., Schneewind, O., & Narayana, S. V. (2004). Crystal structures of *Staphylococcus aureus* sortase A and its substrate complex. *Journal of Biological Chemistry*, *279*(30), 31383-31389.

10. Guimaraes, C. P., Witte, M. D., Theile, C. S., Bozkurt, G., Kundrat, L., Blom, A. E., & Ploegh, H. L. (2013). Site-specific C-terminal and internal loop labeling of proteins using sortase-mediated reactions. *Nature protocols*, 8(9), 1787.

Chapter 7

Biocompatible Conjugation of Tris Base to 2-Acetyl and 2-Formyl Phenylboronic

Acid

This work was done in collaboration with Dr. Kaicheng Li.

7.1 Introduction

7.1.1 Biocompatible Conjugation Chemistries with APBA

Evaluating and picking appropriate libraries for a specific target is an important aspect in phage display. As the previous work discussed in this thesis demonstrates, the right library can identify potent ligands for even the most difficult targets. However, the right library is not the only aspect to consider when screening. Careful set up of the screening process will ultimately identify better and more robust peptide binders, as was seen with incorporation of BSA throughout the panning process. Peptides selected in the screening process will only be as good as the set up and conditions used in the panning procedure. It is unlikely a peptide will possess characteristics beyond what was selected for. With this in mind it is important to be aware of every detail during the panning process. This is especially true when developing new and unique libraries. The libraries we have created incorporate APBA which is found to conjugate with biological amines in a dynamic manner to give iminoboronates (**Figure 7-1A**). We were curious if the APBA headgroup in the library would be affected by Tris base, which also possesses an amine group.

The dynamic iminoboronate formation of 2-FPBA/APBA typically favors unhindered amines such as the side chain amine of lysines. However, the Gao lab and others have recently shown that cysteine and 2,3-diaminopropionic acid (Dap) can rapidly conjugate with 2-FPBA to give a thiazolidinoboronate (TzB) and imidazolidoboronate (IzB) complex respectively.¹⁻³ The TzB/IzB formation proceeds with an iminoboronate intermediate, which is rapidly converted to more stable cyclic products (**Figure 7-1B**).

Interestingly, we have found that Tris base, a commonly used buffering agent, undergoes biocompatible conjugation with 2-FPBA/APBA similar to the TzB/IzB formation to give multicyclic products (**Figure 7-1C**). In contrast to the dynamic nature of TzB/IzB formation, the Tris conjugates exhibit much enhanced kinetic stability. While this stability is great for expanding the toolbox of bioorthogonal conjugation reactions, it ultimately can be a hindrance in screening of reversible covalent phage display libraries and needs to be considered when screening future libraries.

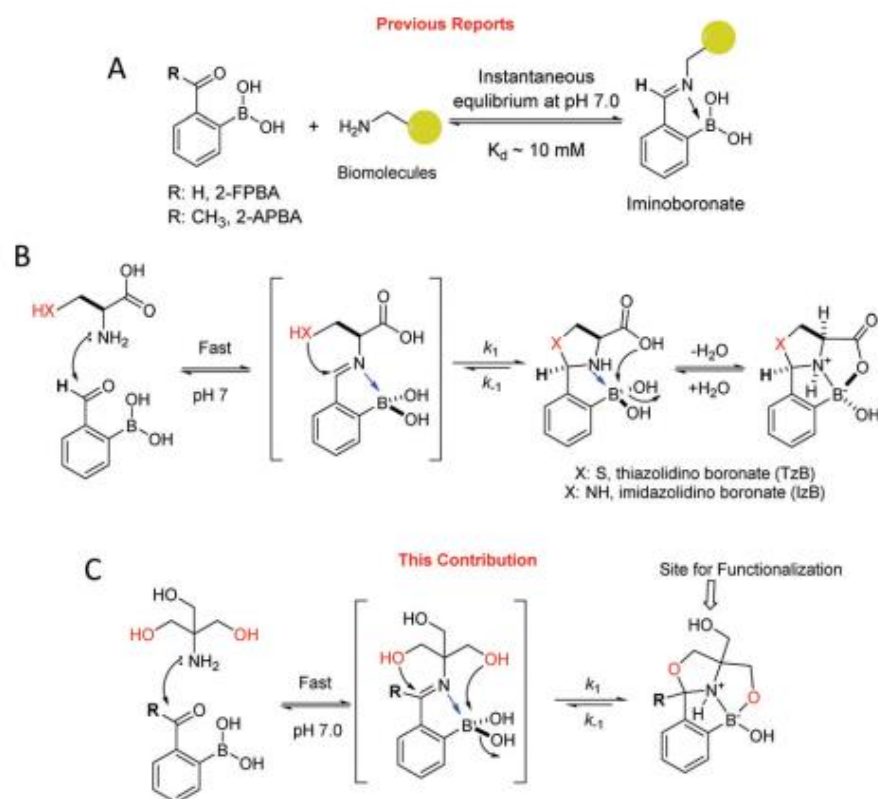


Figure 7-1 Biocompatible conjugation chemistries of 2-FPBA/APBA. (A) Iminoboronate formation; (B) TzB/IzB complex formation of 2-FPBA; (C) 2-FPBA/APBA conjugation with Tris base affording multicyclic products with much enhanced kinetic stability.

7.2 Discovery and Characterization of Tris APBA/FPBA Complex

7.2.1 LC-MS and X-ray Crystallography

The conjugation of Tris base to 2-FPBA/APBA was initially discovered by LC-MS. Peptides identified from the screening process were made via SPPS and then modified with APBA functionality under phage labeling conditions (i.e. in the presence of 50mM Tris). Peptides monitored by LC-MS to check their reaction progress contained an additional 85.05 Da. It was hypothesized that Tris may be reacting with the head group so the modification reaction was switched to PBS buffer and the additional 85.05 Da disappeared (**Table 7-1**)

Table 7-1 Masses of the same peptide labeled APBA head group in Tris vs PBS.

Conditions	Expected Mass M/z	Observed Mass M/z
Labeling in Tris	913.39 $[M - 2H_2O + 2H]^{2+}$	913.39
Labeling in PBS	870.87 $[M + 2H]^{2+}$	870.86

Following this, the Tris base APBA/FPBA interaction was characterized further by X-ray crystallography. Detailed conditions of crystallization can be found in the general methods. As expected for the symmetric (achiral) structure of Tris, the conjugates with 2-FPBA and 2-APBA were obtained as a racemic mixture as indicated by the space group of the crystallography results. To compare with the TzB and IzB structures that we previously reported,^{1,2} the structures of the Tris conjugates are shown with the same stereochemistry as TzB/IzB (**Figure 7-2**). Analogous to the TzB and IzB complexes, the FPBA-Tris conjugate features an oxazolidinoboronate (OzB) core, which further cyclizes

with another $-\text{CH}_2\text{OH}$ arm of Tris to give a three-ring fused structure (**Figure 7-2**). Note that similar cyclization was observed in TzB/IzB complexes, although with a $-\text{COOH}$ group to give mixed anhydrides that show poor stability due to quick hydrolysis.¹ A similar structure was obtained for the Tris conjugate with 2-APBA, which again features a multicyclic structure with an OzB core. Interestingly, although 2-APBA is also known to form a TzB complex with cysteine,⁴ this TzB complex has so far eluded crystallography characterization possibly due to its low stability and rapid dissociation.⁴

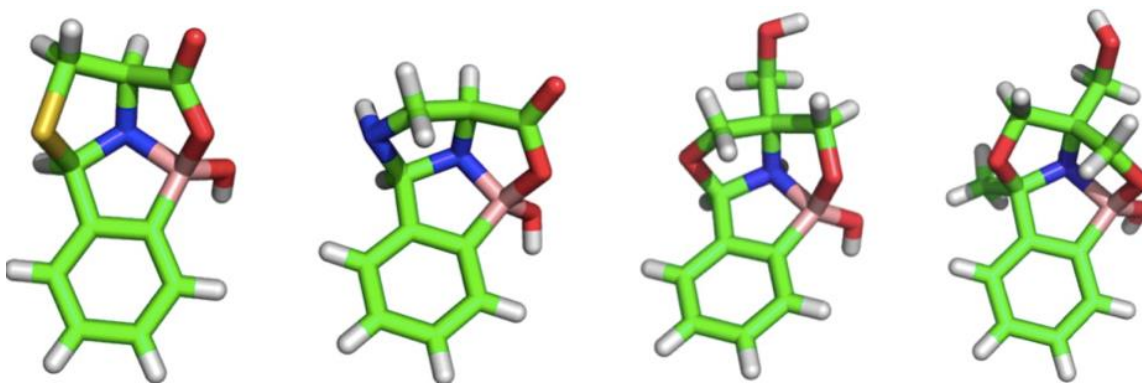


Figure 7-2 Characterization of the FPBA/APBA-Tris conjugates by X-ray crystallography. Crystal structures of the Tris conjugates in comparison to the TzB and IzB complexes. C: Black; N: blue; O: red; B: pink; H: white.

7.2.2 Kinetic Studies

The kinetics of these conjugation reactions was determined by mixing equimolar Tris with 2-FPBA (2 mM) or 2-APBA (8 mM) respectively. The progression of the reactions was monitored by $^1\text{H-NMR}$ (work done by Dr. Li). The conjugation with 2-FPBA reached equilibrium after 2 h giving 80% product. Tris conjugation with 2-APBA was significantly slower and it took ~ 30 h to reach equilibrium affording 57% conversion. The kinetic profiles were fitted according to the mechanism of relaxation kinetics, from which the

forward and backward reaction rate constants (k_1 and k_{-1}) were extracted and shown in

Figure 7-3.

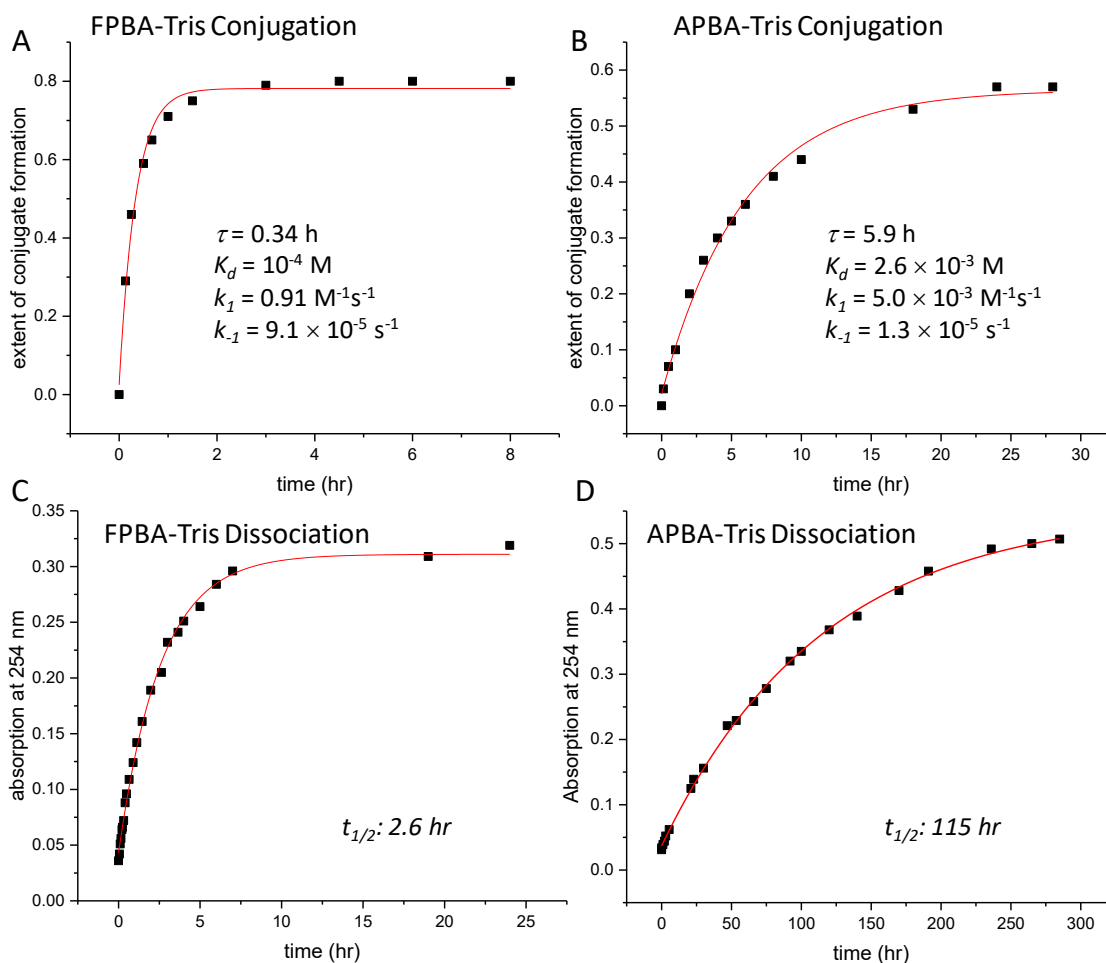


Figure 7-3 Kinetics analysis of Tris conjugation with 2-FPBA/APBA. (A) Associative relaxation of 2-FPBA and Tris at 2 mM concentration. (B) Associative relaxation of 2-APBA and Tris at 8 mM concentration. (C) Dissociation kinetics of 2-FPBA-Tris conjugate monitored by monitoring absorption at 254 nm. (D) Dissociation kinetics of 2-APBA-Tris conjugate monitored by monitoring absorption at 254 nm. For C and D, the conjugates were diluted to 100 μ M to initiate the experiments.

The forward reaction rate constant (k_1) was found to be 0.9 and 0.005 M⁻¹ s⁻¹ for 2-FPBA and 2-APBA respectively. The faster reaction of 2-FPBA is consistent with its more favorable binding (via iminoboronate formation) to hindered amines.⁵ Tris

conjugation with 2-FPBA is sufficiently fast to give 67% Tris conversion with just 0.5 mM 2-FPBA over 3 h (**Figure 7-3A**) The conjugation with 2-APBA is slower and needed 2 mM 2-APBA and overnight incubation (20 h) to give ~50% Tris conversion (**Figure 7-3B**). The rate constant of the backward reaction (k_{-1}) was determined to be 9.1×10^{-5} and $1.3 \times 10^{-5} \text{ s}^{-1}$ respectively, which indicate much slower dissociation in comparison to the TzB or IzB complexes.^{1,2} Indeed, a dilution experiment revealed a half-life of 2.6 h and 115 h for the FPBA-Tris and APBA-Tris conjugate respectively (**Figure 7-3 C and D**). For comparison, the TzB complex of cysteine and 2-FPBA was found to dissociate within an hour,¹ while the APBA-cysteine conjugate dissociates in seconds.⁴ The much slower dissociation makes the APBA-Tris conjugate comparable in kinetic stability to typical oximes and hydrozones.^{6,7}

7.3 Conclusions and Discussion

In summary, this contribution describes the discovery and characterization of biocompatible conjugation chemistry of 2-FPBA and 2-APBA to Tris base, a commonly used buffering agent. The FPBA-Tris conjugate was shown to have a half-life of 2.6 hours while the APBA-Tris conjugate was significantly longer at 115 hr. The much-enhanced stability and excellent biocompatibility make the Tris conjugation chemistry appealing to various biological applications. However, any use of Tris buffer in combination with APBA phage display libraries may have a negative impact. The half-life of the APBA-Tris conjugate makes it clear that any screening done in the presence of Tris will cap the APBA head groups. Even if phage are removed from Tris buffer and allowed to equilibrate

overnight, the majority of the library will remain capped. It is because of this interaction, that one needs to be aware of every condition in the screening set up.

7.4 Experimental Protocols

7.4.1 General Methods and Procedures

2-formylphenylboronic acid (2-FPBA), 2-acetylphenylboronic acid (2-APBA) were purchased from Fisher Scientific or Sigma-Aldrich. UV spectra were collected on a Nanodrop UV-vis spectrometer. Mass-spec data were collected on an Agilent 6230 LCTOF mass spectrometer. Method for LC/MS: isocratic 95% buffer A for 5min, 95% buffer A to 5% buffer A in 15 min, isocratic 5% buffer A for 5 min, 5% buffer A to 95% buffer A in 1 min and then isocratic 95% buffer A for 7 min. Buffer A: nano pure water with 0.1% formic acid Buffer B: acetonitrile with 0.1% formic acid.

7.4.2 Crystallographic Information

100 mM 2-FPBA or 2-APBA and 100 mM Tris were dissolved in 75% Acetonitrile/25% water in a loosely capped 5 mL glass vial at room temperature. After a few days, crystals were observed for both complexes.

Table 7-2 Crystallography data and structure refinement for APBA-Tris.

Identification code	C12H16BNO4
Empirical formula	C12 H16 B N O4
Formula weight	249.07
Temperature	100(2) K
Wavelength	1.54178 \approx
Crystal system	Orthorhombic
Space group	Pca2 ₁
Unit cell dimensions	a = 11.3174(2) \approx a = 90 ∞ . b = 13.2547(3) \approx b = 90 ∞ . c = 7.8913(2) \approx g = 90 ∞ .
Volume	1183.76(5) \approx^3
Z	4
Density (calculated)	1.398 Mg/m ³
Absorption coefficient	0.851 mm ⁻¹
F(000)	528
Crystal size	0.220 x 0.130 x 0.050 mm ³
Theta range for data collection	3.334 to 69.741 ∞ .
Index ranges	-12 \leq h \leq 13, -15 \leq k \leq 16, -9 \leq l \leq 9
Reflections collected	7352
Independent reflections	2045 [R(int) = 0.0299]
Completeness to theta = 67.679 ∞	100.0 %
Absorption correction	Semi-empirical from equivalents
Max. and min. transmission	0.7533 and 0.6610
Refinement method	Full-matrix least-squares on F ²
Data / restraints / parameters	2045 / 4 / 173
Goodness-of-fit on F ²	1.066
Final R indices [I $>$ 2 σ (I)]	R1 = 0.0276, wR2 = 0.0729
R indices (all data)	R1 = 0.0287, wR2 = 0.0740
Absolute structure parameter	0.00(8)
Extinction coefficient	n/a
Largest diff. peak and hole	0.250 and -0.166 e. \approx^{-3}

Table 7-3 Atomic coordinates ($\times 10^4$) and equivalent isotropic displacement parameters ($\approx 2 \times 10^3$) for C₁₂H₁₆NO₄. U(eq) is defined as one third of the trace of the orthogonalized U^{ij} tensor.

	x	y	z	U(eq)
O(1)	3606(1)	7334(1)	5203(2)	17(1)
O(2)	7568(1)	8463(1)	4306(2)	14(1)
O(3)	6132(1)	8179(1)	2222(2)	14(1)
O(4)	3767(1)	10207(1)	2494(2)	16(1)
N(1)	5346(1)	8291(1)	5079(2)	11(1)
C(1)	4764(2)	7402(2)	5937(3)	13(1)
C(2)	5500(2)	6492(2)	5452(3)	14(1)
C(3)	5274(2)	5522(2)	6033(3)	18(1)
C(4)	6059(2)	4760(2)	5588(3)	21(1)
C(5)	7038(2)	4967(2)	4578(3)	20(1)
C(6)	7234(2)	5940(2)	3990(3)	17(1)
C(7)	6465(2)	6724(1)	4432(3)	14(1)
C(8)	4878(2)	8178(1)	2174(3)	15(1)
C(9)	4479(2)	8686(2)	3818(3)	13(1)
C(10)	3311(2)	8287(2)	4477(3)	18(1)
C(11)	4677(2)	7567(2)	7833(3)	16(1)
C(12)	4569(2)	9833(2)	3731(3)	16(1)
B(1)	6528(2)	7896(2)	3923(3)	12(1)

Table 7-4 Crystallography data and structure refinement for FPBA-Tris.

Identification code	C11H14BNO4
Empirical formula	C11 H14 B N O4
Formula weight	235.04
Temperature	100(2) K
Wavelength	1.54178 \approx
Crystal system	Monoclinic
Space group	P2 ₁ /c
Unit cell dimensions	a = 13.3622(6) \approx a = 90 ∞ . b = 9.2625(4) \approx b = 94.734(2) ∞ . c = 8.6950(4) \approx g = 90 ∞ .
Volume	1072.49(8) \approx^3
Z	4
Density (calculated)	1.456 Mg/m ³
Absorption coefficient	0.906 mm ⁻¹
F(000)	496
Crystal size	0.420 x 0.180 x 0.100 mm ³
Theta range for data collection	5.819 to 69.802 ∞ .
Index ranges	0 \leq h \leq 16, -11 \leq k \leq 11, -10 \leq l \leq 10
Reflections collected	3453
Independent reflections	3453 [R(int) = ?]
Completeness to theta = 67.679 ∞	99.2 %
Absorption correction	Semi-empirical from equivalents
Max. and min. transmission	0.7533 and 0.5156
Refinement method	Full-matrix least-squares on F ²
Data / restraints / parameters	3453 / 3 / 164
Goodness-of-fit on F ²	1.049
Final R indices [I \geq 2 σ (I)]	R1 = 0.0543, wR2 = 0.1538
R indices (all data)	R1 = 0.0598, wR2 = 0.1598
Extinction coefficient	n/a
Largest diff. peak and hole	0.397 and -0.217 e. \approx^{-3}

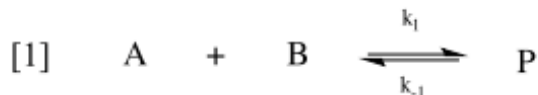
Table 7-5 Atomic coordinates ($\times 10^4$) and equivalent isotropic displacement parameters ($\approx 2 \times 10^3$) for C₁₁H₁₄BNO₄. U(eq) is defined as one third of the trace of the orthogonalized U^{ij} tensor.

	x	y	z	U(eq)
O(1)	6562(1)	3964(2)	6685(2)	30(1)
O(2)	9305(1)	6946(2)	5558(2)	28(1)
O(3)	8930(1)	6269(2)	8096(2)	27(1)
O(4)	8811(1)	1611(2)	8371(2)	27(1)
N(1)	8079(1)	4893(2)	5997(2)	24(1)
B(1)	8528(2)	6541(3)	6501(3)	26(1)
C(1)	6953(2)	4978(2)	5669(3)	28(1)
C(2)	6677(2)	6530(3)	5952(3)	29(1)
C(3)	5693(2)	7044(3)	5810(3)	35(1)
C(4)	5527(2)	8482(3)	6126(3)	37(1)
C(5)	6329(2)	9393(3)	6561(3)	33(1)
C(6)	7305(2)	8868(2)	6690(3)	30(1)
C(7)	7490(2)	7419(2)	6376(3)	27(1)
C(8)	9098(2)	4784(2)	8381(3)	26(1)
C(9)	8276(2)	3965(2)	7408(2)	25(1)
C(10)	7247(2)	3992(3)	8047(3)	29(1)
C(11)	8593(2)	2440(2)	7003(3)	26(1)

7.4.3 Relaxation Kinetics

The forward reaction kinetics data were fitted according to the equations of second order relaxation. The following equations were used to calculate the relaxation constant. Equation 1 describes the reaction mechanism, equation 2 describes the second order relaxation kinetics, equation 3 describes the relaxation time constant τ , equation 4-6 correlates the concentration of the reactants and the reaction rates. $[A]_0 = 2 \text{ mM}$ for FPBA and 8 mM for APBA. $[AB]$ is the concentration of the conjugates at equilibrium, which equals 1.6 mM for FPBA-Tris and 4.6 mM for APBA-Tris according to the integration

of NMR spectrum (done by Dr. Li). $[A]$ and $[B]$ represent the reactant concentrations at equilibrium.



$$[4] \quad \overline{[A]} = \overline{[B]}$$

$$[2] \quad y = y_0 + Ae^{(-t/\tau)}$$

$$[5] \quad \overline{[A]} + \overline{[AB]} = [A]_0$$

$$[3] \quad \tau = \frac{1}{k_{-1} + k_1(\overline{[A]} + \overline{[B]})}$$

$$[6] \quad K_d = \frac{\overline{[A]}\overline{[B]}}{\overline{[AB]}} = \frac{k_{-1}}{k_1}$$

7.5 References

1. Bandyopadhyay, A., Cambray, S., & Gao, J. (2016). Fast and selective labeling of N-terminal cysteines at neutral pH via thiazolidino boronate formation. *Chemical science*, 7(7), 4589-4593.
2. Li, K., Weidman, C., & Gao, J. (2018). Dynamic formation of imidazolidino boronate enables design of cysteine-responsive peptides. *Organic letters*, 20(1), 20-23.
3. Faustino, H., Silva, M. J., Veiros, L. F., Bernardes, G. J., & Gois, P. M. (2016). Iminoboronates are efficient intermediates for selective, rapid and reversible N-terminal cysteine functionalisation. *Chemical science*, 7(8), 5052-5058.
4. Bandyopadhyay, A., Cambray, S., & Gao, J. (2017). Fast diazaborine formation of semicarbazide enables facile labeling of bacterial pathogens. *Journal of the American Chemical Society*, 139(2), 871-878.
5. Cal, P. M., Vicente, J. B., Pires, E., Coelho, A. V., Veiros, L. F., Cordeiro, C., & Gois, P. M. (2012). Iminoboronates: a new strategy for reversible protein modification. *Journal of the American Chemical Society*, 134(24), 10299-10305.

6. Kalia, J., & Raines, R. T. (2008). Hydrolytic stability of hydrazones and oximes. *Angewandte Chemie International Edition*, 47(39), 7523-7526.
7. Dirksen, A., & Dawson, P. E. (2008). Rapid oxime and hydrazone ligations with aromatic aldehydes for biomolecular labeling. *Bioconjugate chemistry*, 19(12), 2543-2548.